

Recalibration of damage equivalence factors for fatigue verification of road bridges

Colin Vaccari

Thesis to obtain the Master of Science Degree in

Civil Engineering

Supervisors

Prof. Dr. Alain Nussbaumer

Prof. Dr. José Joaquim Costa Branco de Oliveira Pedro

Jury

Chairperson: Prof. Dr. Mário Manuel Paisana dos Santos Lopes

Supervisor: Prof. Dr. Alain Nussbaumer

Members of the committee: Prof. Dr. Francisco Batista Esteves Virtuoso

June 2021

I declare that this document is an original work of my own authorship and that it fulfils all the requirements of the Code of Conduct and Good Practices of the Universidade de Lisboa

Abstract

The current works of revision of the Eurocodes (CEN250 project 2nd Eurocode generation), is an opportunity to update the simplified method (lambda factor method) for fatigue verification for steel road bridges. Especially as this method is based on old traffic models, it is necessary to establish an update consistent with current European road traffic.

This thesis focuses on the λ_{max} factor used in the simplified verification method. The aim is to be able to determine new λ_{max} curves using modern traffic models that are more reliable according to current trends. In addition to this, an improvement is to be made to cover a larger number of cases, both in terms of influence lines and span lengths.

The objective remains to propose new λ_{max} curves taking into account the current European traffic observed in order to best monitor the behaviour of steel road bridges. Several types of traffic were used in order to have an overview and to be able to make a comparison between different models and especially Weight in Motion measurements.

In conclusion, a new proposal adapted for the verification method with lambdas factors is presented. This proposal considers a total of 44 influences lines that are regrouped into 4 λ curves. The results obtained shows also a dependency on the traffic volume that can now be considered with the update of the lambda curves

Keywords

Fatigue, Lambda Factor, Traffic Model, Road bridges, Structural Steel Design

Resumo

Os actuais trabalhos de revisão dos Eurocódigos (projecto CEN250 2ª geração dos Eurocódigos), constituem uma oportunidade para actualizar o método simplificado (método dos factores lambda) de verificação da fadiga das pontes rodoviárias, nomeadamente porque este método se baseia em antigos modelos de tráfego que se justifica tornar coerentes com o actual tráfego rodoviário europeu.

Esta tese centra-se no factor de verificação l_{max} . O objectivo é determinar novas curvas de l_{max} utilizando modelos de tráfego modernos que são mais fiáveis em comparação com as tendências actuais. Além disso, é realizado um melhoramento na determinação das novas curvas de λ_{max} para ter em consideração um maior número de casos, tanto em termos de linhas de influência como de comprimentos e de relação entre vãos.

São assim propostas novas curvas λ_{max} tendo em conta o actual tráfego europeu observado, a fim de melhor controlar o comportamento à fadiga das pontes rodoviárias. São utilizados vários tipos de tráfego a fim de se ter uma visão geral e poder fazer uma comparação entre diferentes modelos e especialmente medições de tráfego WIM.

Em conclusão, é apresentada uma nova proposta adaptada para o método de verificação utilizando os factores lambda. Esta proposta tem em conta os resultados das numerosas simulações numéricas realizadas para uma grande variedade de sistemas estáticos e considerando diversos tipos de tráfego.

Palavras-chave

Fadiga, Factor Lambda, Modelo de Trânsito, Pontes rodoviárias, Concepção de Estruturas Metálicas

Contents

1	Introduction	1
1.1	Motivation	1
1.2	Thesis Outline	2
2	Basic concepts of fatigue design	3
2.1	Fatigue Resistance	4
2.1.1	Parameters influencing the service life	4
2.2	Fatigue strength curve	6
2.3	Fatigue safety verification	7
2.3.1	Verification with the fatigue limit	7
2.3.2	Verification with the cumulative damage	8
2.3.3	Verification with the lambda factor	8
2.4	The λ correction factor	11
2.4.1	λ_1 - Damage effect of traffic	11
2.4.2	λ_2 - Traffic volume	12
2.4.3	λ_3 - Design life	12
2.4.4	λ_4 - Traffic on other lanes	12
2.4.5	λ_{max} - Upper limit	13
2.4.6	Fatigue critical length	13
3	Previous simulations and λ_{max} factor determination	15
3.1	Sedlacek and Merzenich, 1995	15
3.1.1	Traffic Model	16
3.1.2	Comparison with Sedlacek and Merzenich simulations	19
3.2	Maddah, 2013	21
3.3	λ_{max} determination	22
3.3.1	Fatigue Load Models	22
3.3.2	Real traffic data	23
3.3.3	Adopted criterion	23
4	λ_{max} calibration procedure	25
4.1	Influence lines	26
4.2	Slopes $m k$ Wöhler curve	27
4.2.1	Slopes $m k = 3 5$	27
4.2.2	Slopes $m = 3$	27
4.2.3	Slopes $m k = 4 6$	28
4.2.4	Slopes $m = 5$	28
4.2.5	Slopes $m k = 5 9$	29
4.3	Fatigue Load Model 3	29
4.3.1	Comparison - 1 or 2 lorries FLM3	30
4.4	Real Traffic Model	31
4.4.1	Fatigue Load Model FLM4	31
4.4.2	Weight In Motion (WIM)	33
4.4.3	Comparison of real traffic models on λ_{max}	37
4.5	Dynamic amplification factor	39

4.5.1	Relevance of dynamic consideration	39
4.5.2	Dynamic amplification in Load models	42
4.5.3	Dynamic amplification factor for λ curves determination	43
5	Analysis of the results	46
5.1	Final parameters for the λ_{max} curves	46
5.1.1	Spans length	46
5.1.2	Critical length L_λ	46
5.2	λ_{max} results	47
5.2.1	A16, Netherland	47
5.2.2	Switzerland	50
5.2.3	Sweden	52
5.3	λ_{max} results comparison	54
5.3.1	λ_{max} corrected results - mid-span moment	55
5.3.2	λ_{max} corrected results - support moment	55
5.3.3	λ_{max} corrected results - mid-span shear	57
5.3.4	λ_{max} corrected results - intermediate shear	57
5.3.5	λ_{max} corrected results - support shear	57
5.4	λ_{max} curves proposition	58
5.4.1	λ_{max} proposition - mid-span moment	58
5.4.2	λ_{max} proposition - support moment	59
5.4.3	λ_{max} proposition - mid-span shear force	59
5.4.4	λ_{max} proposition - support shear force and reaction	60
5.5	Comparison with current eurocode curves	60
5.5.1	Mid-span bending moment	60
5.5.2	Support bending moment	61
5.5.3	Mid-span shear force	61
5.5.4	Support shear force and reaction	62
5.6	New λ_{max} curves	63
5.7	Effects of the slopes of the Wöhler curve	65
5.7.1	Comparison for concrete bridge decks - reinforcing steel	68
5.8	λ_1 and λ_{max} - possible update to EN 1993-2	70
6	Conclusions	71
6.1	Future works	73

List of Figures

- 1.1 λ_{max} factor computation procedure 1
- 2.1 Possible location of fatigue cracks in a road bridge, (extracted from [5]) 3
- 2.2 Stress range definition and effect of residual stress, (extracted from [5]) 4
- 2.3 Fatigue crack evolution phases, (extracted from [5]) 5
- 2.4 Fatigue resistance according to the detail category | m=3, k=5, (extracted from [5]) 6
- 2.5 common FAT detail categories for steel structures assemblies, (extracted from [24]) 7
- 2.6 Fatigue Load Model 3 - axles configuration, (extracted from [18]) 9
- 2.7 Fatigue Load Model 3 - configuration with second lorry, (extracted from [13]) 9
- 2.8 Damage equivalence factor λ_1 calculation procedure, (extracted from [3]) 10
- 2.9 λ_1 for bending moment in road bridges, (extracted from [20]) 11
- 2.10 λ_{max} for bending moment in road bridges, (extracted from [20]) 13
- 2.11 Location of mid-span or support section, (extracted from [20]) 14
- 3.1 Determination of λ_{max} , (adapted from [8]) 15
- 3.2 λ_{max} for moments for road bridges, (extracted from [10]) 16
- 3.3 Auxerre traffic model - percentage of type of lorries, (extracted from [8]) 16
- 3.4 Justification for Auxerre traffic choice as basis for the European traffic loading model, (extracted from [8]) 17
- 3.5 Reduction of Auxerre traffic to 4 vehicles types and distribution to lane 1 and lane 2, (extracted from [8]) 17
- 3.6 Auxerre model - Distribution of vehicle weight, (extracted from [8]) 18
- 3.7 Approximation of distribution as measured by normal distributions, (extracted from [8]) 18
- 3.8 Statistical data of lorry traffic at Auxerre after filtering out dynamic effects, (extracted from [8]) 19
- 3.9 Distribution of vehicle loads on axles and of distances between axles, (extracted from [8]) 19
- 3.10 Comparison with previous simulations - mid-span moment DLT 1 20
- 3.11 Comparison with previous simulations - support moment DLT 3 20
- 3.12 Schematic diagram for acceptance of 1% of the total damage, (extracted from [1]) 21
- 3.13 Comparison of the reduction of maximal stress range on λ_{max} , (extracted from [1]) 21
- 3.14 λ_{max} obtained for Götthard main road traffic with PHV = 25%, (extracted from [1]) 22
- 3.15 Diagram for acceptance of 1% of the total damage, (adapted from [9]) 23
- 3.16 Total Damage when determining λ_{max} with 1% relative damage above CAFL 23
- 3.17 Total Damage when determining λ_{max} with 1% relative damage above CAFL 24
- 3.18 Analysis of tests on full scale welded cover plates: (a) CA test data and average regression curve using a random fatigue limit model; (b) VA test data versus damage calculated with the average regression curve for CA data, extracted from [14] 24
- 4.1 λ_{max} factor computation procedure 25
- 4.2 Static systems for the recalibration of λ_{max} 26
- 4.3 set of influence lines 26
- 4.4 Fatigue strength curve - mk = 3|5 27
- 4.5 Fatigue strength curve - m = 3 27
- 4.6 Fatigue strength curve - mk = 4|6 28
- 4.7 Fatigue strength curve - m = 5 28
- 4.8 Fatigue strength curve - mk = 5|9 29
- 4.9 Comparison with simplified FLM3 - mid-span moments 30
- 4.10 Comparison with simplified FLM3 - support moments 30

4.11 Fatigue Load Model 4, extracted from [18]	31
4.12 Inter-vehicle distribution free-flowing and congested, extracted from [2]	32
4.13 Influence of light vehicles, 3S-MM and 3S-SM	32
4.14 A16 WIM traffic 2018	33
4.15 proposed "European lorry" based on WIM A16 database, extracted from [14]	34
4.16 Sweden WIM Traffic 2002-2009	34
4.17 Löddeköpinge WIM Traffic 2009	35
4.18 Gotthard WIM Traffic 2019	35
4.19 Ceneri WIM Traffic 2019	36
4.20 Denges WIM Traffic 2019	36
4.21 λ_{max} comparison real traffic model	37
4.22 Total Damage - comparison real traffic model	38
4.23 Effects of the stress histogram repartition	38
4.24 Vehicle vibration model, extracted from [8]	39
4.25 Power spectral density of roadway roughness, extracted from [8]	40
4.26 classification of roadway roughness, extracted from [8]	40
4.27 Stochastic unevenness profile, extracted from [8]	40
4.28 Comparison of time-histories for speeds of 15 km/h (L) and 65 km/h (R), extracted from [8]	41
4.29 Dynamic increments of moment as a function of the fundamental frequency, extracted from[8]	41
4.30 Dynamic increments of moment as a function of the fundamental frequency, extracted from[8]	41
4.31 Dynamic increments of moment for convoy of vehicles, extracted from[8]	42
4.32 Dynamic factor in weight measurements, extracted from[8]	42
4.33 Impact factor for local irregularities, extracted from[8]	43
4.34 Additional amplification factor near expansion joints, extracted from [16]	43
4.35 Cross section of the bridge and influence lines (validation test in Dutch A16), extracted from [14]	44
4.36 Measured and calculated bridge response in validation test in Dutch A16, extracted from [14]	44
4.37 Stress ranges histogram using strain gauges and WIM measurements, extracted from [14]	45
4.38 Weekly damage for $\Delta\sigma_D = 59$ MPa, extracted from [14]	45
5.1 λ_{max} curves for mid-span(L) and intermediate bending moment(R)	47
5.2 λ_{max} curves for support bending moment(L) and support shear(R)	47
5.3 λ_{max} curves for mid-span shear(L) and intermediate shear(R)	48
5.4 λ_{max} for mid-span (L) and support bending moments(R) - A16, Netherlands	49
5.5 λ_{max} for shear forces - A16, Netherlands	49
5.6 λ_{max} for mid-span bending moments - Switzerland	50
5.7 λ_{max} for support bending moments - Switzerland	50
5.8 λ_{max} results for mid-span(L) and intermediate shear forces(R) - Switzerland	51
5.9 λ_{max} results for support shear force - Switzerland	51
5.10 λ_{max} for mid-span bending moments - Sweden	52
5.11 λ_{max} for support bending moments - Sweden	52
5.12 λ_{max} results for mid-span(L) and intermediate shear forces(R) - Sweden	53
5.13 λ_{max} results for support shear force - Sweden	53
5.14 λ_{max} comparison for WIM measurements	54
5.15 λ_{max} results for mid-span moment corrected with $N_0 = 500'000$ (L) and $N_0 = 2'000'000$ (R)	55

5.16	λ_{max} results for support moment corrected with $N_0 = 500'000$ (L) and $N_0 = 2'000'000$ (R)	56
5.17	Typical 7-axles lorry from swedish WIM measurement	56
5.18	comparison 5-axle and 7-axle lorry	56
5.19	λ_{max} results for mid-span shear corrected with $N_0 = 500'000$ (L) and $N_0 = 2'000'000$ (R)	57
5.20	λ_{max} results for intermediate shear corrected with $N_0 = 500'000$ (L) and $N_0 = 2'000'000$ (R)	57
5.21	λ_{max} results for support shear corrected with $N_0 = 500'000$ (L) and $N_0 = 2'000'000$ (R)	57
5.22	λ_{max} fitting curve for mid-span moment corrected with $N_0 = 500'000$ (L) and $N_0 = 2'000'000$ (R)	58
5.23	λ_{max} fitting curve for support moment corrected with $N_0 = 500'000$ (L) and $N_0 = 2'000'000$ (R)	59
5.24	λ_{max} fitting curve for mid-span shear corrected with $N_0 = 500'000$ (L) and $N_0 = 2'000'000$ (R)	59
5.25	λ_{max} fitting curve for support shear force and reaction corrected with $N_0 = 500'000$ (L) and $N_0 = 2'000'000$ (R)	60
5.26	Mid-span moment - λ_{max} fitting curve comparison(L) and gap to confidence interval comparison(R)	60
5.27	Support moment - λ_{max} fitting curve comparison(L) and gap to confidence interval comparison(R)	61
5.28	Mid-span shear - λ_{max} fitting curve comparison(L) and gap to confidence interval comparison(R)	62
5.29	Support shear - λ_{max} fitting curve comparison(L) and gap to confidence interval comparison(R)	62
5.30	λ_{max} final curves	63
5.31	λ_{max} comparison for different slopes of the fatigue strength curve	65
5.32	Comparison of $\Delta\sigma_C$ for various slopes $m k$	66
5.33	λ_{max} corrected for $m=5$ (L) $m k=4 6$ (R)	67
5.34	Comparison with EN 1992-2 [19] for reinforcing steel - in span verification	68
5.35	Comparison with EN 1992-2 [19] for reinforcing steel - support area	69
5.36	λ_1 and λ_{max} curves	70
6.1	λ_{max} final curves - bending moments	71
6.2	λ_{max} final curves - shear forces	72

List of Tables

4.1	WIM characteristics	37
5.1	λ_2^* factor for $N_0 = 500'000$ and $N_0 = 2'000'000$ heavy vehicles	55
5.2	λ_{max} curves equations	63
5.3	λ_{max} curves parametric equations	64
5.4	λ_{max} curves parameters	64
5.5	Comparison of fatigue strength curves	66

List of Symbols

Capital Letters

D_{CAFL}	Damage above CAFL
D_{tot}	Total damage
E_d	Design value of the effects of fatigue actions
L_λ	Critical length
M	Bending moment
N	Number of cycles
N_j	Number of lorries per year on lane j
N_{obs}	Number of lorries per year on the slow lane
Q_0	Average weight of the model
Q_{fat}	Fatigue Load Model
Q_i	Average weight of the considered lorries
Q_{m1}	Average weight of the lorries in the slow lane
Q_{mj}	Average weight of lorries on lane j
R_d	Design value of the resistance
R_{fat}	Fatigue resistance

Letters

d_0	Mean distance between vehicles
d_m	Modal distance between vehicles
d_{max}	Maximum distance between vehicles
d_{min}	Minimum distance between vehicles
j	Number of lanes subjected to heavy traffic
k	Fatigue resistance curve slope
m	Fatigue resistance curve slope
n_i	Number of lorries considered
t_{Ld}	Bridge design life
t_{ref}	Standard design life
v	Vehicle speed

Abbreviations

CAFL	Constant Amplitude Fatigue Limit
COL	Cut-Off Limit
DAF	Dynamic Amplification Factor
EN	European Norm
FAT	Equivalent stress
FLM	Fatigue Load Model
MM	Mid-span Bending Moment
MV	Mid-span Shear
SM	Support Bending Moment
SV	Support Shear
WIM	Weight in Motion

Greek Letters

α	Coefficient for traffic flow conditions
β	Coefficient for traffic flow conditions
γ_{Ff}	Fatigue action effects safety factor
γ_{Mf}	Fatigue strength safety factor
$\Delta\sigma$	Stress range
$\Delta\sigma_C$	Fatigue strength at 2 millions cycles
$\Delta\sigma_D$	Fatigue strength at 5 million cycles
$\Delta\sigma_L$	Fatigue strength at 100 million cycles
$\Delta\sigma_{E,2}$	Equivalent direct stress range at 2 million cycles
λ	Damage equivalence factor
λ_1	Partial factor for the damage effect of traffic
λ_2	Partial factor for the traffic volume
λ_3	Partial factor for the design life
λ_4	Partial factor for the traffic on other lanes
λ_{max}	Maximum damage equivalent factor
σ_{max}	Maximum stress
σ_{min}	Minimum stress
σ_{res}	Residual stress

1 Introduction

1.1 Motivation

Fatigue is a key issue in the design and verification of road bridges. Repeated cycling loading as road traffic can have a negative impact on the durability of structures. This thesis proposes improvements to the simplified method for fatigue verification with the lambda correction factors. The lambda correction factors are damage equivalent factors to be used with the fatigue load model 3 (FLM3). These factors are intended to calibrate the fatigue load from load model with real effects of traffic.

The lambda curves in the current standards need to be revised to be in line with the current European traffic. Indeed, the European standards are based on 30 year old traffic models which not necessarily represents the current trends. It is therefore required to evaluate and update the lambda values defined in the current standards.

The aim of the thesis is the work on the recalibration of the lambda factors, focusing in particular on the λ_{max} factor. For this purpose, current European traffic is evaluated through numerical simulations to determine an update to the λ_{max} factor. In order to assess present traffic, the use of Weight in Motion (WIM) measurements is part of the development of the new λ_{max} curves. This allows a variety of European road traffic to be assessed and compared with the fatigue models described in the standards. The new numerical simulations, which procedure is defined in 4.1, are based on a much larger number of influence lines and aim to define lambda values for spans up to 200m as opposed to 80m.

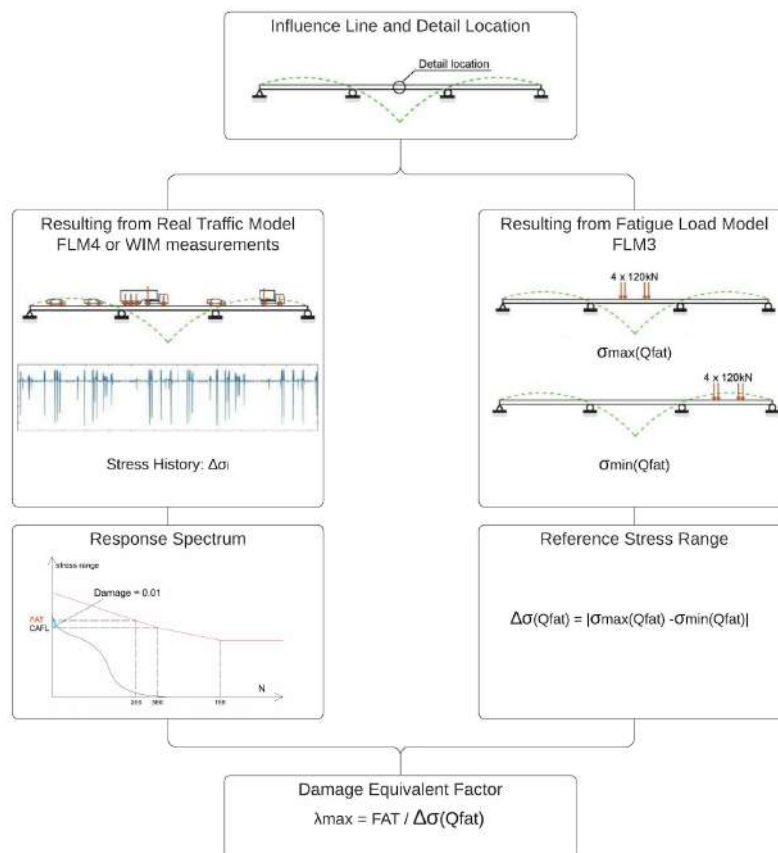


Figure 1.1. λ_{max} factor computation procedure

1.2 Thesis Outline

This thesis is divided in 6 chapters, with the following contents:

- **Chapter 1 - Introduction**
- **Chapter 2 - Basic concepts of fatigue design** This chapter describes the basic concepts used in the following sections of the thesis, including an overview of fatigue strengths and possible verification methods. The simplified method with lambda factors that needs to be recalibrated is also described in detail.
- **Chapter 3 - Previous simulations and λ_{max} factor determination** This chapter examines the previous simulations that were determined in particular for the development of the current European curves. In addition, the second part of the chapter focuses on the criterion that should be used for the determination of λ_{max} .
- **Chapter 4 - λ_{max} calibration procedure** The method of calibration of the new lambda curves and the various parameters used are described in detail in this chapter. The main parameters include the influence lines, the resistance curves and the traffic models used.
- **Chapter 5 - Analysis of the results** The chapter analyses the results of the numerical simulations, especially for the traffic from the WIM measurements. This section compares the λ_{max} results obtained for the different traffic types and proposes new lambda curves which are also compared to the current λ_{max} curves defined in the standards.
- **Chapter 6 - Conclusions** The chapter summarises the various aspects studied and includes the new λ_{max} curves.

2 Basic concepts of fatigue design

The fatigue phenomenon occurs when a member is subjected to repeated cycling loadings such as road traffic. This phenomenon is part of the main causes of damages in steel structures, together with corrosion and wear. Fatigue damage is manifested by the propagation of cracks and results in a loss of resistance over time. It rarely occurs in base materials, but rather in assemblies, which remain the critical location when fatigue loading is checked. It has been demonstrated that geometrical changes, discontinuities and stress concentrations affect the formation and propagation of cracks.

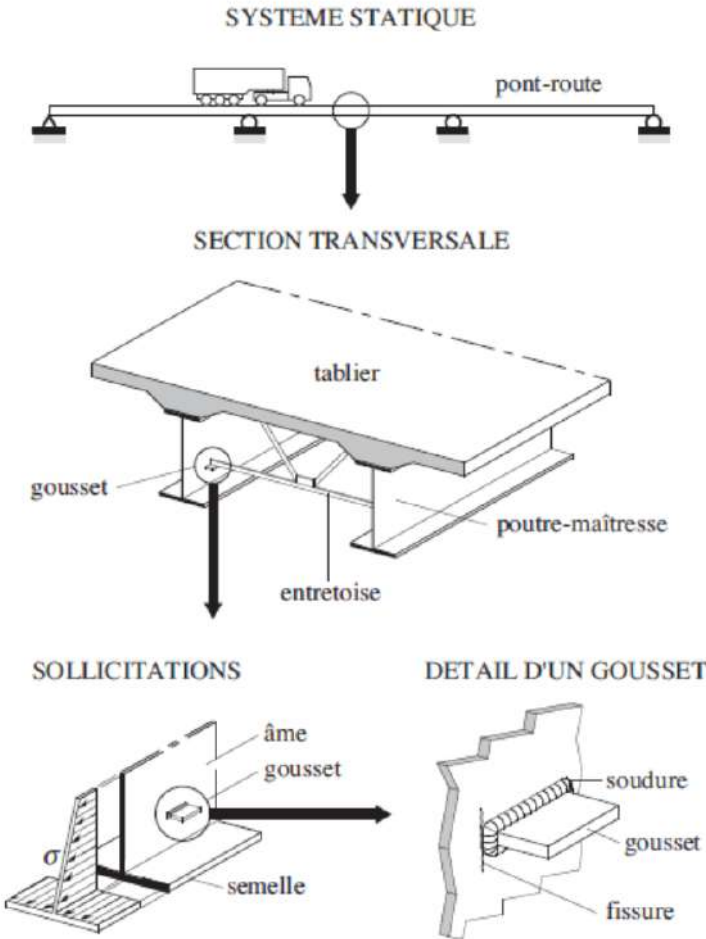


Figure 2.1. Possible location of fatigue cracks in a road bridge, (extracted from [5])

The combined effect of anomalies and stress concentrations can be the source of fatigue crack formation and propagation, even if the applied stresses remain well below the yield point. This crack propagation can lead to yielding or brittle failure. For this reason, the design and fabrication of a structure subjected to repeated variable loads must be done with care in the design and fabrication of the elements and construction details, in order to avoid brittle failure.

2.1 Fatigue Resistance

2.1.1 Parameters influencing the service life

The service life of a member or a construction detail subjected to cycling loading is defined as the number of stress cycles supported until failure. The fatigue strength can be influenced by 4 main parameters:

- stress range
- the geometry of assemblies
- material properties
- environmental impacts

Stress range - $\Delta\sigma$ is the most determinant parameter for assemblies. The stress range is defined as:

$$\Delta\sigma = \sigma_{max} - \sigma_{min} \quad (1)$$

- σ_{max} : maximal stress value
- σ_{min} : minimal stress value

Other parameters such as maximum stress, minimum stress or cycle frequency are less decisive than the applied stress range. Furthermore we might think that compressive stresses could be beneficial to increase the service life of the element, but this is often not the case, especially for welded elements. This is because of the tensile residual stresses σ_{res} introduced during welding. The effect of the residual stresses is shown in figure 2.2 :

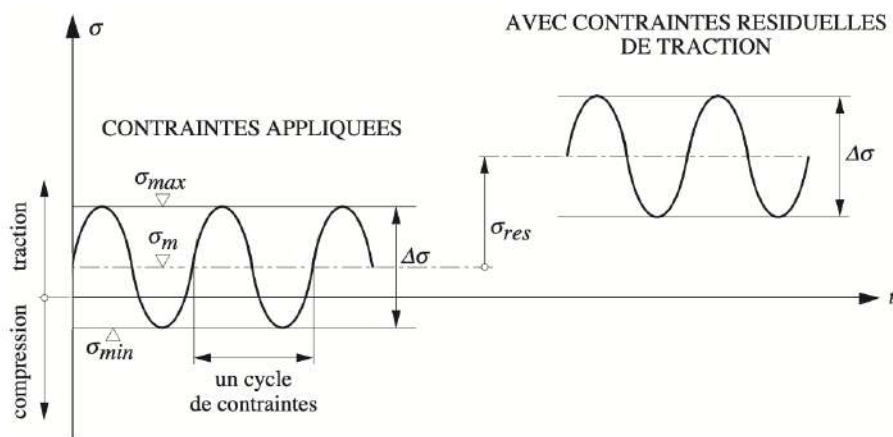


Figure 2.2. Stress range definition and effect of residual stress, (extracted from [5])

Geometry of assemblies - is decisive for the location of the fatigue crack and for its propagation speed. These factors are therefore directly related to the service life. The categories of geometric influence are:

- The effect of the structure geometry
- The effect of stress concentrations
- The effect of weld faults

These effects can be positively influenced by a good conception. A well designed detail means that we avoid abrupt changes in the geometry in order to reduce stress concentrations. As far as weld defects are concerned, these can be avoided by using proper manufacturing and inspection methods which will greatly reduce the risks associated with fatigue loading.

Material properties - It has been observed in many sample test that the chemical composition, mechanical properties and microscopic structures can have a good influence on the service life of members, in particular through an increase in the crack initiation phase. For welded elements, as the service life is mainly governed by the propagation phase, the benefits of the chemical properties are less determinant as they only affect the crack initiation phase. The phases of crack evolution are represented in figure 2.3

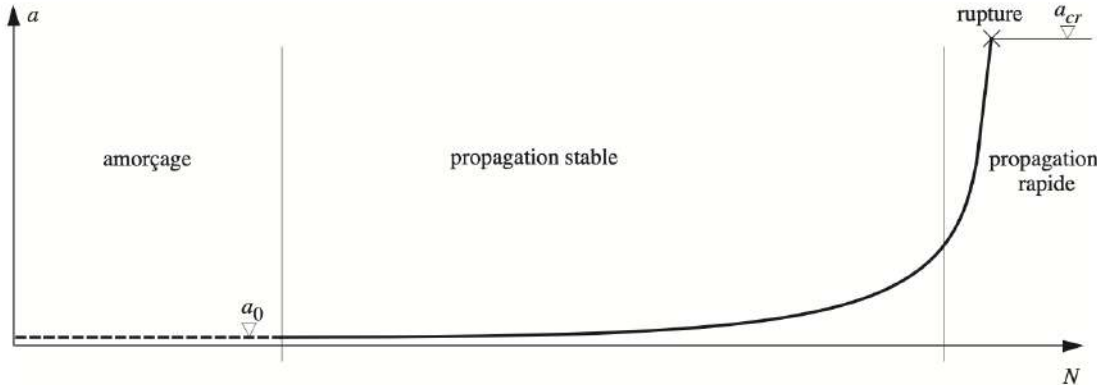


Figure 2.3. Fatigue crack evolution phases, (extracted from [5])

Environmental impacts - As with many other characteristics, the environment can also have an influence on the service life. A damp and corrosive environment can have a major influence, as it can increase the speed of crack propagation. Therefore, for certain situation with aggressive environment, it is necessary to consider and to provide adequate protection of the steel elements. Surface corrosion, on the other hand, has practically no influence on the service life. Indeed, surface corrosion remains less critical than original defects in welded assemblies.

2.2 Fatigue strength curve

In order to know the fatigue resistance of steel structures, standardised resistance curves have been established in European construction standards on the basis of a large number of tests. The results are represented in a diagram in which we find, on the y-axis, the stress range $[\Delta\sigma_R]$ and, on the x-axis, the number of cycles $[N]$ observed until failure. These curves can be seen in figure 2.4, according to the detail category.

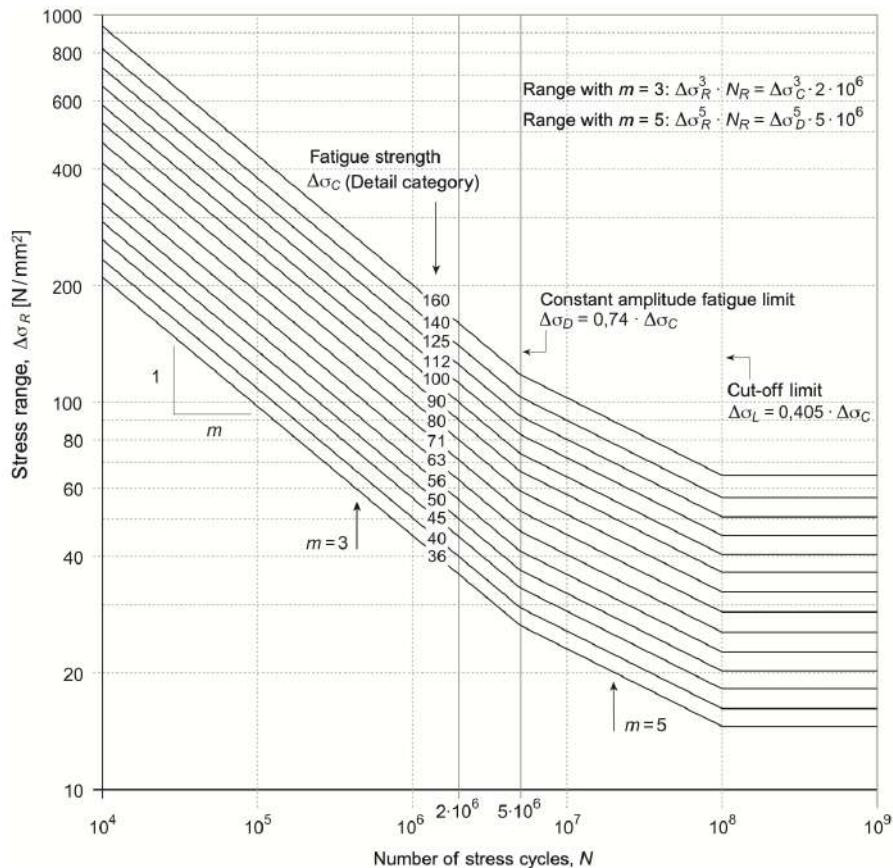


Figure 2.4. Fatigue resistance according to the detail category | $m=3$, $k=5$, (extracted from [5])

- N : Number of cycles [-], m, k : slopes of the curve
- $\Delta\sigma_C$: resistance for the category of detail [MPa]
- $\Delta\sigma_D$: constant amplitude fatigue limit CAFL [MPa]
- $\Delta\sigma_L$: cut-off limit COL [MPa]

The resistance curves are each defined by their reference value $\Delta\sigma_C$ which corresponds to a value of $2 \cdot 10^6$ cycles. This value $\Delta\sigma_C$ indicates that a detail with this resistance resists a stress difference equal to $\Delta\sigma_C$ during $2 \cdot 10^6$ cycles until failure. The constant amplitude fatigue limit, $\Delta\sigma_D$, is where the slope of the curve changes from m to k and corresponds to a number of cycles of $5 \cdot 10^6$. The truncation limit, which corresponds to $1 \cdot 10^8$ cycles, represents the limit below which the effect of stresses can be neglected for the calculation of the cumulative damage.

The type of detail are classified according to the type of connections and their geometry. The classification of details can be found in the EN 1993-1-9, such an example is represented in the figure 2.5.

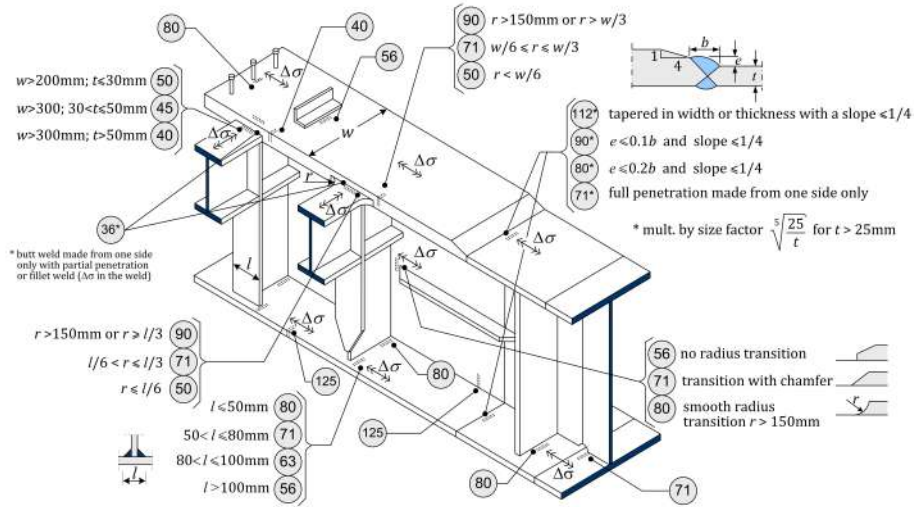


Figure 2.5. common FAT detail categories for steel structures assemblies, (extracted from [24])

2.3 Fatigue safety verification

Fatigue verification is a complementary verification to structural safety check, which can be done in a similar way. Generally, we can express:

$$E_d \leq R_d = \frac{R_{fat}}{\gamma_{Mf}} \quad (2)$$

- E_d : design value of the effects of fatigue actions
- R_d : design value of the resistance
- R_{fat} : fatigue resistance
- γ_{Mf} : fatigue resistance safety factor

The equation 2 can be verified with 3 different methods, that are presented below.

2.3.1 Verification with the fatigue limit

The first verification method remains the simplest and most conservative. Indeed, this verification only takes into account the maximum stress difference. On the basis of tests, it has been shown that the service life of a construction detail tends towards infinity when the stress differences remain below the fatigue limit $\Delta\sigma_D$. Based on this principle, the following relationship can be expressed:

$$\gamma_{Ff} \cdot \Delta\sigma_{i,max} \leq \frac{\Delta\sigma_D}{\gamma_{Mf}} \quad (3)$$

- γ_{Ff} : partial load factor, usually 1.0 [-]
- γ_{Mf} : fatigue resistance factor, 1.0 to 1.35 according to the failure consequences [-]
- $\Delta\sigma_{i,max}$: maximum stress range of the stress histogram [MPa]
- $\Delta\sigma_D$: constant amplitude fatigue limit CAFL [MPa]

This verification method is intended to be conservative as it provides long service life to the element subjected to cycling loading. Moreover it is also very sensitive to future increases in stresses as this could lead to stress ranges above the fatigue limit.

2.3.2 Verification with the cumulative damage

The cumulative damage method is different and allows to take into account the whole stress histogram, instead of the maximum value. The cumulative damage is based on a linear accumulation which is sequence independent. Starting from the following damage accumulation expression:

$$D_{tot} = \sum_{i=1}^k n_i \cdot d_i \leq D_{lim} = 1.0 \quad (4)$$

- D_{tot} : Total Damage [-]
- n_i : number of cycles applied for the stress range $\Delta\sigma_i$ [-]
- d_i : Damage due to a single cycle of stress range $\Delta\sigma_i$ [-]

For the verification, it is possible to compute the equivalent stress range $\Delta\sigma_{E,2}$, which correspond to $2 \cdot 10^6$ cycles, from the cumulative damage in order to obtain a single stress level which is a sort of weighting of all the stress ranges of the histogram. The following relationship is then used for verification:

$$\gamma_{Ff} \cdot \Delta\sigma_{E,2} \leq \frac{\Delta\sigma_c}{\gamma_{Mf}} \quad (5)$$

- $\Delta\sigma_{E,2}$: equivalent stress value corresponding to $2 \cdot 10^6$ cycles [MPa]
- $\Delta\sigma_c$: fatigue resistance of the detail [MPa]
- γ_{Ff} : partial load factor, usually 1.0 [-]
- γ_{Mf} : fatigue resistance factor, 1.0 to 1.35 according to the failure consequences [-]

2.3.3 Verification with the lambda factor

Since cumulative damage method is rather complicated and requires a large number of calculations, a simplified verification method has been established in order to carry out a fast and efficient calculation while satisfying fatigue safety. Approach is to calculate the maximum and minimum stresses using a load model defined in the standard. In order to obtain these stress values, it is simply a matter of placing the load at the most favourable (respectively the most unfavourable) location along the influence lines. It allows, in a first step, to determine the value of the stress range $\Delta\sigma(Q_{fat})$:

$$\Delta\sigma(Q_{fat}) = \sigma_{max}(Q_{fat}) - \sigma_{min}(Q_{fat}) \quad (6)$$

- $\Delta\sigma(Q_{fat})$: stress range according to the fatigue load Q_{fat} [MPa]
- $\sigma_{max}(Q_{fat})$: maximal stress obtained subjected to the load Q_{fat} [MPa]
- $\sigma_{min}(Q_{fat})$: minimal stress obtained subjected to the load Q_{fat} [MPa]

The load model used to calculate $\Delta\sigma(Q_{fat})$ is the FLM3 (Fatigue Load Model 3). This model consists of two 4-axle lorries, the first with a weight of 480 kN and the second with a weight of 144 kN. The inter-vehicle distance between the 2 lorries is at least 40 meters. In fact, the model was defined on the basis of traffic data from Auxerre damage equivalent load for single axle, tandem axle and for the vehicle

(see [8]). The first lorry FLM3 has been set with very close loads to these damage equivalent loads. As explained in [8], the single axle load of 120 kN corresponds to the most damaging single load of 131 kN, the tandem load of 240 kN is close to the tandem most damaging load of 252 kN and the vehicle load of 480 kN is approximately equal to the vehicle damage equivalent load of 469 kN. The addition of the second lorry FLM3 was necessary, as it was found that the single vehicle model underestimated the moment compared to the Auxerre traffic in some cases, especially for the support moment on a beam. The model was therefore adjusted to remain safe in all cases. The load is therefore distributed between the axles with the spacings described in figures 2.6 and 2.7:

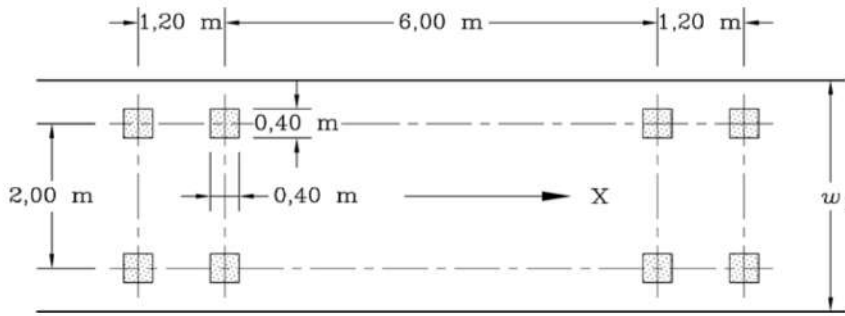


Figure 2.6. Fatigue Load Model 3 - axles configuration, (extracted from [18])

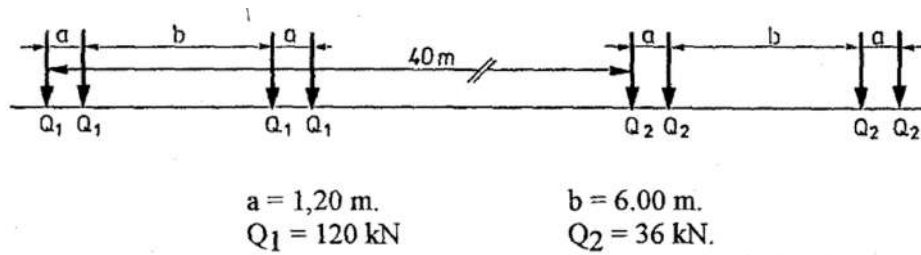


Figure 2.7. Fatigue Load Model 3 - configuration with second lorry, (extracted from [13])

Once the fatigue stress range $\Delta\sigma(Q_{fat})$ is set, the following expression which incorporates the correction factor λ is used:

$$\Delta\sigma_{Ed,2} = \lambda \cdot \gamma_{Ff} \cdot \Delta\sigma(Q_{fat}) \leq \frac{\Delta\sigma_c}{\gamma_{Mf}} \quad (7)$$

- $\Delta\sigma_{E,2}$: equivalent stress value corresponding to $2 \cdot 10^6$ cycles [MPa]
- $\Delta\sigma(Q_{fat})$: stress range according to the fatigue load Q_{fat} [MPa]
- $\Delta\sigma_c$: fatigue resistance of the detail [MPa]
- γ_{Mf} : fatigue resistance factor, 1.0 to 1.35 according to the failure consequences [-]
- γ_{Ff} : partial load factor, usually 1.0 [-]
- λ : damage equivalence factor

This verification is very simple to perform as it only requires a quick static calculation based on the influence lines and using the λ factors associated with the analyzed case.

The correction factor λ depends on the static system, the location of the construction detail, the operating loads, the traffic volume, the expected service life as well as the fatigue strength curves. The correction factor λ can then be broken down into partial correction factors λ_i :

$$\lambda = \lambda_1 \cdot \lambda_2 \cdot \lambda_3 \cdot \lambda_4 \quad \text{with} \quad \lambda \leq \lambda_{max} \quad (8)$$

However, to establish this simplified fatigue check for the convenience of engineers, it was necessary to realistically determine the λ correction factors and to calibrate them to obtain an efficient result with the λ factor method. The calibration method that was used and that is the subject of this thesis is the method described in the figure 2.8.

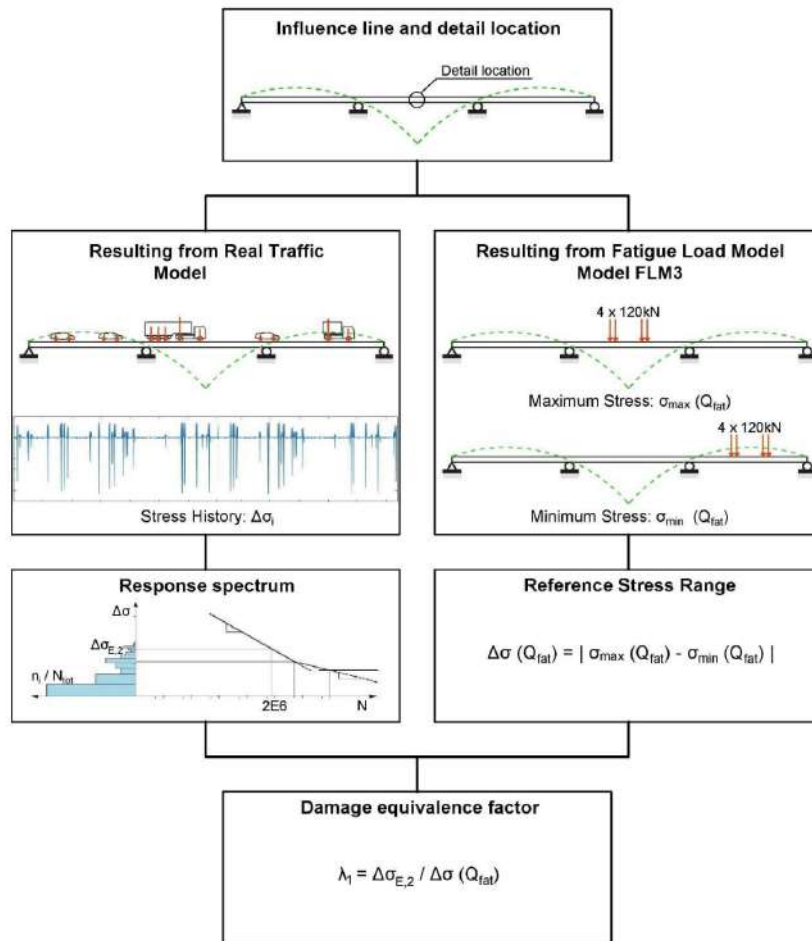


Figure 2.8. Damage equivalence factor λ_1 calculation procedure, (extracted from [3])

In the figure above, the procedure is described for the correction factor λ_1 . The procedure contains two parallel calculations. On one hand, the computation of $\Delta\sigma(Q_{fat})$ with the Fatigue Load Model 3 (FLM3). On the other hand, the calculation with the cumulative damage method for real traffic model. The cumulative damage method therefore considers the entire stress histogram. To obtain the value of the equivalent stress $\Delta\sigma_{Ed,2}$, the algorithm shifts the fatigue strength curve vertically until the total damage due to the stress histogram equals 1.0. The λ_1 factor is the fraction between these 2 values, it is the factor between the stress range from the Fatigue Load Model 3 and the real damage effects of traffic.

$$\lambda = \frac{\Delta\sigma_{Ed,2}}{\Delta\sigma(Q_{fat})} \quad (9)$$

2.4 The λ correction factor

As mentioned previously, the λ factor consists of 4 partial correction factors :

$$\lambda = \lambda_1 \cdot \lambda_2 \cdot \lambda_3 \cdot \lambda_4 \quad \text{with} \quad \lambda \leq \lambda_{max} \quad (10)$$

- λ_1 is the factor for the damage effect of traffic and depends on the length of the critical influence line or area
- λ_2 is the factor for the traffic volume
- λ_3 is the factor for the design life of the bridge
- λ_4 is the factor for the traffic on other lanes
- λ_{max} is the maximum possible λ -value taking account of the fatigue limit

2.4.1 λ_1 - Damage effect of traffic

The λ_1 factor represents the effect of traffic on the damage as a function of the equivalent span length. According to the Eurocode EN 1993-2 [20], two curves are described to determine the value of λ_1 . These curves defines the value λ_1 for span length going from 10m to 80m for both mid-span and support bending moment. These graphs are shown in the figure 2.9:

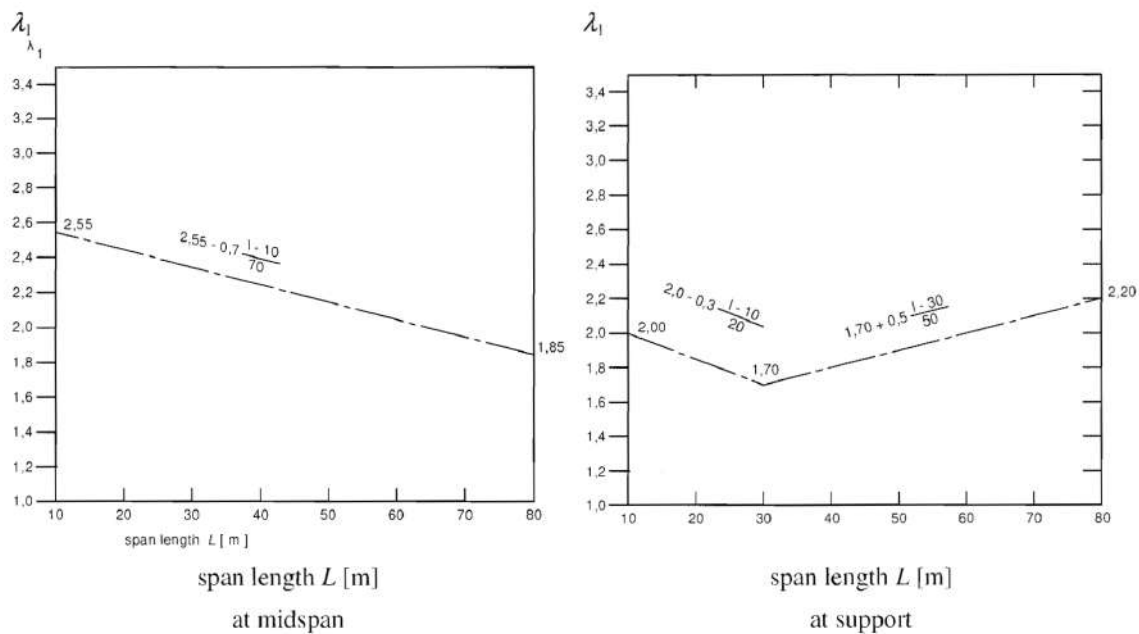


Figure 2.9. λ_1 for bending moment in road bridges, (extracted from [20])

2.4.2 λ_2 - Traffic volume

The λ_2 factor takes into account the volume of traffic, it is a function of the average weight of the lorries and the total annual number of lorries on the slow lane.

$$\lambda_2 = \frac{Q_{m1}}{Q_0} \cdot \left[\frac{N_{obs}}{N_0} \right]^{1/m} \quad (11)$$

- Q_{m1} : average weight of the lorries in the slow lane [kN]
- Q_0 : average weight of the model, equals 480 [kN]
- N_0 : number of lorries per year according to the model, equals $0.5 \cdot 10^6$ [-]
- N_{obs} : number of lorries per year on the slow lane [-]
- $m = 5$: slope of the fatigue strength curve [-]

Q_{m1} is obtained by :

$$Q_{m1} = \left[\frac{\sum n_i \cdot Q_i^m}{\sum n_i} \right]^{1/m} \quad (12)$$

- Q_i : average weight of the considered lorries [kN]
- n_i : number of considered lorries

2.4.3 λ_3 - Design life

The λ_3 factor takes into account the design life of the bridge, in comparison to the standard design life of 100 years.

$$\lambda_3 = \left[\frac{t_{Ld}}{t_{ref}} \right]^{1/m} \quad (13)$$

- t_{Ld} : design life of the bridge [years]
- t_{ref} : standard design life, equals to 100 [years]

2.4.4 λ_4 - Traffic on other lanes

In the case where there are several lanes of traffic on the road bridge, the factor λ_4 takes into account the traffic on the other lanes and thus the transverse distribution of stresses.

$$\lambda_4 = \left[1 + \frac{N_2}{N_1} \left(\frac{\eta_2 Q_{m2}}{\eta_1 Q_{m1}} \right)^m + \frac{N_3}{N_1} \left(\frac{\eta_3 Q_{m3}}{\eta_1 Q_{m1}} \right)^m + \dots + \frac{N_j}{N_1} \left(\frac{\eta_k Q_{mj}}{\eta_1 Q_{m1}} \right)^m \right]^{1/m} \quad (14)$$

- j : number of lane subjected to heavy traffic [-]
- N_j : number of lorries per year on lane j [-]
- Q_{mj} : average weight of lorries on lane j [kN]
- η_j : value of the influence line for the force producing the stress range at the middle of lane j (with positive sign) [-]. This allows the stress level to be adjusted by taking into account the transverse distribution in relation to the stress in the case of a single lane road bridge.

2.4.5 λ_{max} - Upper limit

The λ_{max} factor is the upper limit taking account of the fatigue limit. The values of λ_{max} are defined in Eurocode EN 1993-2 [20] in a similar way to the λ_1 factor for equivalent spans ranging from 10m to 80m. There are also 2 distinct curves, one for mid-span sections and one for support sections.

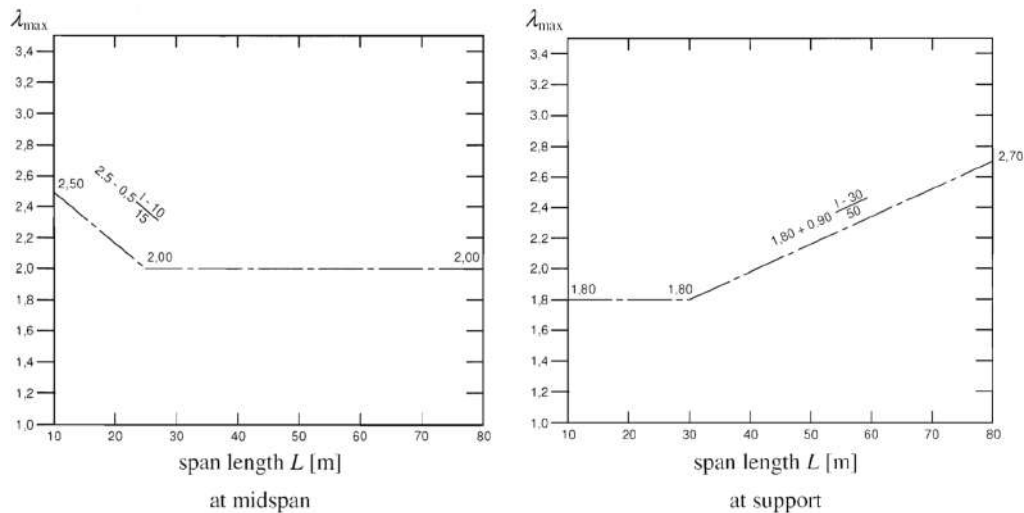


Figure 2.10. λ_{max} for bending moment in road bridges, (extracted from [20])

2.4.6 Fatigue critical length

To obtain the λ_1 and λ_{max} value from the graphs given in the Eurocode EN 1993-2 [20], the critical length need to be determined. To do so, the European norm gives indication for road bridges:

- for moments
 - for a simply supported span, the span length L_i
 - for continuous spans in mid-span sections, the span length L_i of the span under consideration
 - for continuous spans in support sections, the mean of the two spans L_i and L_j adjacent to that support
 - for cross girders supporting stringers, the sum of the two adjacent spans of the stiffeners carried by the cross girders
- for shear for a simply supported span and a continuous span
 - for the support section, the span under consideration L_i
 - for the mid-span section, 0.4 x the span under consideration L_i
- for reactions
 - for end support, the span under consideration L_i
 - for intermediate supports, the sum of the two adjacent spans L_i and L_j
- for arch bridges
 - for hangers, twice the distance between hangers
 - for arch, half the span of the arch

The Eurocode EN 1993-2 [20] gives also an indication to determine whether the section is considered as a mid-span or support section according to its location.

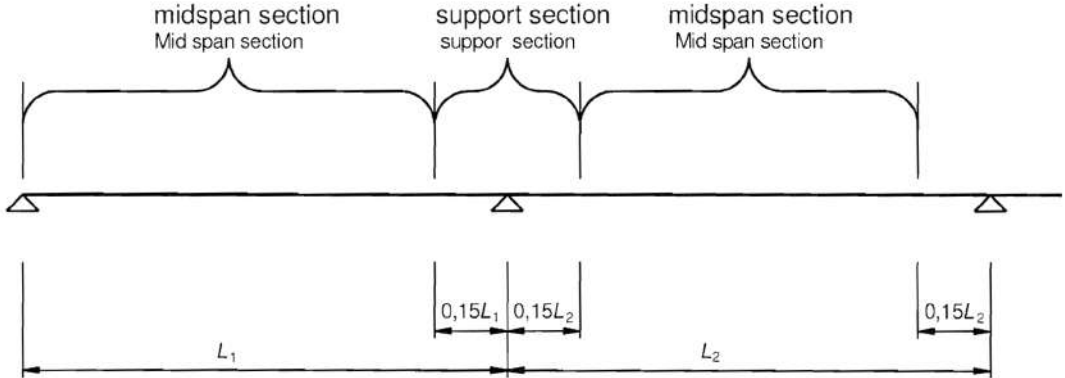


Figure 2.11. Location of mid-span or support section, (extracted from [20])

3 Previous simulations and λ_{max} factor determination

The λ_{max} factor, as introduced in the previous section, is an upper limit that the λ factor can take. This factor is intended to be a limit value that ensure "infinite life" of the considered element subjected to fatigue loads. λ_{max} is function of the maximum loads that can occur over the service life. To ensure, as it is called, an "infinite life", the concept is that the maximum stress ranges must remain under the constant amplitude fatigue limit (CAFL). In this case, it is assumed that the greatest stress cycles will not result in a crack initiation and therefore ensure a great safety over time. The figure 3.1 shows the determination of λ_{max} considering the stress histogram and the associated fatigue strength curve.

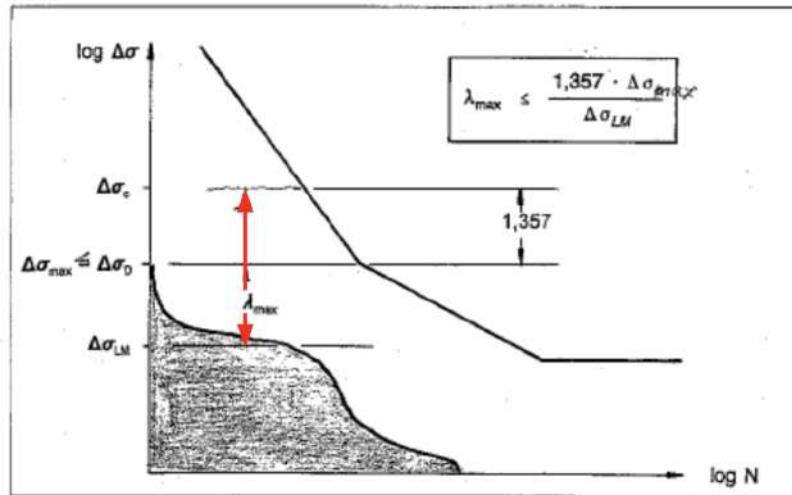


Figure 3.1. Determination of λ_{max} , (adapted from [8])

The category of resistance required to ensure that the maximum stress range remains under the CAFL can be determined with the stress histogram obtained for a real traffic model. Then the determination of λ_{max} is the ratio between the category $\Delta\sigma_C$ and the stress range $\Delta\sigma_{LM}$ issued from the fatigue load model. When using standard fatigue resistance curve with slopes $m|k = 3|5$, the proportion between the resistance category $\Delta\sigma_C$ and the constant amplitude fatigue limit is equal to:

$$\Delta\sigma_D = \Delta\sigma_C \cdot \left[\frac{N_D}{N_C} \right]^{1/m} = \Delta\sigma_C \cdot \left[\frac{5 \cdot 10^6}{2 \cdot 10^6} \right]^{1/3} = 1.357 \cdot \Delta\sigma_C \quad (15)$$

The λ_{max} factor can then be computed in function of the maximum stress range $\Delta\sigma_{max}$:

$$\lambda_{max} = \frac{\Delta\sigma_C}{\Delta\sigma_{LM}} \geq 1.357 \cdot \frac{\Delta\sigma_{max}}{\Delta\sigma_{LM}} \quad (16)$$

3.1 Sedlacek and Merzenich, 1995

To introduce current λ_{max} curves in EN 1993-2 [20], previous simulations from Sedlacek and Merzenich's work were performed. These numerical simulations date from 1995 and were published in Heft 711 [10]. At the time, the λ_{max} simulations only present results of 2 influence lines such as 3 spans - mid-span moment (DLT1) and 3 spans - support moment (DLT3). The computation is done for different traffic models such as Fatigue Load Model 1, Fatigue Load Model 2 and a real traffic model based on Auxerre traffic measurements. Moreover, for Auxerre traffic model, dynamic amplification factors have been applied according to various road surface quality. This allows the modelling of traffic on the influence line to be compared with the FLM1 and FLM2 models which are simplified representations of

frequent road traffic loads. The FLM1 and FLM2 models are described precisely for verification where the calculated stresses of these models must remain under the CAFL, similarly to the definition of the λ_{max} factor. The final simulations of Merzenich and Sedlacek are presented in figure 3.2.

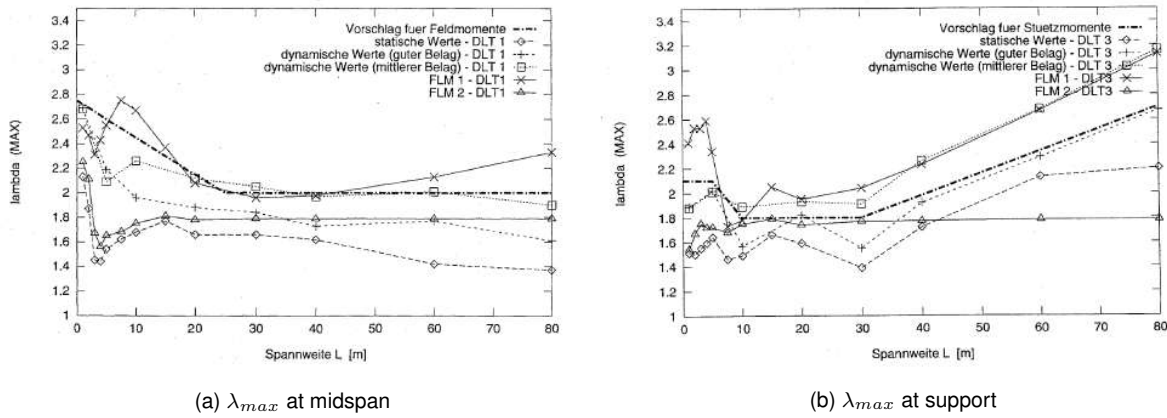


Figure 3.2. λ_{max} for moments for road bridges, (extracted from [10])

Sedlacek and Merzenich's λ_{max} simulations must surely be improved with actualised traffic parameters. The presented results in figure 3.2 use parameters such as: flowing traffic (no congested traffic or jam situations are considered), fixed distance of 50 meters between vehicles and no cars considered. These parameters are questionable, especially for the fixed inter-vehicle distance and the flowing traffic. Many unfavourable situations are not considered as the possibility of interaction between vehicles is greatly reduce. The influence of this key parameter is set aside in Sedlacek and Merzenich's simulations.

3.1.1 Traffic Model

Sedlacek and Merzenich's simulations used the Auxerre traffic data which was considered to be the heaviest traffic in Europe according to various traffic measurements across the continent. Further analysis allowed the modelling of real traffic to be compared with FLM1 and FLM2 models. Current λ_1 and λ_{max} curves of the Eurocodes are based on Auxerre traffic from 1986 which data were documented over a large time period on two slow lanes of a four-lane highway. The figure 3.3 present the percentage of lorry types obtained from various traffic measurement (Auxerre traffic distribution is highlighted).

	1	2	3	4	5	6	7	8	9	10
	CARONNE 1997 - 1977	NOTULIBAY 1977	AUXERREVILLE 1977	WALSCHTTE FORNIE 1980	BRIDEN 1980	LEHJENBERG JAN 1980	MOREN 1980	MANCHRETEK 1980	BO VERDE 1980	AUXERRE 1986
	F	F	F	NL	NL	D	GB	GB	I	F
	(2)	(2)	(2)	(2)	(2)	(2)	(1)	(1)	(1)	(2)
	49,2	57,2	39,2	80,3	52,1	41,3	89,1	94,1	58,1	22,7
	4,8	4,3*	3,5*	4,4*	6,1*	3,1	1,9	1,1	2,0	1,3
	-	-	-	-	-	-	1,0	-	-	-
	17,8	8,4	12,5	3,1	4,1	4,1	2,3	0,6	3,6	-
	22,6*	18,1*	28,5	4,6*	11,8	5,5	5,6*	3,7*	3,3	65,2
	-	0,8*	8,2	1,1	6,9*	5,4*	-	-	10,8	-
	-	5,0	-	0,3	1,2	2,7*	-	-	-	-
	-	-	-	0,5	1,2*	-	-	-	-	-
	3,4	5,7	3,7*	3,6	7,6	13,8	-	-	1,9	-
	-	-	-	0,3	1,4	6,9	-	-	-	10,8
	1,1	-	2,3	0,7	3,8	16,2	-	-	2,6	-
	0,4	-	-	-	-	-	-	-	4,2	-
Divers	0,6	0,5	2,1	1,4	5,2	1,0	0,1	0,5	16,8*	-

* véhicules déterminants pour les charges 1) tous véhicules 2) camions seuls

Figure 3.3. Auxerre traffic model - percentage of type of lorries, (extracted from [8])

The figure 3.4 shows the accumulated distribution of total vehicle loads and axle loads. n_{10} is the number of axle loads with $P_A \geq 10kN$ and n_{30} is the number of vehicles with $G \geq 30kN$. Once again the Auxerre traffic appears to be the most aggressive traffic observed from various traffic measurements.

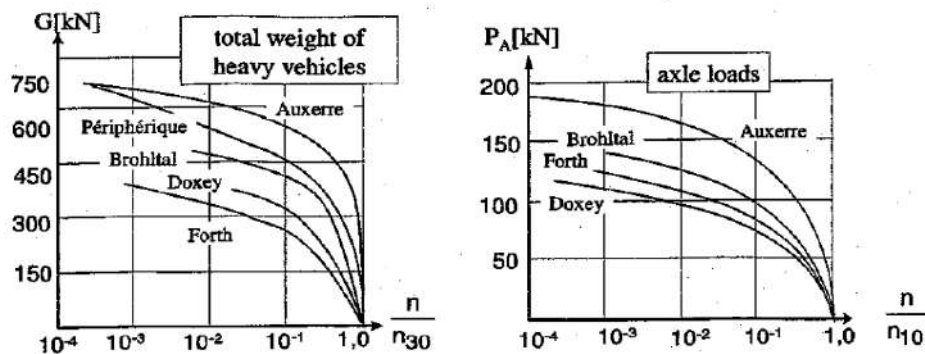


Figure 3.4. Justification for Auxerre traffic choice as basis for the European traffic loading model, (extracted from [8])

As explained in [8], Auxerre has been chosen as the reference location due to:

- The composition of the traffic corresponds to the estimation of future trends;
- The portion of lorries in the traffic composition is 32% in lane 1 and 10% in lane 2 and in relation to other locations rather high;
- The portion of loaded lorries from all lorries is 66% and hence mirrors the trend for an improved transport management;
- Data were fully documented for a large time period for lane 1 and lane 2 in a 4 lane-highway.

It was therefore for safety reasons and with a view to a possible increase in future trends that this traffic was chosen at the time. The Auxerre traffic has therefore been classified in order to model it. This classification made it possible to isolate 4 representative types of lorries as shown in figure 3.5. The distribution of these vehicles was also measured for lanes 1 and 2.

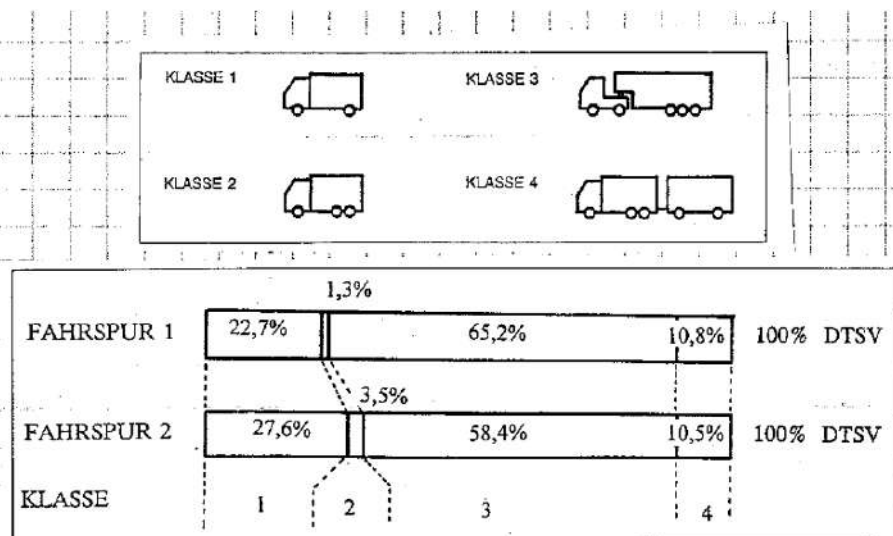


Figure 3.5. Reduction of Auxerre traffic to 4 vehicles types and distribution to lane 1 and lane 2, (extracted from [8])

For the four vehicle types determined, the figure 3.6 presents the weight distribution in order to best determine the traffic model that should be considered to represent the measured trends.

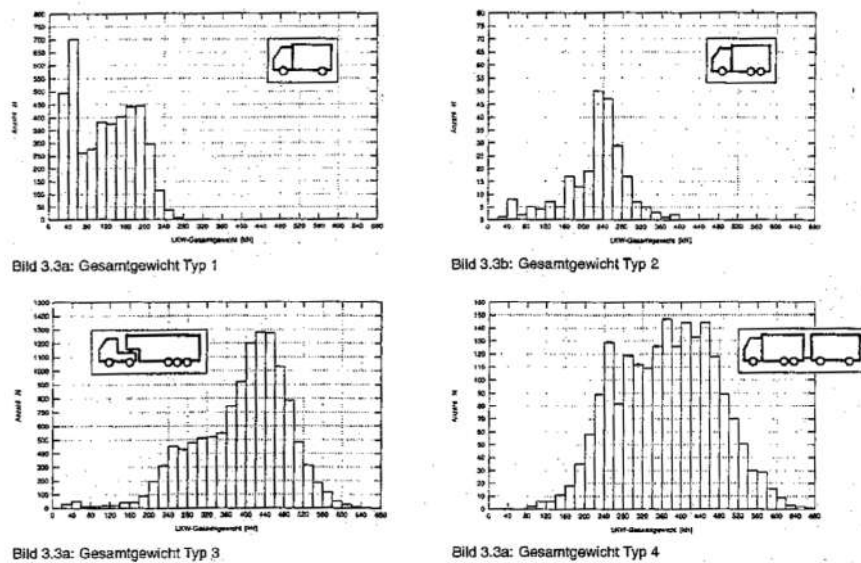


Figure 3.6. Auxerre model - Distribution of vehicle weight, (extracted from [8])

The best way to statically represent the distribution of vehicle weights has been to represent them by normal distributions (see figure 3.7). In this case, 2 distributions had to be determined for each type of lorry. One distribution represents fully loaded lorries and the second one represents lorries when they are empty or very lightly loaded. The distinction between these two cases seems obvious and fairly representative of reality. Indeed, it is clear that the trucks in the circulation cannot be fully loaded all the time due to the purpose of transporting goods.

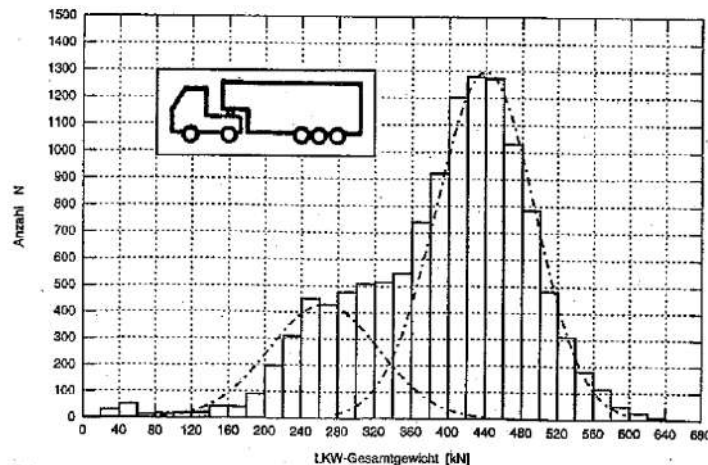


Figure 3.7. Approximation of distribution as measured by normal distributions, (extracted from [8])

In addition to this, normal distributions were also carried out to estimate the distribution of weights on each axle and also to find out the distribution of axle spacings. The data are all presented in tabular form (figure 3.8 and 3.9). The figure is determined after filtering out the different dynamic effects. The filtering of the dynamic effects is not explained in detail in [8], it is assumed that the filtering took place with calibrations of the measurement tools. However, it is difficult to know the accuracy of the measurements that were done at the time and there are many doubts about the confidence that can be attributed to

these measurements which may have led to a certain overestimation of the measured values. It should be noted that the dynamic filtration used does not influence the average values defined in the table but only the standard deviation.

		Mittelwert der Fahrzeuggewichte \bar{Q}		Standardabweichung der Fahrzeuggewichte σ_Q		Aufretenshäufigkeit f	
		[kN]		[kN]		[%]	
		Spur 1	Spur 2	Spur 1	Spur 2	Spur 1	Spur 2
Klasse 1	LLKW	74	64	31	29	13,3	17,2
	SLKW	183	195	23	28	9,4	10,4
Klasse 2	LLKW	123	107	40	39	0,3	1,3
	SLKW	251	257	31	35	1,0	2,2
Klasse 3	LLKW	265	220	51	68	17,1	28,0
	SLKW	440	463	42	65	48,1	30,4
Klasse 4	LLKW	254	196	37	60	3,6	4,1
	SLKW	429	443	55	64	7,2	6,4
$\Sigma = 100\%$							

Figure 3.8. Statistical data of lorry traffic at Auxerre after filtering out dynamic effects, (extracted from [8])

		Klasse 1		Klasse 2		Klasse 3		Klasse 4		PKW									
		LLKW	SLKW	LLKW	SLKW	LLKW	SLKW	LLKW	SLKW	LLKW	SLKW								
		m	σ	m	σ	m	σ	m	σ	m	σ								
Anteil der Achse i am Gesamtgewicht [%]	Achse 1	50,0	8,0	35,0	7,0	40,5	8,4	28,4	5,7	50,6	5,8	17,1	2,4	31,7	5,7	18,5	4,1	50,0	10,0
	Achse 2	50,0	8,0	66,0	7,0	36,2	6,8	42,8	4,2	27,5	4,4	26,9	4,4	31,3	5,8	28,1	4,2	50,0	10,0
	Achse 3	-	-	-	-	25,3	7,3	27,8	5,3	16,2	3,6	19,9	3,0	13,4	4,1	18,9	3,6	-	-
	Achse 4	-	-	-	-	-	-	-	-	13,6	3,1	19,0	2,8	13,7	3,5	16,3	3,4	-	-
	Achse 5	-	-	-	-	-	-	-	-	12,1	3,1	16,7	3,8	9,9	3,3	15,2	4,3	-	-
Abstand zwischen Achse i und i+1 [m]	Achse 1 - 2	3,71 1,10		3,78 0,71		3,30 0,26		4,27 0,48		3,00 0,50									
	Achse 2 - 3			1,25 0,03		4,71 0,78		4,12 0,31											
	Achse 3 - 4					1,22 0,13		4,00 0,42											
	Achse 4 - 5					1,23 0,14		1,28 0,03											

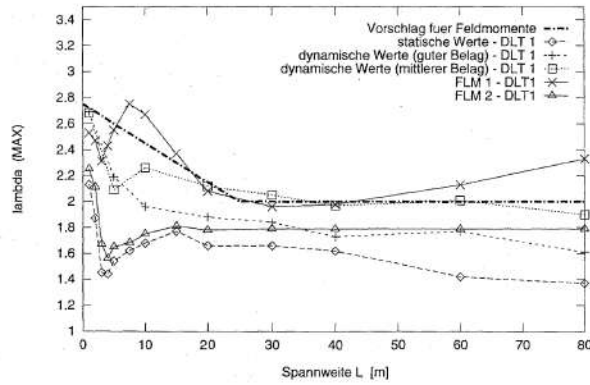
Figure 3.9. Distribution of vehicle loads on axles and of distances between axles, (extracted from [8])

In Sedlacek and Merzenich's simulations, traffic is defined according to the 2 figures above. However, for the traffic extrapolation, only the half-normal distribution fitted to the upper part of the real distribution was used [8].

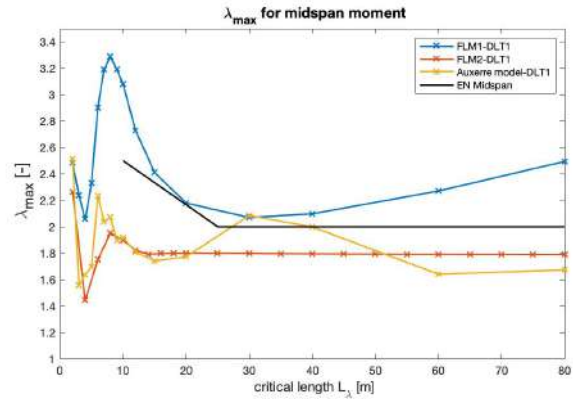
3.1.2 Comparison with Sedlacek and Merzenich simulations

Being aware of the traffic model that was used in Sedlacek and Merzenich's simulations, it is possible to use the same model and parameters of traffic to confirm the results provide in the previous numerical simulations and to confirm the validity of our algorithm. The parameters applied in our numerical simulations are the same as described in the Background document to EN 1991-2 [8]:

- only free-flowing traffic, modelled with a fixed inter-vehicle distance of 50 m;
- heavy vehicles only (eliminating cars), proportion of trucks as mentioned in figure 3.5 for slow lane.
- axles distances and weights distributions: half-normal distribution, maximum value = mean + 5 standard deviations. Parameters described in figures; 3.8 and 3.9 for slow lane;
- no dynamic amplification factor.

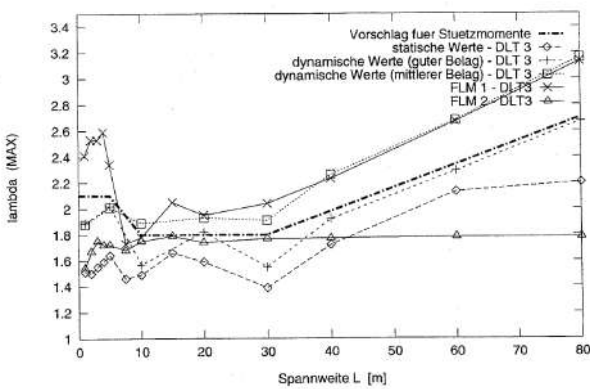


(a) Sedlacek and Merzenich Results

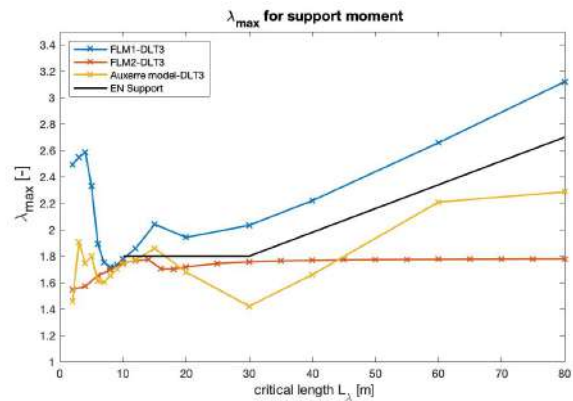


(b) Implemented code Results

Figure 3.10. Comparison with previous simulations - mid-span moment DLT 1



(a) Sedlacek and Merzenich Results



(b) Implemented code Results

Figure 3.11. Comparison with previous simulations - support moment DLT 3

The results obtained are quite or very similar to those in the Eurocode Background [8], the only difference is the peak obtained for FLM1-DLT1, nevertheless the behaviour of the curve seems similar. It also allows us to confirm the validity of our algorithm before presenting and analysing future results. However, it is now necessary to question the justification of the parameters used. As far as the traffic model is concerned, it is largely representative of the measurements modelled by the half-normal distribution. But nevertheless, it turns out that the distribution is cut at 5 standard deviations. To approximate average traffic values it is clear that the method is very satisfactory, but in the case of λ_{max} , it is necessary to know the real maximum values that is applied on the structures. Especially since the criteria does not admit any stress ranges above the CAFL. The results are then mainly influenced by the parameters we use. For example, when the distribution should be cut off, why congested traffic is not taken into account when it would cause higher stress peaks, and the distance between vehicles that is always fixed and greatly reduces the possible interactions between lorries. For this reason, the parameters must be carefully defined, as well as the criterion to be applied to determine the λ_{max} factor.

3.2 Maddah, 2013

In the PhD thesis of Maddah in 2013 [1], numerous simulations to determine the λ_{max} factor were performed. These simulations used real traffic data from Gotthard, Switzerland. To determine λ_{max} , the criterion used was the one proposed by the Eurocode which accept exceedance for a damage contribution of less than 1% of the total damage.

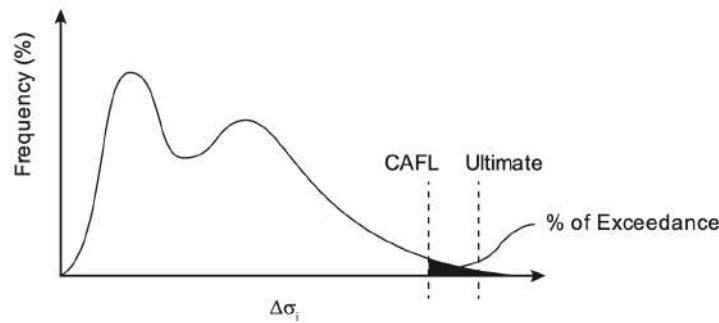


Figure 3.12. Schematic diagram for acceptance of 1% of the total damage, (extracted from [1])

However, as explain in Maddah's thesis, the occurrence of very few cycles above CAFL may lead to failure in some cases. This is not necessarily due to the number of cycles above the threshold, but mainly due to the eventuality that such a cycle above this limit could lead to a crack initiation. This would lower the CAFL threshold and therefore increase the damage as many stress ranges will not necessarily remain below the constant amplitude fatigue limit. Caution should therefore be exercised when applying this criterion of 1% relative damage as it does not necessarily mean that the total damage will remain below 1.0. The figure 3.13 extracted from Maddah's thesis shows the difference between both criteria ($\Delta\sigma_{max}$ equals to CAFL, and the one which accept an exceedance of 1% of the total damage).

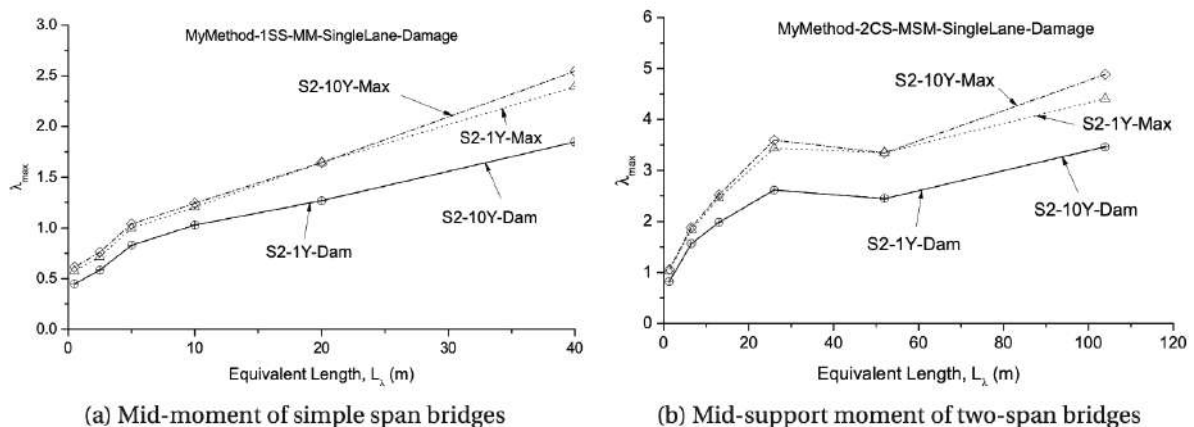


Figure 3.13. Comparison of the reduction of maximal stress range on λ_{max} , (extracted from [1])

For both cases, the graphs shows the results for 1 year and 10 years of Götthard main road traffic. It is clear that the absolute maximum stress is more sensible to difference between 1 and 10 years traffic as the 1% relative damage threshold gives the same results for 1 year and 10 years traffic.

The figure 3.14 extracted from Maddah's thesis show the result of λ_{max} for mid-span and support sections, using Götthard main road traffic (with 25% of heavy vehicle). In this case, the 1% threshold above constant amplitude fatigue limit is used to determine λ_{max} .

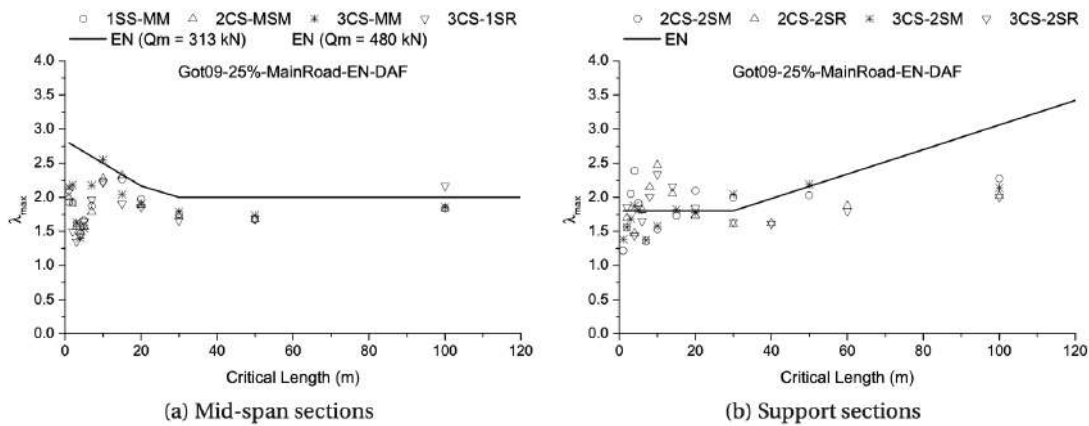


Figure 3.14. λ_{max} obtained for Götthard main road traffic with PHV = 25%, (extracted from [1])

3.3 λ_{max} determination

The criterion for determining λ_{max} has evolved a little over time. Originally the criterion, for Sedlacek and Merzenich, was that the constant amplitude fatigue limit was set at the level of the maximum stress range $\Delta\sigma_{max}$. This was to ensure sufficient safety to structures checked by assuming that the stress ranges were all below the constant amplitude fatigue limit and therefore did not cause damage that would cause the structure to collapse. This criterion especially limits the potential for crack initiation as all the stress ranges are limited by the constant amplitude fatigue limit.

This criterion is very sensitive to the traffic parameters since it only considers the maximum stress range. This can differ greatly from one traffic to another, and even within a single traffic depending on the time scale used. This is demonstrated in figure 3.13 (extracted from Maddah's Phd thesis [1]), which shows the difference in λ_{max} between using real traffic data over a 1 year period and a 10 years period.

3.3.1 Fatigue Load Models

4 fatigue load models were introduced into the Eurocode, based on the 1986 Auxerre traffic, considered to be the heaviest traffic in Europe at that time. Fatigue Load models 1 and 2 are intended to check whether the structure life can be considered unlimited against fatigue when the constant amplitude fatigue limit is set. While fatigue load models 3 and 4 are intended to estimate the service life of a structure with reference to the fatigue strength curve.

Fatigue Load Model 1 and 2 therefore reflect the characteristic loads to which road bridges can be subjected on the basis of the probability of occurrence obtained from the Auxerre traffic data. In a similar way, when λ_{max} is calibrated, one could think about the traffic characteristics that should be applied to the real traffic model. By using the maximum stress range as the only reference for calculating λ_{max} , it is then sensitive to the chosen probability rules, such as the characteristic value of the total weight and the inter-axles distances. In addition to this, the criterion appears to be very safe since by lowering the stress spectrum below the constant amplitude fatigue limit, the damage caused can become very low. Very little damage would mean that one could end up with many cases of over-strength design.

3.3.2 Real traffic data

This criterion does not seem applicable when using real traffic. Especially due to the fact that the maximum loads can become very high while in the load models characteristic values are chosen. Moreover, these values will vary greatly depending on the time period used. The criterion has also been adapted to accept the exceedance of which would produce a damage contribution of less than 1% of the total damage. This reduced the sensitivity of the factor to traffic and time period as shown in figure 3.13. The results obtained remains the same for a 1 year and a 10 years traffic.

3.3.3 Adopted criterion

The criterion defined as a basis for developing the Eurocode, proposed by Sedlacek in [13], of 1% exceedance of the total damage is less sensitive to the occurrence of maximum loads. This means that the stress ranges above the constant amplitude fatigue limit produces less than 1% of the total damage.

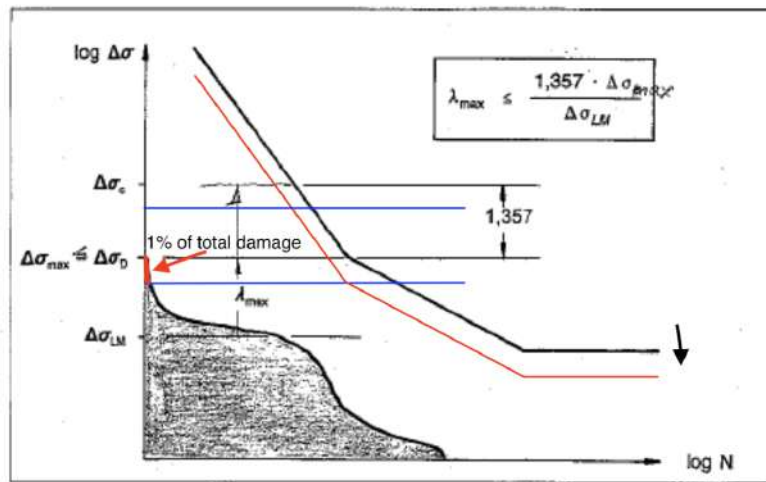


Figure 3.15. Diagram for acceptance of 1% of the total damage, (adapted from [9])

However, allowing 1% relative damage above CAFL does not guarantee that the total damage due to the stress histogram will remain below 1.0. The effect of this criterion on the results of λ_{max} is also very different depending on the span length. The figure 3.16 represents the total damage when computing λ_{max} with an acceptance of 1% relative damage.

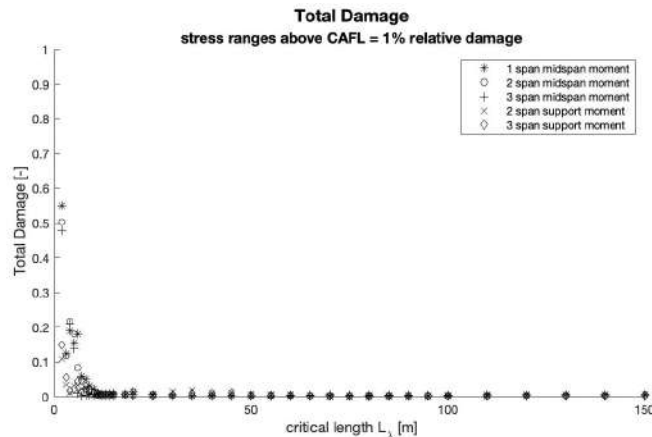


Figure 3.16. Total Damage when determining λ_{max} with 1% relative damage above CAFL

For spans longer than 20 meters, the criterion of 1% of relative damage become very difficult to reach because the total damage is already very small. The total damage, using this method, is approximately equals to 0.001 for span from 20 meters. in this case the values are quickly overestimated and give higher values for λ_{max} which is not desirable. To use a more appropriate criterion, it is proposed to allow an absolute damage of 0.01 for stress ranges above the constant amplitude fatigue limit while ensuring that the total damage remains below 1.0. This criterion is the one that is selected for the simulations presented in the next sections. In comparison with the previous figure, the figure 3.17 represents the total damage when computing λ_{max} by this method.

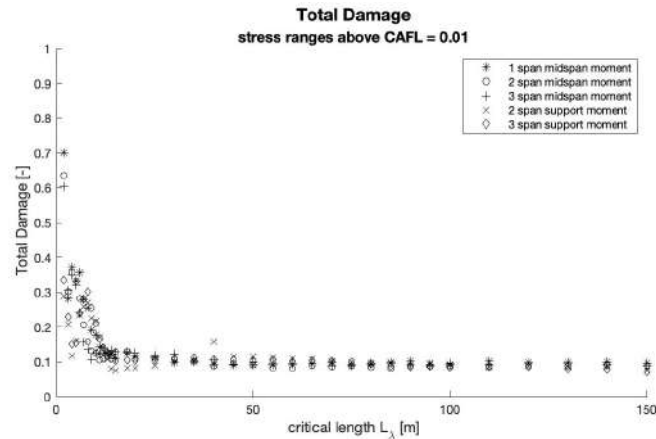


Figure 3.17. Total Damage when determining λ_{max} with 1% relative damage above CAFL

The results of the total damage are still widely below the limit of 1.0 which is important to satisfy. Otherwise the criterion would not be applicable because it would not be safe, let alone to satisfy an "infinite" service life. For longer spans, the total damage is approximately equals to 0.1 which is still safe. It will result in reducing the values of λ_{max} and generate more economic designs than those that could happen when using the previous criterion.

To confirm our choice, an even less strict criterion was adopted in [14]. The criterion is that damage above the constant amplitude fatigue limit D_{CA} is equal to (or smaller to) $D_{lim}=0.02$. This limit was determined on the basis of variable amplitude (VA) test, with Rayleigh stress range spectra. And in some cases, the stress range spectra is set with various additional cycles above CAFL. The figure 3.18 shows the number of cycles up to failure and the damage determined by calculation. It is then shown that all but 3 tests failed when the damage above CAFL was greater than 0.02. The limit for non-propagative crack was then set for D_{lim} equals to 0.02.

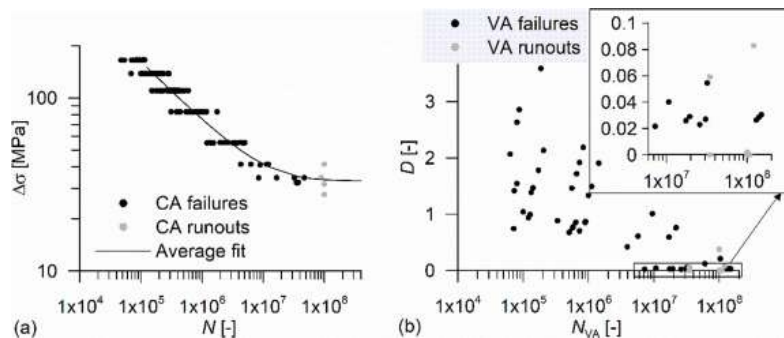


Figure 3.18. Analysis of tests on full scale welded cover plates: (a) CA test data and average regression curve using a random fatigue limit model; (b) VA test data versus damage calculated with the average regression curve for CA data, extracted from [14]

4 λ_{max} calibration procedure

The procedure to determine λ_{max} is very similar to the procedure used to obtain λ_1 . Therefore, the algorithm implemented was adapted from the Master thesis of Gianluca Bianchi [3]. A new routine, with the procedure described in figure 4.1, has been introduced in the code.

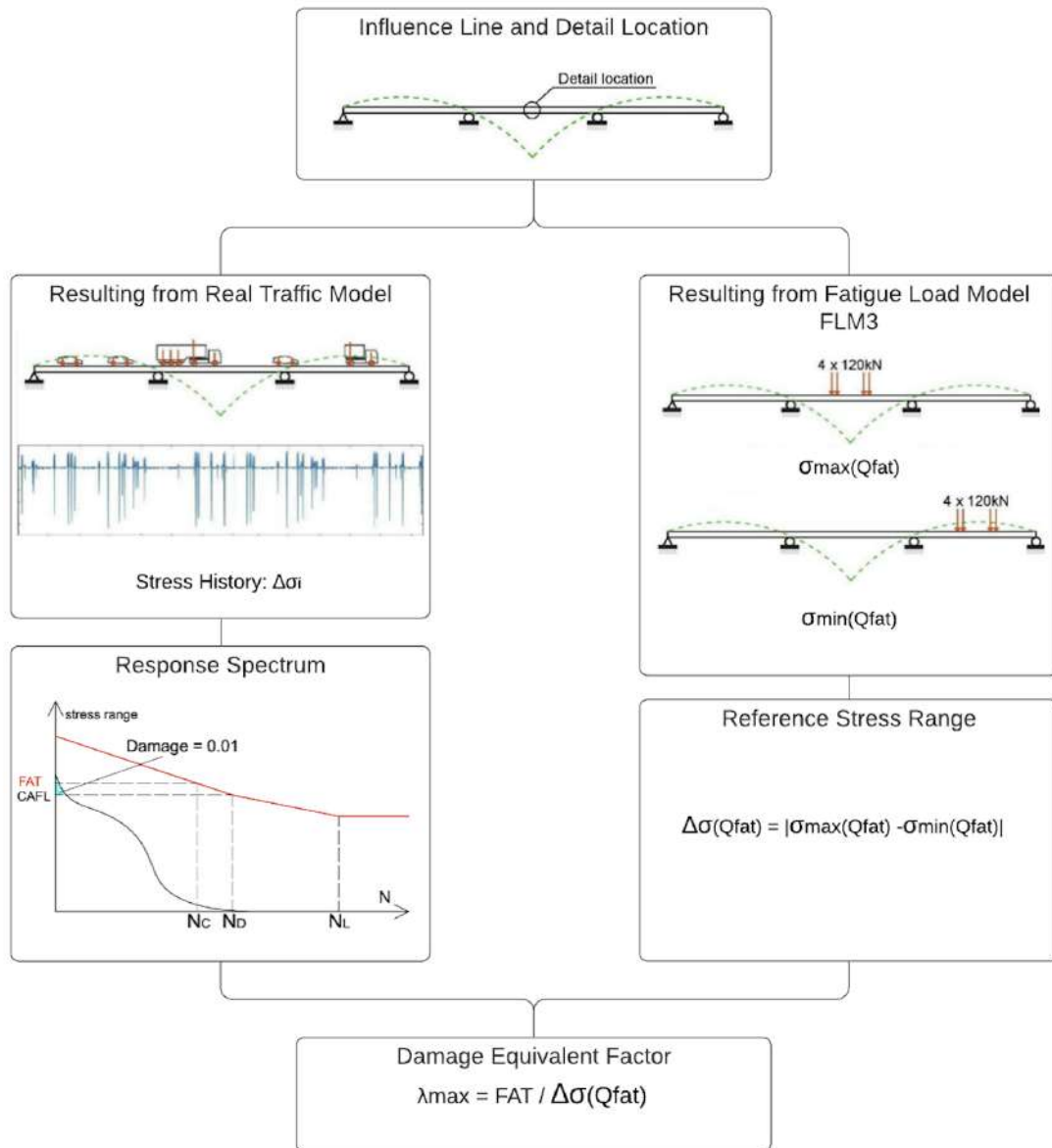


Figure 4.1. λ_{max} factor computation procedure

The method allows the calibration of the factor by comparing a real traffic model with the FLM3 model described in the Eurocode for the fatigue design of road bridges. On the one hand, the fatigue load calculation from the FLM3 model is performed, and on the other hand, a cumulative damage calculation is used for the real traffic model, which could be for instance FLM4. In contrast to the λ_1 calculation, the calculation of the cumulative damage does not have to reach one. Here the resistance curve is adjusted to find a damage equals to 0.01 for stress ranges located above the constant amplitude fatigue limit. Then, λ_{max} is the ratio between the resistance of the strength curve and the reference stress range $\Delta\sigma_{Qfat}$. The main parameters used in the computer algorithm, such as traffic parameters and fatigue strength curves, are described in the next sections.

4.1 Influence lines

In the development of the λ_1 and λ_{max} curves for EN 1993-2, the simulations of Merzenich and Sedlacek used a small number of influence lines. In order to have a good overview and to propose new λ_{max} curves that take into account a large number of influence lines, a larger number of influence lines are considered. It will be possible to confirm the results obtained and to apply them to several types of structure configurations. To do this, the simulations carried out for the λ_{max} calculations use 5 static configurations presented below.

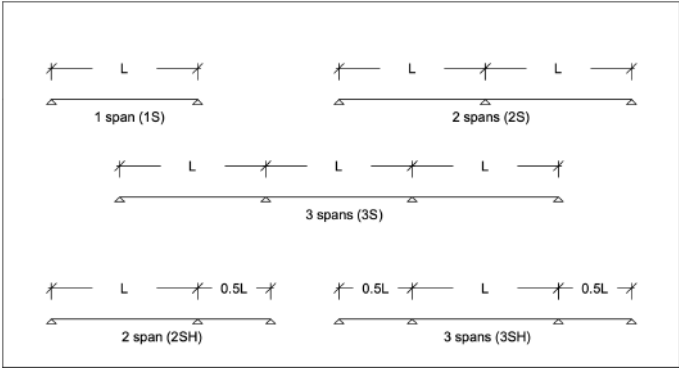


Figure 4.2. Static systems for the recalibration of λ_{max}

In addition to the conventional configurations, 2 systems use lateral spans that are half the length of the centre span. This will determine whether the effect of having different span lengths has an effect on the λ_{max} values or whether they can be associated with the same values as for structures with identical spans. In the results presented in the EN 1993-2[20], those have been calculated for influence lines such as mid-span moment, support moment, support shear force and mid-span shear force. Various influence lines were added, including support reactions and mid-span moments on the end spans. Moreover, 2 influence lines such as intermediate moment and intermediate shear evaluate the respective forces for a section located at $0.15 \cdot L$ from the support, which is currently the limit between span and support sections (defined in EN 1993-2, and presented in figure 2.11). The annex A also shows all the influence lines and the critical length L_λ graphically.

Influence line	1S	2S	3S	2SH	3SH
Midspan M	1S-MM	2S-MM	3S-MM	2SH-MM	3SH-MM
Midspan V	1S-MV	2S-MV	3S-MV	2SH-MV	3SH-MV
Support M	-	2S-SM	3S-SM	2SH-SM	3SH-SM
Support V	1S-SV	2S-SV	3S-SV	2SH-SV	3SH-SV
Lateral Midspan M	-	-	3S-LM	2SH-LM	3SH-LM
Lateral Midspan V	-	-	3S-LV	2SH-LV	3SH-LV
Intermediate M	1S-IM	2S-IM	3S-IM	2SH-IM	3SH-IM
Intermediate V	1S-IV	2S-IV	3S-IV	2SH-IV	3SH-IV
Central Reaction	-	2S-CR	3S-CR	2SH-CR	3SH-CR
Lateral Reaction	1S-LR	2S-LR	3S-LR	2SH-LR	3SH-LR

Figure 4.3. set of influence lines

These new set of influence lines will allow a thorough evaluation of the behaviour of the λ values and to determine the similarities of the results between the influence lines. This will also allow the results to be grouped together to produce new λ curves that include a wider variety of results and condense a larger number of situations.

4.2 Slopes m | k Wöhler curve

Several resistance curves with different slopes are described in the European standards. In order to evaluate the behaviour of the λ_{max} results, the curves with the following slopes were used.

4.2.1 Slopes m|k = 3|5

This curve is the standard curve used, especially for the classification of details. This curve consists of a slope $m=3$ up to the constant amplitude fatigue limit (at $5 \cdot 10^6$ cycles, $\Delta\sigma_D = 0.74 \cdot \Delta\sigma_C$), and a second slope $k=5$ up to the cut-off limit at 10^8 cycles (which corresponds to $\Delta\sigma_L = 0.405 \cdot \Delta\sigma_C$). This resistance curve is the reference curve that is used for the λ_{max} simulations.

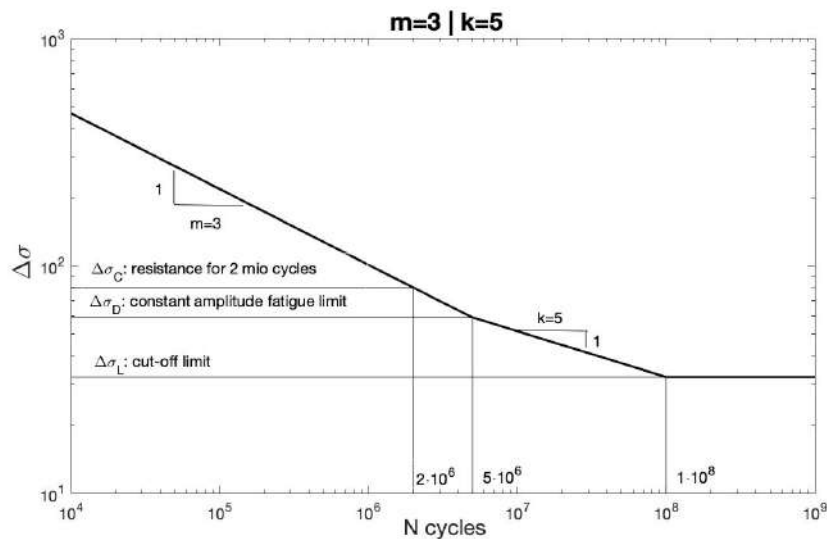


Figure 4.4. Fatigue strength curve - mk = 3|5

4.2.2 Slopes m = 3

This curve is a unique slope $m=3$ with a cut-off limit at 10^8 cycles (which corresponds to $\Delta\sigma_L = 0.271 \cdot \Delta\sigma_C$).

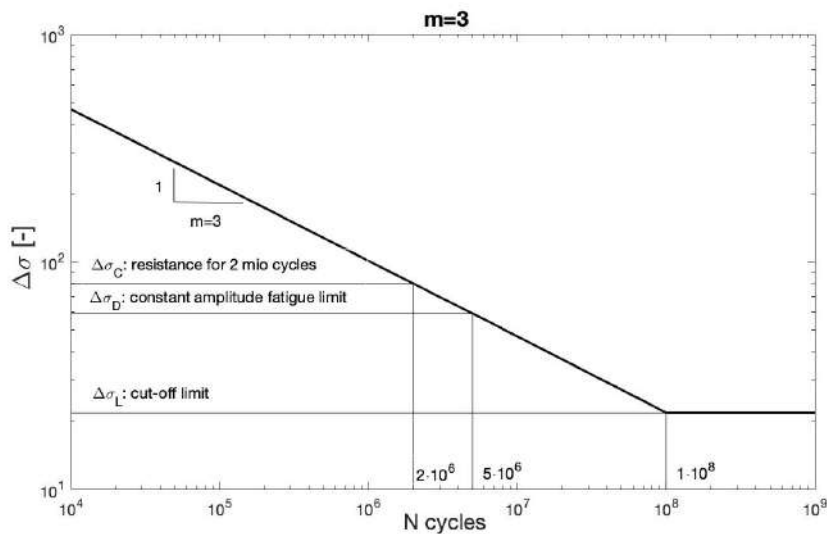


Figure 4.5. Fatigue strength curve - m = 3

4.2.3 Slopes $m|k = 4|6$

This curve is also a double slope curves with $m=4$ and $k=6$. For this curve, there is no cut-off limit admitted, but this time the slope change occurs at $2 \cdot 10^6$ cycles. This is particularly defined for the strength of tension components, such as cables (for instance in cable-stayed bridges).

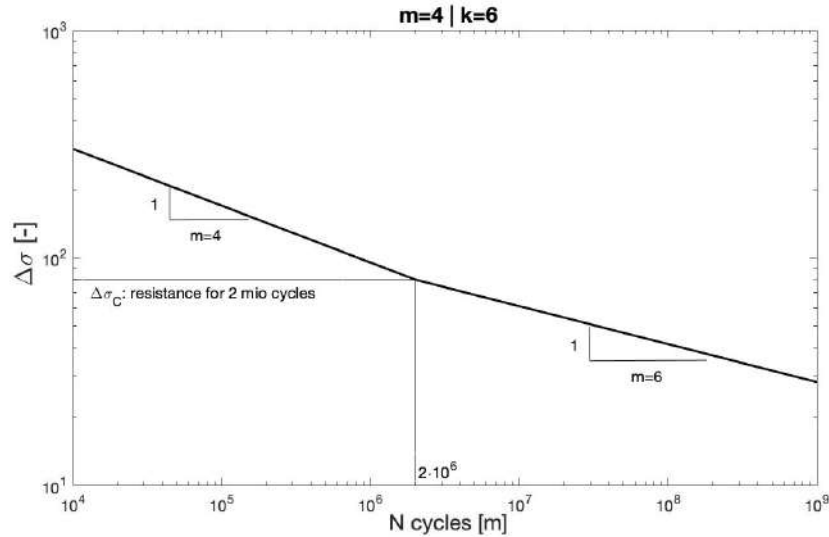


Figure 4.6. Fatigue strength curve - $mk = 4|6$

4.2.4 Slopes $m = 5$

This curve is a simple slope with $m=5$ and with a cut-off limit at 10^8 cycles (which corresponds to $\Delta\sigma_L = 0.457 \cdot \Delta\sigma_C$). Generally, the resistance curve is used for elements under shear stress.

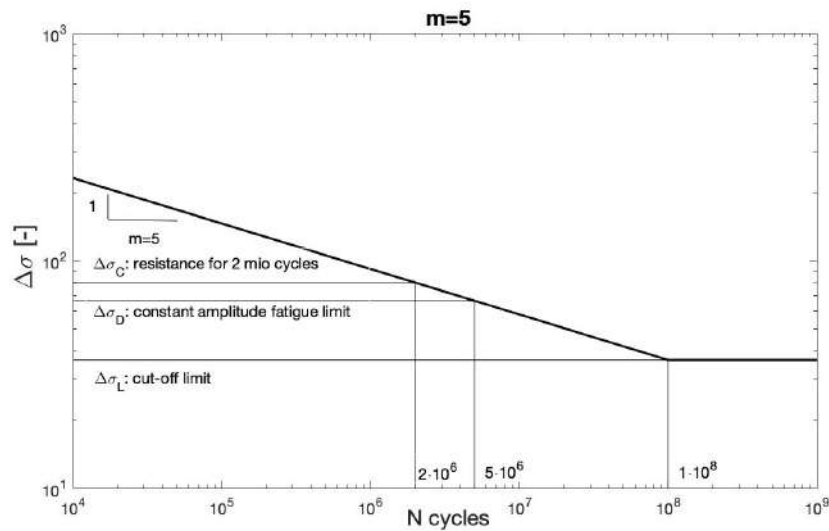


Figure 4.7. Fatigue strength curve - $m = 5$

4.2.5 Slopes m|k = 5|9

This curve is a double slope with $m=5$ and $k=9$ that is used for verification of rebars in bridge deck. The constant amplitude fatigue limit is set at $2 \cdot 10^6$ cycles and a cut-off limit at 10^8 cycles (referring to EN1992-1-1: 2021).

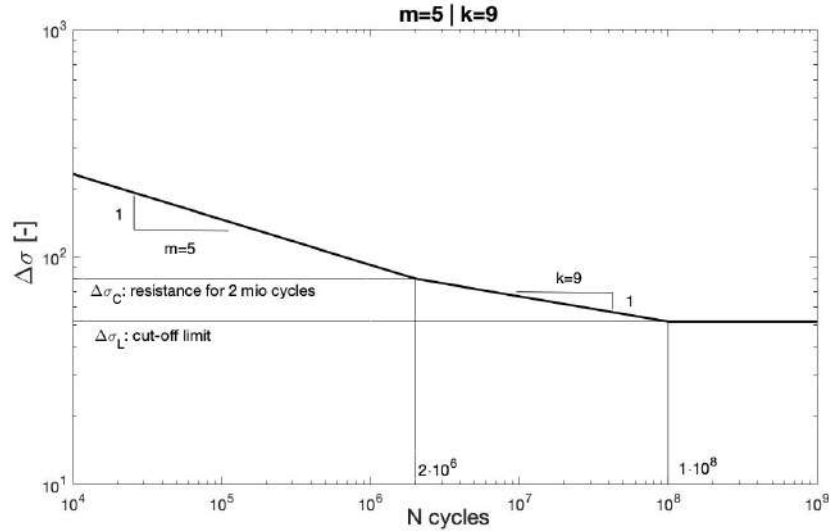


Figure 4.8. Fatigue strength curve - $mk = 5|9$

4.3 Fatigue Load Model 3

For the fatigue design of road bridges using the simplified method with correction factors, the load model prescribed by the Eurocode is the Fatigue Load Model 3. As explained in section 2, This consists of 2 equivalent lorries that can act on the influence line of the defined static system. Depending on the length of the influence line, the second lorry must be introduced to calculate the fatigue stress range $\Delta\sigma_{Q_{fat}}$. The only condition to complete is the minimum distance between the 2 vehicles, the hindrance must be greater than 40 meters (see fig. 2.7).

The fatigue stress range $\Delta\sigma_{Q_{fat}}$ is then calculated by positioning the loads at the relevant points along the influence line to obtain the maximum and minimum stresses ($\Delta\sigma_{max}$ and $\Delta\sigma_{min}$). The absolute difference between these two gives the fatigue stress range.

$$\Delta\sigma(Q_{fat}) = \sigma_{max}(Q_{fat}) - \sigma_{min}(Q_{fat}) \quad (17)$$

The use of a second lorry considerably increases the possibility of mistakes when calculating $\Delta\sigma_{max}$. This is due to the positioning of the second lorry as it is not fixed. For the recalibration of the λ factors, it was therefore decided to use only the first FLM3 lorry. This simplification will avoid possible mistakes and will clarify any doubts that may be present when using the FLM3 model. Although the second FLM3 lorry was introduced for obvious reasons, explained in section 2, in order to best match the real traffic behaviour for every influence lines. The use of only one truck will not change the veracity of the results as this difference will be directly taken into account in the calibration of the lambda factors.

4.3.1 Comparison - 1 or 2 lorries FLM3

As the use of a single lorry FLM3 is proposed for the recalibration of the lambda curves, the effects of neglecting the second lorry have to be known to analyze the results of the new λ_{max} values correctly. To do this, the following figures show the difference that occurs in the $\Delta\sigma(Qfat)$ calculation when the second FLM3 lorry is removed. Influence lines results are shown below, the figure 4.9 represent the results for mid-span bending moments and the figure 4.10 is for the support bending moments.

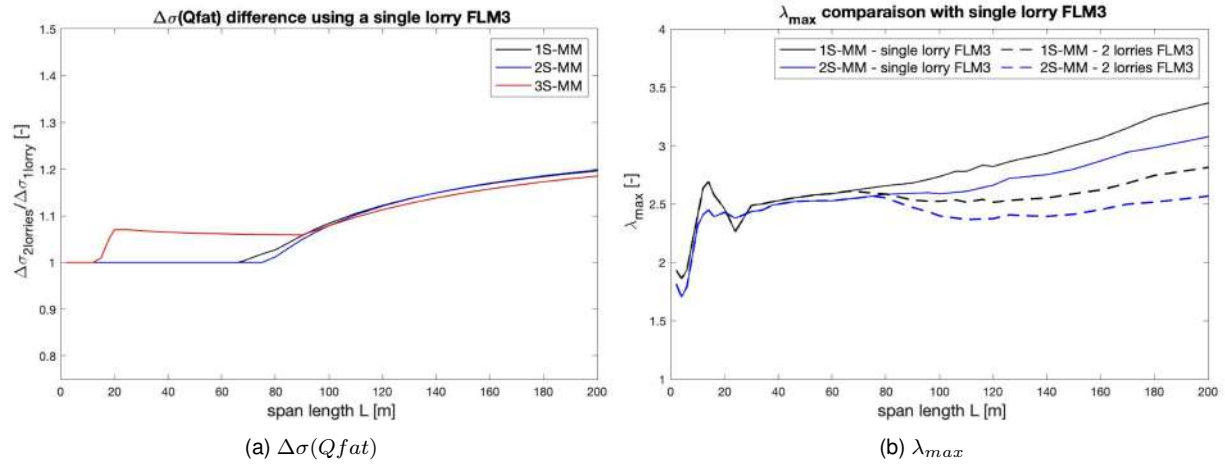


Figure 4.9. Comparison with simplified FLM3 - mid-span moments

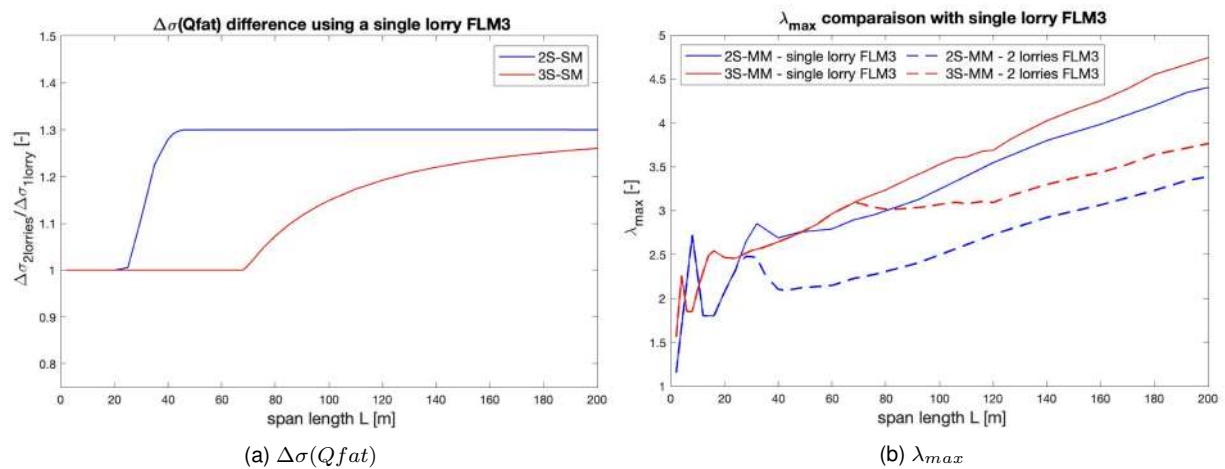


Figure 4.10. Comparison with simplified FLM3 - support moments

The figure shows the ratio between the stress range calculated for the 2 vehicles and the single vehicle FLM3 model. Depending on the static systems, the difference does not occur for the same span length. This depends on the number of spans in the system, as the second vehicle must be at least 40m away from the first one. There is therefore no difference in the calculation when the span length remains short. A reduction of up to 30% is determined, especially for the 2 spans - support moment system. This will result in the same increase for the lambda values. This significant effect will automatically increase the lambda values, especially for longer spans. Using a single lorry FLM3 considerably reduces the dispersion between the curves, we observe a continuity of the curves with this simplified model. The addition of the second vehicle causes a jump in the λ_{max} curves and it is then more complicated to group the results. The effect is all the more important for the influence lines for support moment as the second lorry was introduced especially to correct the model for such influence lines.

4.4 Real Traffic Model

In order to determine the lambda values, it is necessary to use a real traffic model to calculate the cumulative damage. It is possible to use either the FLM4 model (with additional assumption for traffic flow conditions) or real traffic data from the Weight In Motion (WIM) measurement for instance. The different traffics used by the algorithm for the recalibration of λ_{max} are described in the following sections.

4.4.1 Fatigue Load Model FLM4

FLM4 set of lorries consists in 5 standard lorries described in figure 4.11. This model is based on damage equivalent loads from Auxerre traffic. In contrast to FLM3, which is intended for the verification of bridge main component with influence lengths greater than 20m, the FLM4 model is intended for bridge decks or elements with short influence lines (less than 20m), and orthotropic decks. This was done using a model much closer to the characteristic weights observed in the measurements with 5 vehicles configurations. These silhouettes are based on the average geometries observed in the Auxerre measurements. The model is therefore more appropriate when it comes to elements where local effects are predominant. In addition to this, the wheel type is defined for each axle, again to define the distribution and local effects as accurately as possible. The proportion of each type of lorry is determined for 3 types of traffic (long distance, intermediate distance and local traffic). The λ curve represents the calibration between FLM3, which is used for the calculation of the equivalent stress $\Delta\sigma_{E2}$, and the real traffic represented by FLM4.

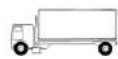



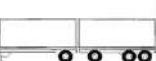
VEHICLE TYPE			TRAFFIC TYPE			
1	2	3	4	5	6	7
			Long distance	Medium distance	Local traffic	
LORRY	Asse spacing (m)	Equivalent axle loads (kN)	Lorry percentage	Lorry percentage	Lorry percentage	Wheel type
	4,5	70 130	20,0	40,0	80,0	A B
	4,20 1,30	70 120 120	5,0	10,0	5,0	A B B
	3,20 5,20 1,30 1,30	70 150 90 90 90	50,0	30,0	5,0	A B C C C
	3,40 6,00 1,80	70 140 90 90	15,0	15,0	5,0	A B B B
	4,80 3,60 4,40 1,30	70 130 90 80 80	10,0	5,0	5,0	A B C C C

Figure 4.11. Fatigue Load Model 4, extracted from [18]

Other parameters must be determined in order to produce a complete traffic model. In particular, a distance law between vehicles must be chosen. In addition, it would be too severe to use only fully-loaded vehicles, while it is not likely that freight transport is completely efficient. In our case, the proportion of "empty" vehicles was set at 33%, which is the most efficient system that was recorded in Auxerre in 1986. This proportion recorded in Auxerre was by far the lowest observed in Europe and this traffic assumption remains safe today. The weight of these empty vehicles is set at 40% of the weight of a fully-loaded lorry. A new parameter introduced in the numerical simulations is a variable to produce a slight fluctuation in vehicle weights described in FLM4. To avoid considering systematically equal loads,

it was preferable to insert this variable which allows to spread the stress histogram. It was therefore decided to arbitrarily set a fluctuation ranging from +5 to -5 kN per axles.

To define the distances between vehicles in traffic, flowing and congested traffic must be distinguished and defined. For free-flowing traffic, the distance between vehicles is defined according to their speeds. The distribution is done according a Gamma distribution based on the density function of Davenport calculated for a speed of 80 km/h, which is also the average speed found in traffic measurements. For congested flow, the inter-vehicle distance is calculated according to a Beta distribution for a speed of 20 km/h. The algorithm also allows for the mixing of traffic so that a certain traffic share is congested. A share of 10% of congested traffic was chosen, knowing that this remains an upper bound in comparison with real portion of congested traffic.

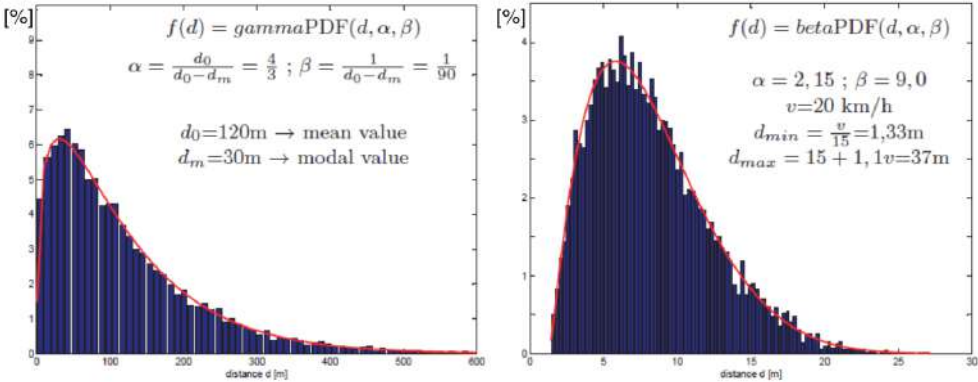
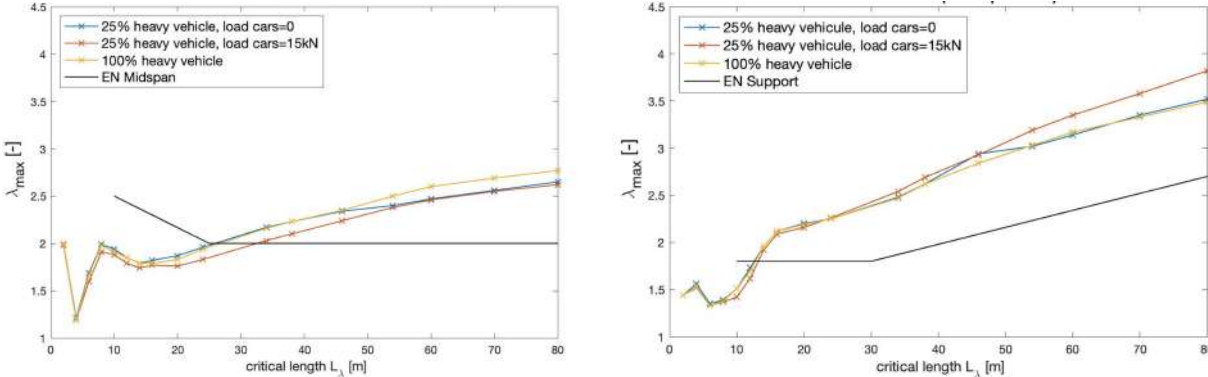


Figure 4.12. Inter-vehicle distribution free-flowing and congested, extracted from [2]

Light vehicles can also be considered, even if their load is small, they greatly influences the distance between heavy vehicles. It is therefore important to evaluate their effect on λ_{max} results. In theory, the effect of cars is null for short spans since the influence line is too short to allow vehicles interactions. However, for longer spans, the influence should be noticeable since the presence of cars will increase the distance between lorries reducing the possibility of interaction. Small cars can be considered in the numerical simulations. For this purpose, a single car type is defined with a spacing of 2.75m between axles. Usually the chosen load is 15 kN, however due to the small effects, it is also possible to assign a zero load. In figure 4.13, a comparison is done for a calculation with and without cars consideration. Therefore, 3 calculations are computed; using exclusively heavy traffic (hv=100%), using 25% heavy traffic with cars weight of 15 kN; and using the same share (25%) but neglecting the cars weights.



(a) Midspan bending moment (b) Support bending moment

Figure 4.13. Influence of light vehicles, 3S-MM and 3S-SM

The effect of light vehicles is relatively small, however, we can see that they have a real influence on the inter-vehicle distances. It is a secondary effect and is not a determining factor in the calculation of λ_{max} . It is therefore possible to use a simplified traffic model with only heavy vehicles weights without changing the results in a decisive way.

4.4.2 Weight In Motion (WIM)

WIM measuring stations provide real traffic data and are nowadays the standard for traffic load measurements. These data can be used directly to calibrate the lambda factors, which makes it possible to be in line with current European traffic. They provides useful informations such as axles load, inter-vehicle distance, inter-axles distance and speed. Use of WIM also indicates the traffic intensity and helps deriving the annual traffic flow of the measured highway. The various WIM traffic used for the recalibration of the λ_{max} factor are described below.

A16, Netherlands The WIM database from Netherlands, is based on the A16 highway, which is the main highway near the Harbour of Rotterdam. The motorway consists of 3 lanes per direction. The WIM station is installed in the slow lane and in the fast lane which is used for overtaking vehicles in slow lane. The third lane is only allowed to light vehicles. As reported in [14], the proportion of lorries between the slow and fast lane is constant for the 3 measurement periods considered. The slow lane contains approximately 88% of the heavy traffic. The figure 4.14 shows the main parameters of the A16 traffic.

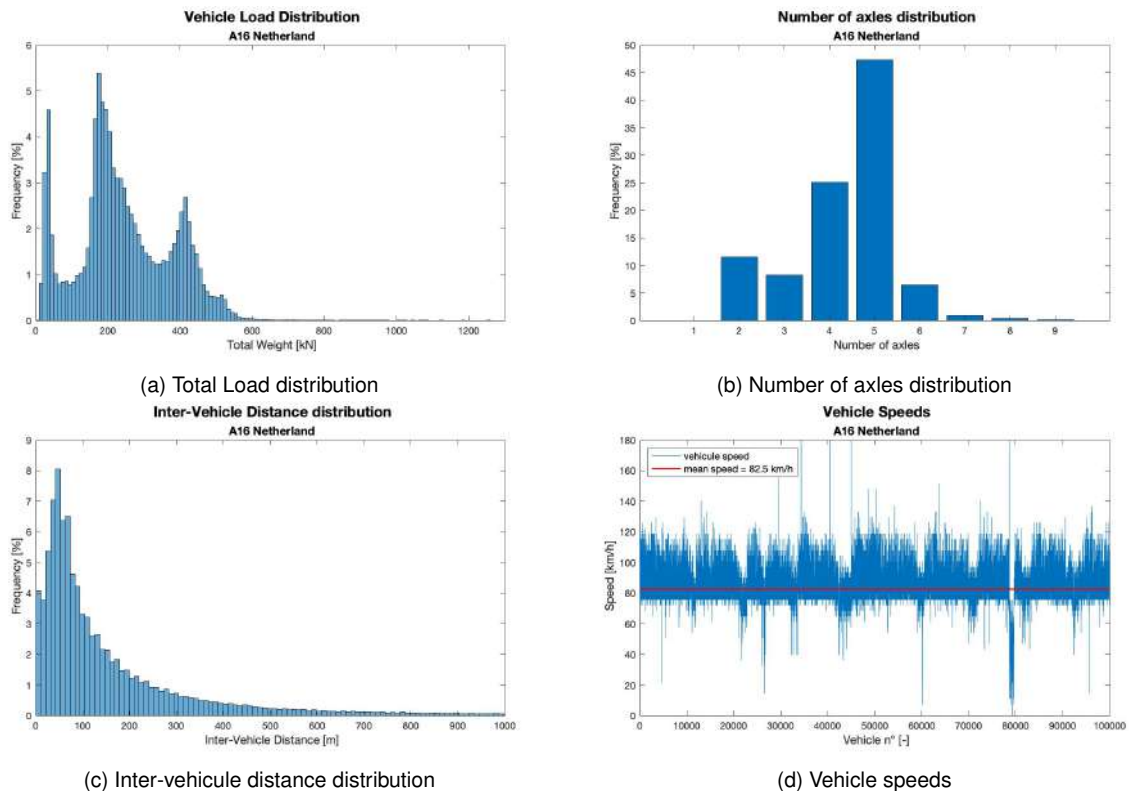


Figure 4.14. A16 WIM traffic 2018

The annual number of heavy vehicles is estimated at 2'100'000 on the slow lane. This is in line with the national road authority's indication that the annual number of heavy vehicles on 3-lane road is approximately 2.5 millions. Considering that 88% of the heavy traffic is on the slow lane, this would represent 2.2 millions vehicles. Moreover, the measurements are rather constant over the 3 measurement periods (2008, 2013, 2018) which indicates according to [14] that the road reached saturation. The numerical

simulation use a sample of 100'000 vehicles issued from the slow lane of the WIM database. In order to best reproduce real traffic, the calculation of λ_{max} is done using the actual number of lorries per year. This sample is multiplied to obtain a value of 2'100'000 lorries per year (during a service life of 100 years). As seen in 4.14, it is clear that the majority of traffic is determined by the 5-axle "European lorry". This lorry represent about 50% of the heavy traffic. In [14], the average 5 axles lorry from the WIM database is determined. This "European" lorry is presented in the figure 4.15.

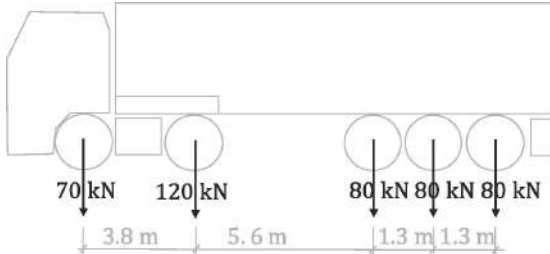


Figure 4.15. proposed "European lorry" based on WIM A16 database, extracted from [14]

It seems that the A16 traffic is representative of the heaviest European traffic nowadays, this traffic is used as the reference traffic for the λ_{max} simulation results. But it will be put in perspective with other WIM traffics in order to compare and interpret the results in a global way.

Sweden The WIM data from Sweden combine several measurement periods at different locations. The measurement periods range from 2002 to 2009 and were carried out at 10 different locations on major roads. The WIM data therefore represents a set that should be a fairly reliable representation of Swedish traffic. As the measurements are not all taken at the same place, it is difficult to estimate the annual number of vehicles correctly as the data combine several traffic. Nevertheless, the average number of heavy vehicles per year is estimated to be 400'000. The load and the number of axles distribution of swedish WIM measurements are presented in figure 4.16

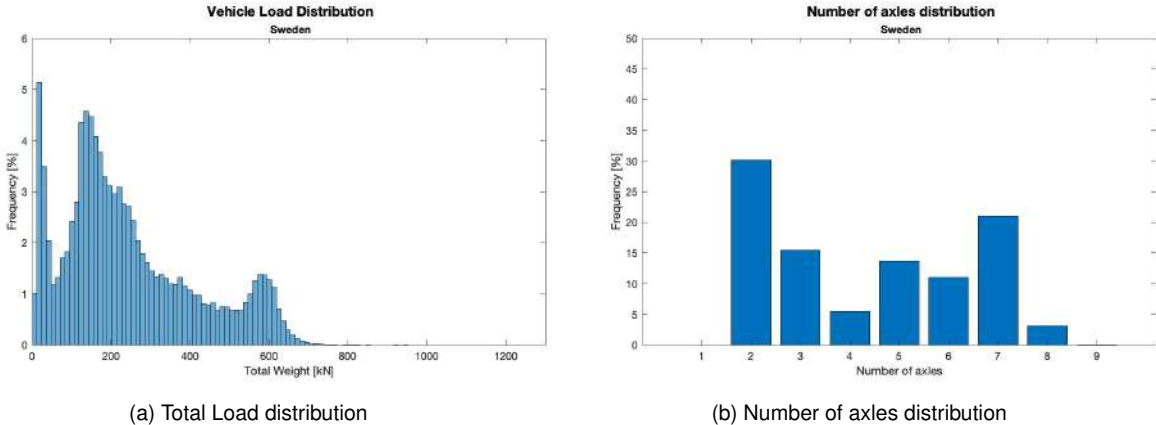


Figure 4.16. Sweden WIM Traffic 2002-2009

The Swedish traffic is less dense, but it is a little heavier than the A16 traffic. Moreover, when we look at the number of axles per lorry, we find a higher proportion of heavy vehicles with 7-8 axles. Whereas in the A16 measurements, the majority of trucks have 5 axles. The average distance between trucks is also higher, which is consistent with the fact that the number of lorries here is only 400'000 vehicles per year. The traffic seems to be less saturated.

Löddeköpinge, Sweden The measurements are based on the E20 motorway which connects Malmö to Göteborg, one of the major roads in Sweden. The measurements date from 2009. The available data covers only 10'000 vehicles, which corresponds to one week of traffic. The sample is low compared to the other WIM data used. One should therefore be cautious as the maximum loads are probably underestimated as the measurement period is quite short. The annual number of heavy vehicles is estimate to be 500'000. The figure 4.17 presents the distributions for Löddekopinge WIM station.

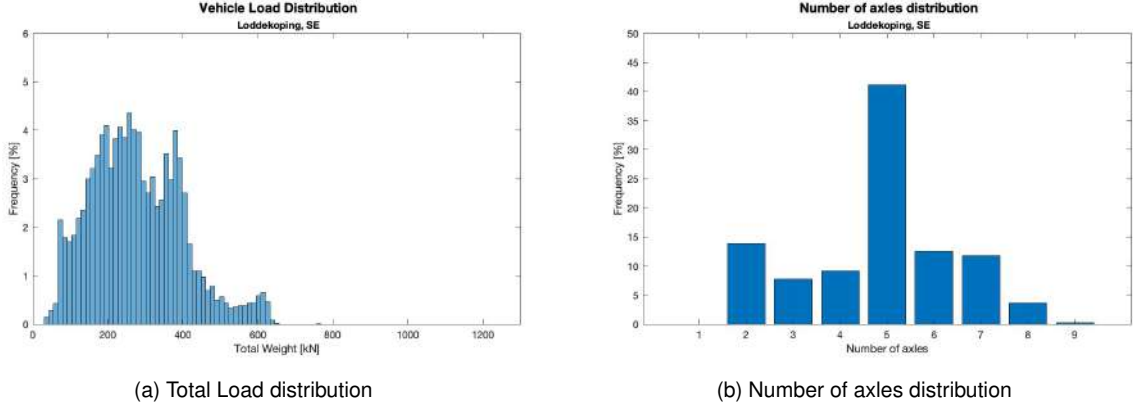


Figure 4.17. Löddeköpinge WIM Traffic 2009

the distribution of the number of axles is somewhat intermediate between the overall Swedish traffic and the A16 traffic. There is a large proportion of 5 axle trucks, but there is also a significant proportion of vehicles with 6-7-8 axles. The average weight is also slightly higher than that of the A16.

Switzerland WIM database Several WIM stations are installed in Switzerland and allow the study of traffic on Swiss roads on an annual basis. The traffic that could be used for the λ_{max} calculations are the Monte Ceneri, Gotthard and Denges traffic. The Swiss traffic is quite light when compared to heavy European traffic such as the A16 or Sweden. The 3 traffics used are relatively similar even if there is a higher number of annual heavy vehicles on the Ceneri station. The typical lorries are very similar, there are no or very few trucks with more than 5 axles. And again, the proportion of lorries with 5 axles is important.

Gotthard, Switzerland

- $Q_{m1} = 307.67$ kN ($m_2=5$), $N_{obs} = 400'000$ heavy vehicles

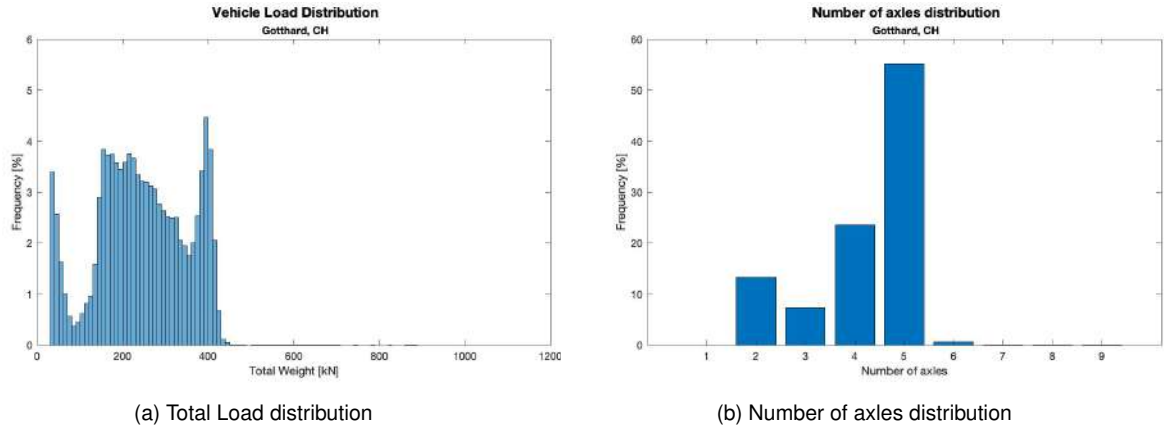


Figure 4.18. Gotthard WIM Traffic 2019

Ceneri, Switzerland

- $Q_{m1} = 280.17 \text{ kN}$ ($m_2=5$), $N_{obs} = 675'000$ heavy vehicles

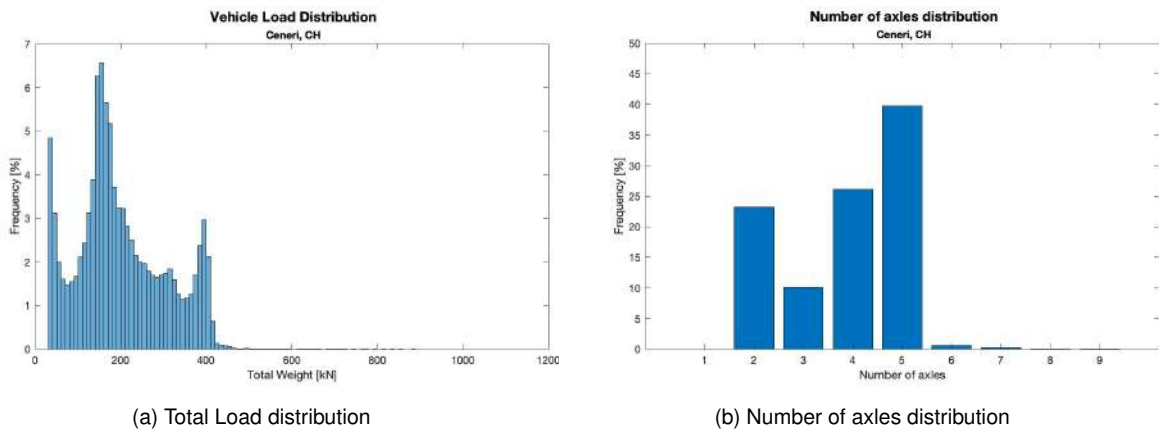


Figure 4.19. Ceneri WIM Traffic 2019

Denges, Switzerland

- $Q_{m1} = 250.58 \text{ kN}$ ($m_2=5$), $N_{obs} = 500'000$ heavy vehicles

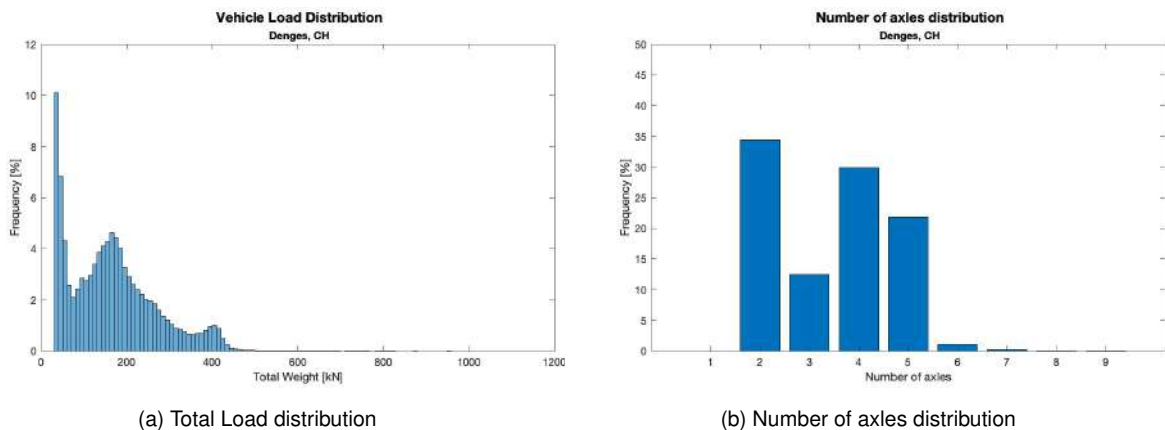


Figure 4.20. Denges WIM Traffic 2019

The 3 Swiss traffics do not all have the same particularity, which can be felt in the distribution of the types of trucks measured at the 3 stations. The traffic from the Gotthard is an international traffic on the North-South European route. And it is the traffic with the highest proportion of so-called "European" lorries. In contrast, the traffic from Denges is rather regional and in its distribution of trucks is closer to an intermediate traffic as described in the FLM4 model. As for Ceneri, the traffic is between the two (long-distance and medium-distance traffic) due to its geographical location. This traffic is rather a mix between international traffic and more regional traffic, which is fairly well described in the typology of trucks passing on this road.

Comparison of the WIM database The simulations use the 6 available WIMs. These WIMs have different and various traffic parameters and will be useful to determine a new λ_{max} curve that will include the traffic diversity. The table 4.1 compare some key parameters of the different WIMs.

	Avg. weight of lorries Q_{m1} [kN] ($m_2 = 5$)	Avg. weight of axles Q_{ma} [kN] ($m_2 = 5$)	Avg. vehicle distance [m]	Nobs	Traffic type
A16, NL	349.28	75.81	255.24	2'100'000	long distance
Sweden	402.85	74.98	1019.79	400'000	long distance
Löddekopinge	366.25	71.23	1076.66	500'000	long distance
Gotthard	307.67	73.02	423.83	400'000	long distance
Ceneri	280.17	69.63	482.73	675'000	medium/long distance
Denges	250.58	67.63	2191.10	500'000	medium distance

Table 4.1. WIM characteristics

The traffic characteristics are quite different, which makes it possible to have a good diversity of traffic between very heavy and very dense European traffic such as the A16 and lighter traffic such as that present in Switzerland. The traffic also allows to study a very heavy traffic but less dense than the one in the Netherlands such as Sweden. All these different data will allow to evaluate if λ_{max} results are linked to these parameters and to propose λ_{max} curves based on various European road traffics. The average lorries weights are all well below the value $Q_0 = 480$ kN defined in [20] to which the λ_{max} values are calibrated. The calibration against this value seems too high, as the weights observed for European heavy traffic are all well below these values, so it would be overestimated to continue using this value. To replace it, with a more suitable value, it has been introduced, especially for λ_1 values, a new reference with $Q_0 = 350$ kN (which corresponds to the average weight in A16 WIM measurements). The value of 480 kN is not in line with the multiple traffic measurements used by far. It can be observed that on the heaviest traffics we have available (Swedish WIM traffic) the average Q_{m1} value never exceeds 405 kN.

4.4.3 Comparison of real traffic models on λ_{max}

It is possible to compare the results according to the traffic used, and especially to check that the modelled traffic does indeed represent the real traffic when these models are used to determine λ_{max} . The comparison is done in figure 4.21 for the FLM4 model, the Auxerre traffic model and the measured WIM traffic of the A16. It should also be noted that in figure 4.21 the simulated traffics (WIM A16, Auxerre and FLM4) uses the FLM3 model with a single vehicle for the computations of λ_{max} , unlike the EN curves which use the FLM3 model with 2 vehicles.

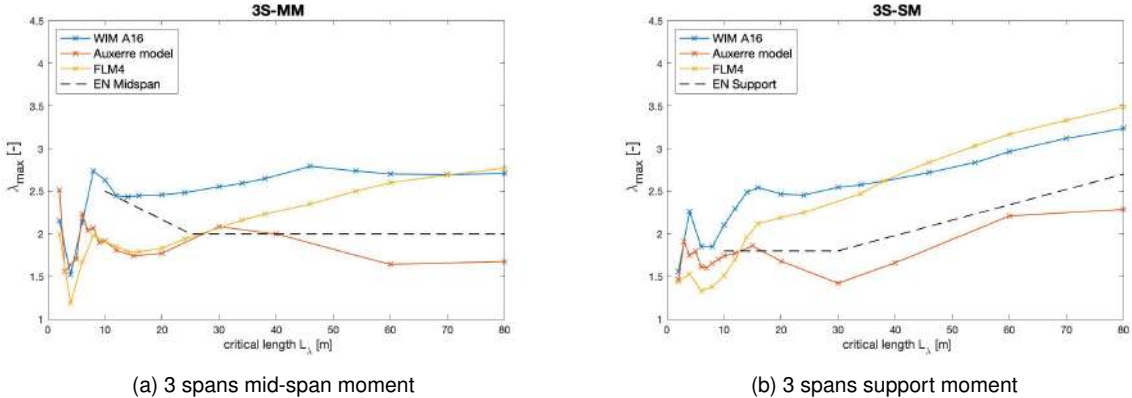


Figure 4.21. λ_{max} comparison real traffic model

The results are still different when using real traffic data from the WIM stations, while the results between the 2 traffic models are already closer. Clearly, λ_{max} factor calculation, using modelled traffic will not be able to accurately relate to real traffic. Due to the criterion applied, which is directly related to the maximum loads that occur on the structure, it is complicated to reproduce this with FLM4 traffic, for instance, which isolates a fixed load value for each FLM4 vehicle types. Although these values describe typical heavy vehicles maximum loads. They do not allow for the more extreme weights that are becoming more and more common on the roads. Traffic models such as FLM4 and Auxerre do not represent the extreme values that are taken into account in the λ_{max} calculation. In addition to this, the application of the criterion of $D=0.01$ above the fatigue limit (CAFL), is not as effective with a traffic model because the load values and stress ranges are quite homogeneous. And in these cases, this limit often does not guarantee that the total damage value remains below 1.0. The following figure shows the total damage value when computing λ_{max} for the 3 traffic types.

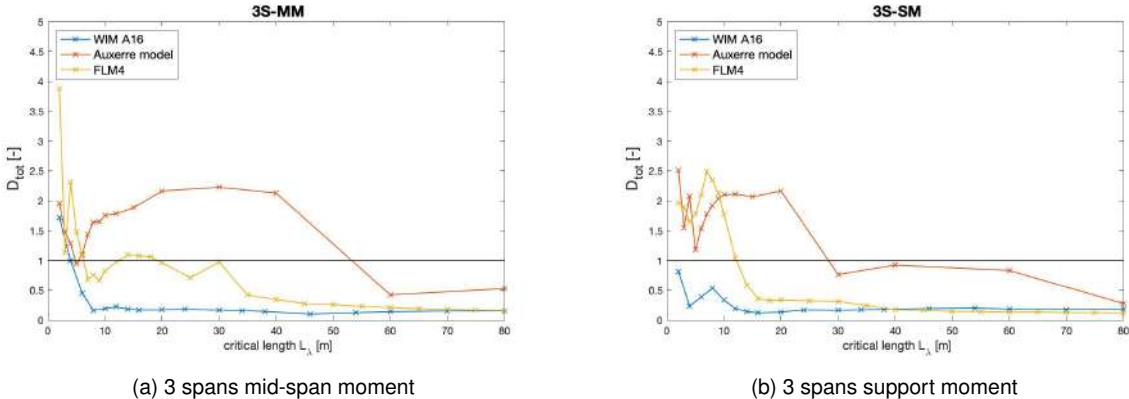


Figure 4.22. Total Damage - comparison real traffic model

The criterion seems to be more effective when calculation is performed with traffic measurements. Indeed, a large number of total damage values are higher than 1.0 for the calculations with FLM4 and Auxerre models. This means that the associated λ_{max} values are not "acceptable" as they are not safe. This also means that the λ_{max} would remain below the one for λ_1 , as the λ_1 values are defined to produce a total damage of $D = 1.0$. As explained above, this is mainly due to the fact that the stress histogram is less spread out for traffic models than for real traffic where extreme values are considered. It is therefore normal that with a fairly clustered histogram with fairly close stress ranges, there is not a great gap between λ_1 and λ_{max} values. It would therefore be a mistake to use modelled traffic that does not consider extreme values of stress, as this would not be representative of reality. The figure 4.23 shows the intended effect of the stress histogram repartition.

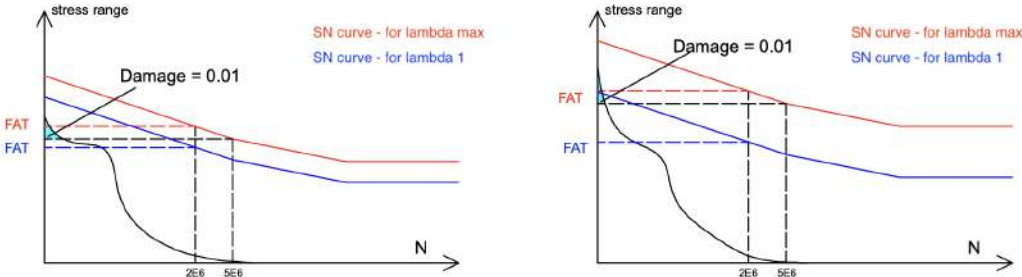


Figure 4.23. Effects of the stress histogram repartition

For traffic load models, the maximum stress ranges are less spread out, this is due to the fact that the vehicles are defined with systematic load values. The stress histogram can then become very homogeneous and very clustered. The risk is then that the difference between the criterion for λ_{max} and λ_1 will become very close and even that the strength curve associated with λ_{max} could end up below λ_1 . This explains why the use of WIM measurements was preferred for the recalibration of the λ_{max} factor.

4.5 Dynamic amplification factor

4.5.1 Relevance of dynamic consideration

Dynamic effects can obviously have an influence when calculating and determining road traffic effects. It is not easy to describe dynamic effects because they depend on many parameters. As referring to road bridges, it is then necessary to determine the behaviour due to the interaction between the structure and the passage of vehicles. There are three main parameters to be considered, namely the dynamic properties of the vehicle, the response of the bridge and the contact surface.

To represent the effect of the vehicle model on the dynamic responses. In the background to EN 1991-2 [8], 2 types of trucks were studied, namely a single truck with single axles connected to a rigid body and an articulated truck where the trailer is connected by elastic coupling. The vehicle model defined the structure of the vehicles, the suspension systems and the tires properties.

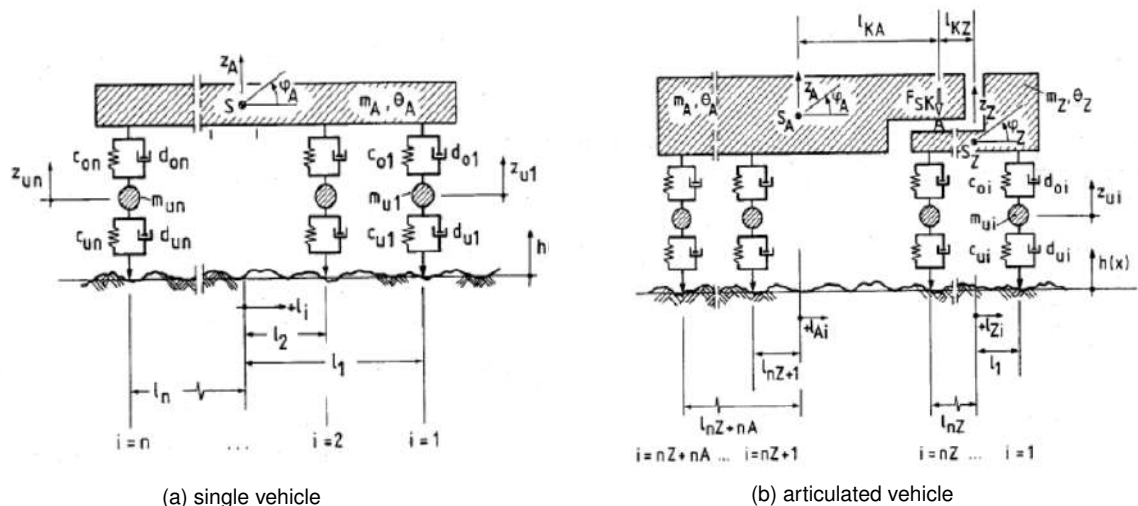


Figure 4.24. Vehicle vibration model, extracted from [8]

The mechanical model of the bridge must also be determined in order to study the interaction between the vehicles and the bridge dynamic response. To do this, the model is described to determine the eigenfrequencies and eigenmodes of the structure and the deflection and action effects resulting from the excitement due to traffic. The bridge can therefore be discretized by finite elements method, assuming planar continuous beam with distributed masses with linear elastic behaviour and viscous damping.

The roughness of the road can be of 3 kinds; local irregularities, regular unevenness (due to fabrication) and irregular unevenness. From power spectral density measurements of roadway roughness, it is possible to characterize the quality of roadway pavements. The figure 4.25 shows the power spectral density $\phi(\Omega_0)$ for typical road surfaces.

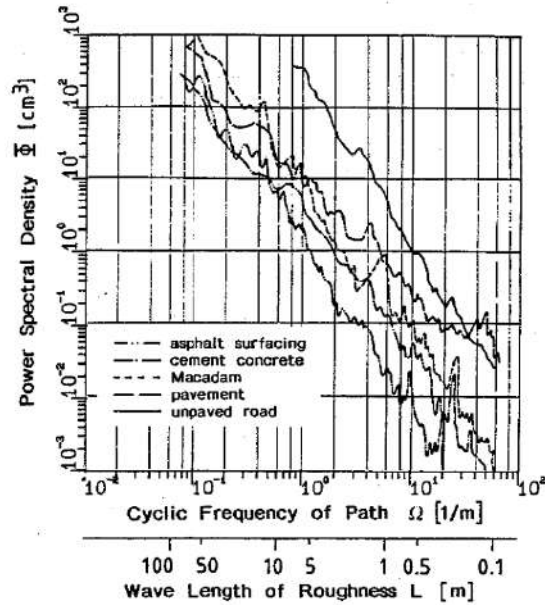


Figure 4.25. Power spectral density of roadway roughness, extracted from [8]

The classification of roughness is therefore a function of the power spectral density and the classification can be done according to the figure 4.26. These values together with power spectral density distribution are then used to determine a discrete profile using a Fourier series which lead to a stochastic profile as in figure 4.27.

Quality of pavement $\sigma(\Omega_0)$ [cm^3] for $\Omega_0 = 1 [m^{-1}]$, $w = 2$			
	lower limit	mean value	upper limit
very good	0.5	1	< 2
good	2	4	< 8
average	8	16	< 32
poor	32	64	< 128
very poor	128	256	< 512

Figure 4.26. classification of roadway roughness, extracted from [8]

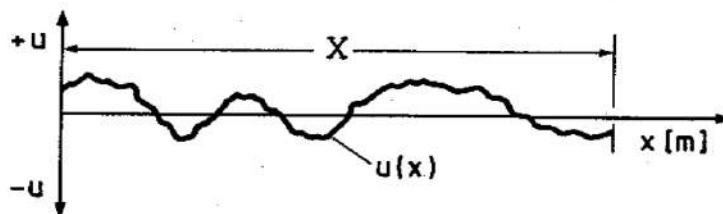


Figure 4.27. Stochastic unevenness profile, extracted from [8]

These models presented above could then be calibrated on the basis of real loading tests, notably during a test performed on a road bridge in Switzerland. This test used a 2-axes lorry with leaf suspension crossing the bridge with speeds from 10 to 70 km/h. The results could then be calibrated and compared between the measurements and the calculated models. It turned out that the calculations reflect the test measurements quite well. The figure 4.28 shows the comparison of time-histories deflection for crossing speeds of 15 km/h and 65 km/h.

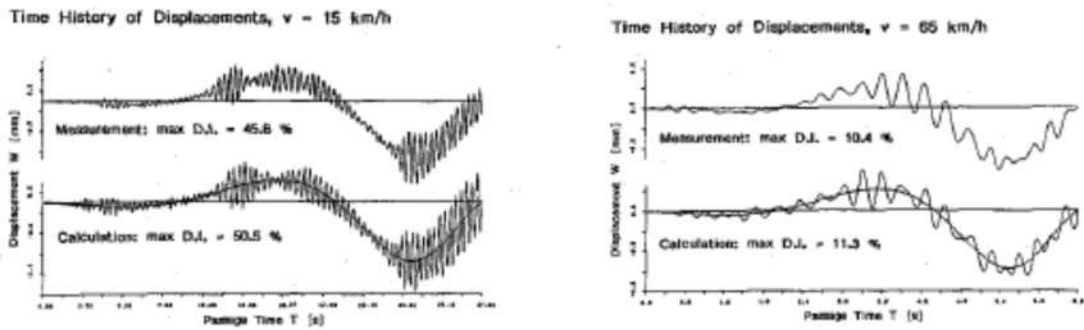


Figure 4.28. Comparison of time-histories for speeds of 15 km/h (L) and 65 km/h (R), extracted from [8]

It is clear that the vibration is composed of a natural vibration due to the response of the bridge accompanied by a secondary oscillation due to the excitation of the vehicle. This calibration allowed calculations to be made for different configurations, with different bays and different truck types. In the following figure the dynamic increment is plotted against the fundamental frequency of the road bridge. The calculation is shown for a single vehicle with pneumatic suspension and leaf suspension.

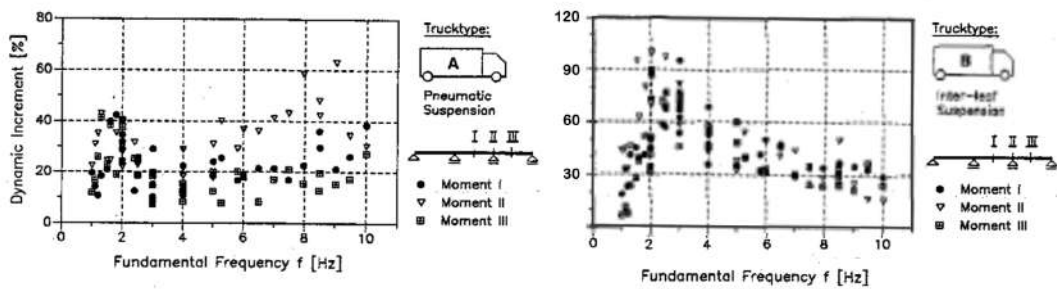


Figure 4.29. Dynamic increments of moment as a function of the fundamental frequency, extracted from [8]

This shows the importance of the vehicle model and in this case the type of suspension which can lead to large differences in the dynamic increment. However, for articulated trucks, the dynamic increment is less important for most of the case as shown in figure 4.30.

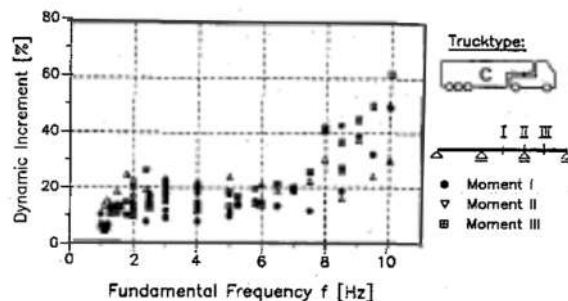


Figure 4.30. Dynamic increments of moment as a function of the fundamental frequency, extracted from [8]

In reality, the effect of vehicles is higher for high frequencies, which corresponds to short span lengths. The dynamic effect is increased to a large extent by the passage of double and triple axles. But for most cases, where the spans are longer, the dynamic effect is considerably reduced compared to single

vehicles. These calculations represent the dynamic effects when a single vehicle passes over the bridge, however it is also necessary to establish what happens when a convoy of vehicles cross the road bridge simultaneously. Similarly, in figure 4.31, the dynamic increment is calculated for a series of vehicles crossing the bridge at a speed of 40 km/h with a inter-vehicle distance of 5 m. What is observed is that the dynamic increment is reduced considerably for span lengths above 30m.

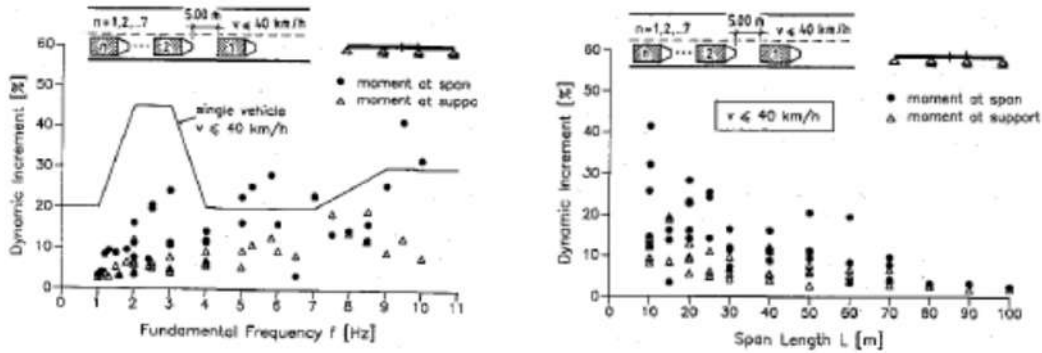


Figure 4.31. Dynamic increments of moment for convoy of vehicles, extracted from[8]

4.5.2 Dynamic amplification in Load models

The determination of Load Models in EN 1991-2 [18] is based on several traffic measurements, but to determine the load values, the dynamic effects has to be considered. Firstly, measurements, although calibrated, inevitably contain dynamic amplification due to the conditions at the point of measurement. Calibration allows to extrapolate the share of dynamic amplification in the measurement. The dynamic amplification factor can be defined as :

$$\varphi = \frac{E_{dyn}}{E_{stat}} \geq 1.0 \quad (18)$$

- E_{dyn} : dynamic action effect
- E_{stat} : static action effect

The implicit dynamic factor has been extrapolated in the background document to EN 1991-2 [8] for characteristic value of axles and vehicles loads. The dynamic factor is equal to 1.10 for vehicle loads and 1.14 for axles loads.

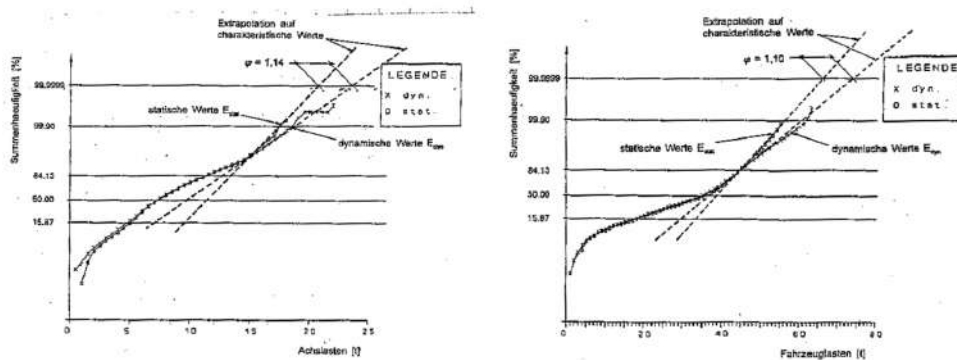


Figure 4.32. Dynamic factor in weight measurements, extracted from[8]

For Load Model 1, it includes a certain amplification factor due to roadway roughness. The deduced characteristic value is therefore equal to $Q_k=300$ kN instead of the characteristic value deduced from

measurements equal to 279 kN. For Load Model 2, the implied dynamic factor of 1.14 was deemed insufficient, particularly as LM2 is specified for elements with small influence lengths $L \leq 20m$. It has been shown that for short span lengths, the effect of local irregularities can become significant. The figure 4.33 shows the amplification factor due to local irregularity (modelled with a thickness of 30 mm).

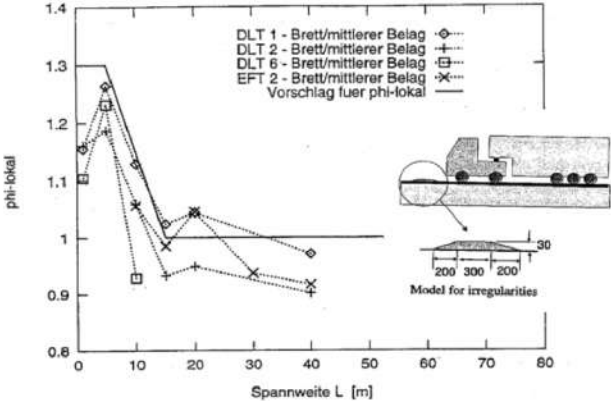


Figure 4.33. Impact factor for local irregularities, extracted from[8]

An additional dynamic factor of 1.3 (with reference to the maximum value in figure 4.33) has been applied in Load Model 2, which lead to a value of 400 kN (approximately 30% more than LM1).

For Fatigue Load Model 1 to 4, they also considers a dynamic amplification factor of 1.10 which is set for good quality pavements. It is necessary to differentiate this dynamic amplification which is directly included in the Fatigue Load Model with the dynamic factor φ_{fat} . This supplementary factor, presented in figure 4.34, needs to be use when check is done for elements near expansion joints.

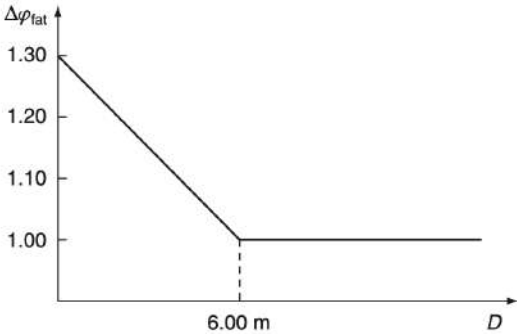


Figure 4.34. Additional amplification factor near expansion joints, extracted from [16]

4.5.3 Dynamic amplification factor for λ curves determination

Dynamic amplification factors are calculated for special cases, e.g. to take into account a vehicle on the adjacent lane, or for the case of very short spans. In reality, high dynamic effects are quite rare and do not necessarily coincide with the highest load cases. It is therefore not easy to find a realistic factor that does not overestimate the dynamic effects, especially when calculating the λ curves. When using traffic measurements for the calibration of λ curves, there is obviously a dynamic effect already included in the measurements, but it may be necessary to multiply these values by an additional dynamic factor. Since an amplification of around 10% is estimated in the measurements, a large part of the dynamic effects

is already included in the computation. This value of about 10% is found in several references, in the background document to EN 1991-2 [8], the extrapolated value is 10 or 14% depending on whether one considers the total vehicle load or only the axle load (see figure 4.29), in the background to SIA codes 160:1989 [11] a value of 1.05-1.15 is mentioned for most of measurements on bridge. In the Maljaars studies [14] using WIM measurements from Dutch A16, the WIM system is classified with an accuracy of 10% between static and measured vehicle weight. Maljaars [14] also shows the calibration that was done with a known vehicle static weight. The structural system of the bridge is presented in figure 4.35, and the comparison between the calculation with static weights and the measured stress for crossing speeds of 20 km/h and 85 km/h is related in figure 4.36.

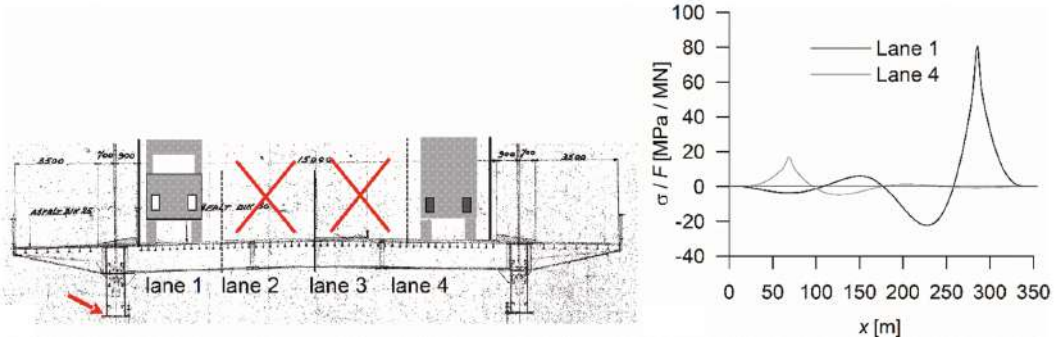


Figure 4.35. Cross section of the bridge and influence lines (validation test in Dutch A16), extracted from [14]

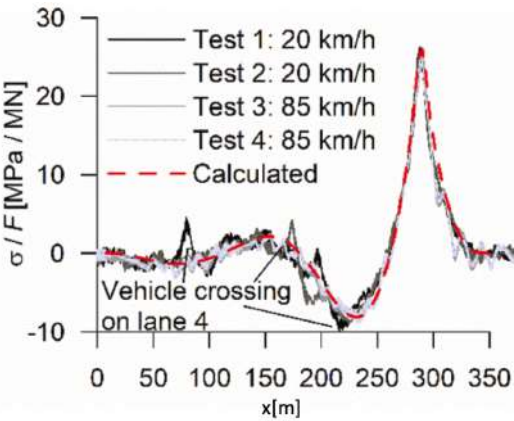


Figure 4.36. Measured and calculated bridge response in validation test in Dutch A16, extracted from [14]

As explained in [14], The test results show a good agreement between the measurements and the calculated stresses. Some peaks are visible at speeds of 20 km/h, which are due to vehicles passing on the opposite lane. Stress variations are indeed observed at a frequency close to the natural frequency of the bridge with a magnitude of 10% of the largest stress recorded, however for the highest measured stress value, it is the same regardless of the speed. The value is also very close to the calculated value without any real amplification from the dynamic point of view. The model represents the extreme stress value very well.

However, the effect of bridge vibration, estimated at 10%, does not necessarily reflect the overall amplification in terms of stress range. The dynamic amplification to be applied in terms of fatigue must certainly be lower. The figure 4.37 from [14] shows the comparison between the stress histogram from measured strains and from WIM simulations applying a dynamic factor of 1.0, 1.03 or 1.05.

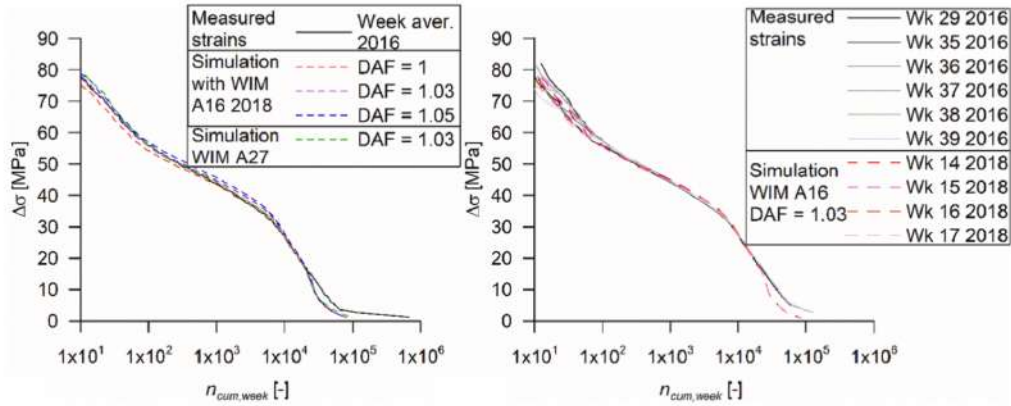


Figure 4.37. Stress ranges histogram using strain gauges and WIM measurements, extracted from [14]

The difference between the values from simulations using the WIM database and the measured values is very small. The only deviation in the stress histogram occurs at very low stress values (smaller than 10 MPa), which is easily explained by the fact that the WIM measurements only take into account heavy vehicles. However, in terms of fatigue, these low stress range values are negligible in the damage calculation and have no real influence on the total damage.

Measured strains	WIM, DAF = 1	WIM, DAF = 1.03	WIM, DAF = 1.05
$2.33 \cdot 10^{-4}$	$2.06 \cdot 10^{-4}$	$2.38 \cdot 10^{-4}$	$2.61 \cdot 10^{-4}$

Figure 4.38. Weekly damage for $\Delta\sigma_D = 59$ MPa, extracted from [14]

The comparison was also made in terms of damage per week for $\Delta\sigma_D=59$ MPa. It seems that this range between 1.0 and 1.03 for DAF is a good match for finding an adequate damage. The numerical simulations presented in the next section therefore not include a dynamic amplification factor on the WIM measurements values as the additional effects are not decisive, even if a DAF of 1.03 could have been justified.

5 Analysis of the results

5.1 Final parameters for the λ_{max} curves

The final simulations for the λ_{max} factor are set with the following parameters:

- Fatigue strength curve slope: $m|k=3|5$
- Fatigue Load Model: FLM3 with a single lorry of 480 kN, divided in axles
- Bridge design life: 100 years
- Criterion: λ_{max} set for $D_{CAFL} = 0.01$
- Real Traffic Model: WIM measurements (A16-NL, Sweden, Löddekopinge, Ceneri, Gotthard, Denges) without dynamic amplification factor
- Heavy vehicles per year: annual heavy vehicles observed for each traffic
- Inter-vehicles distance: measured distances extracted from WIM measurements

5.1.1 Spans length

The final curves are presented for spans length until 200 meters. The simulations use 33 spans length: 2, 4, 6, 8, 10, 12, 14, 16, 18, 20, 24, 30, 34, 38, 46, 54, 60, 70, 80, 90, 96, 100, 106, 110, 116, 120, 126, 130, 140, 150, 160, 170, 180, 200. It will allow to determine the behaviour for longer spans than 80m as defined in the current standards.

5.1.2 Critical length L_λ

To determine the critical length according to the influence line, **adjustments** have been made to the indications prescribed in EN 1993-2 [20].

- for moments
 - for a simply supported span, the span length L_i
 - for continuous spans in mid-span sections, the span length L_i of the span under consideration
 - for continuous spans in support sections, the mean of the two spans L_i and L_j adjacent to that support (**except for static systems with only two spans which have a ratio 1.2, in this case the sum of the two spans L_i and L_j adjacent to that support**)
 - for cross girders supporting stringers, the sum of the two adjacent spans of the stiffeners carried by the cross girders
- for shear for a simply supported span and a continuous span
 - for the support section, the span under consideration L_i
 - **for the mid-span section, the span under consideration L_i**
- for reactions
 - for end support, the span under consideration L_i
 - for intermediate supports, the sum of the two adjacent spans L_i and L_j
- for arch bridges
 - for hangers, twice the distance between hangers
 - for arch, half the span of the arch

5.2 λ_{max} results

As the traffic patterns are significantly different among the available WIMs, the results are classified by country in a first step (Dutch A16, Sweden and Switzerland). This preliminary classification makes it possible to understand the differences in traffic and to verify that the results remain similar for very comparable traffic within the same country. An overall analysis will be made in the next sections. Moreover, the large number of influences lines requires to classify the results in an efficient way. The results are classified in 4 groups: mid-span moment, support moment, mid-span shear and support shear.

5.2.1 A16, Netherland

The simulations used the sample of 100'000 vehicles from the WIM measurement of the A16. The estimated number of lorries per year on slow lane is 2'100'000. The calculations therefore took into account this value of N_{obs} to simulate an annual traffic of 2'100'000 heavy vehicles over a design life of 100 years. The figure 5.1 shows the simulation results for mid-span and intermediate bending moment

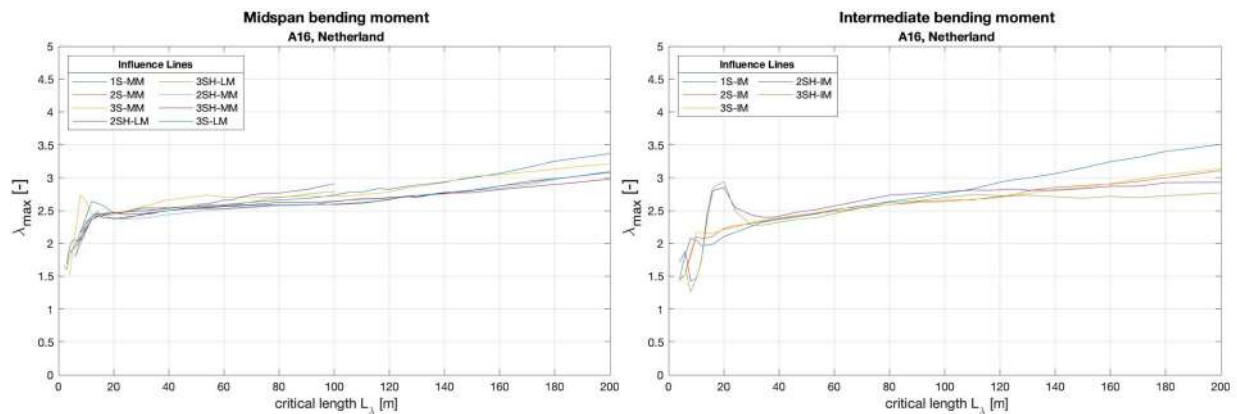


Figure 5.1. λ_{max} curves for mid-span(L) and intermediate bending moment(R)

The results between the mid-span and the intermediate bending moments, which are located at the boundary between the support sections and the span sections (at a distance of 0.15·L from the support), are quite close. For long critical length, the slope of the curve is quite similar. The greatest difference remains in the peak that is a little higher and shifted to the right for the intermediate moments. The figure 5.2 presents this time the λ_{max} results for support bending moment and support shear.

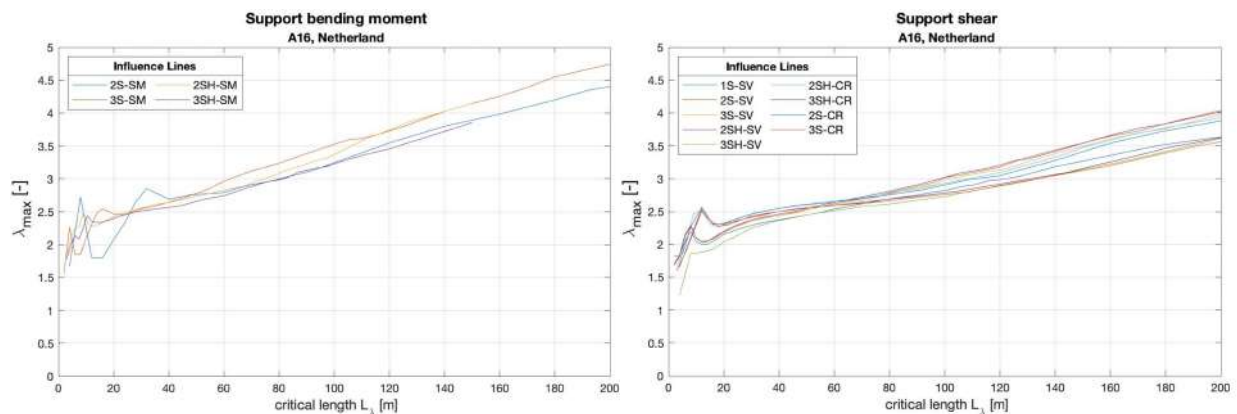


Figure 5.2. λ_{max} curves for support bending moment(L) and support shear(R)

The results for support bending moments confirm that the λ_{max} values obtained for longer spans are relatively higher than for mid-span moments. The results show a steeper curve than for mid-span locations. This shows that for the bending moments, λ_{max} for the intermediate sections are closer to the behaviour of the mid-span sections. In figure 5.3, the results for mid-span and intermediate shear are presented.

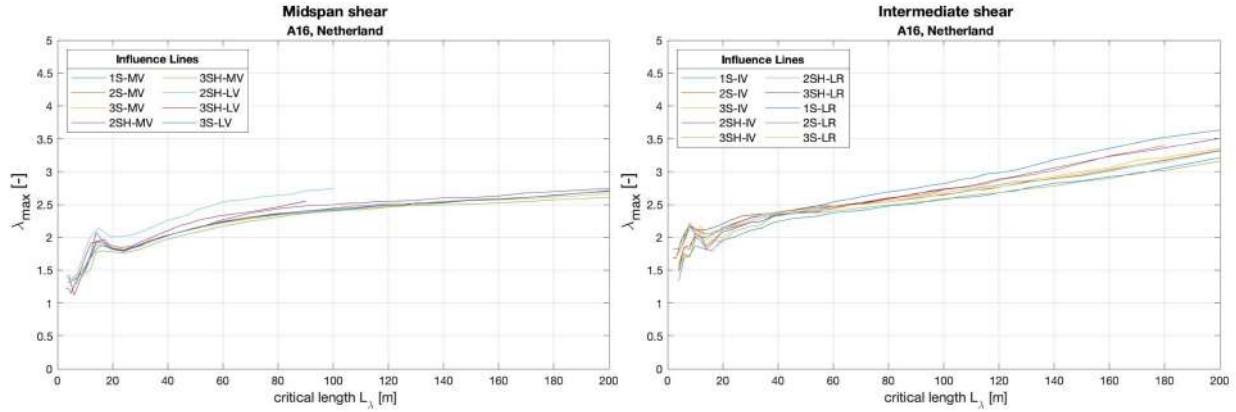


Figure 5.3. λ_{max} curves for mid-span shear(L) and intermediate shear(R)

The λ_{max} results for shear forces have similar behaviours but the difference remains in the evolution of the slope for longer spans. For support sections, the slopes is the steepest, whereas for mid-span sections, these are much lower. In contrast to bending moments, the intermediate section does not refers to mid-span sections, as the results are between the two extremes of mid-span and support sections locations.

Classification To compare the results later on between the different traffics and to be able to propose new λ_{max} curves, the results obtained for the influence lines are checked and processed. Firstly, the results are checked to be acceptable according to the following two conditions: the damage above the constant amplitude fatigue limit must be equal to $D=0.01$ with a tolerance of 3%, and the total damage must be smaller than or equal to 1.0.

$$0.0097 \leq D_{CAFL} \leq 0.0103 \quad (19)$$

$$D_{tot} \leq 1.0 \quad (20)$$

Then the values that satisfy these 2 conditions are kept and a linear interpolation is carried out on the basis of these values. The interpolation is performed meter by meter for span lengths ranging from 10m to 200m. The following figures (5.4 and 5.5) show the results interpolated in this way. The results here are classified into 5 groups:

- Mid-span bending moments: regroups mid-span, intermediate and lateral bending moment.
- Support bending moments
- Mid-span shear: regroups mid-span shear and lateral shear
- Intermediate shear: regroups intermediate shear and lateral reaction
- Support shear: regroups support shear and central reaction

The λ_{max} values for spans from 1 to 10 meters are not interpolated because, depending on the influence lines, a large number of values are not acceptable under the conditions described above. The acceptable values for the short spans are nevertheless shown in the graphs.

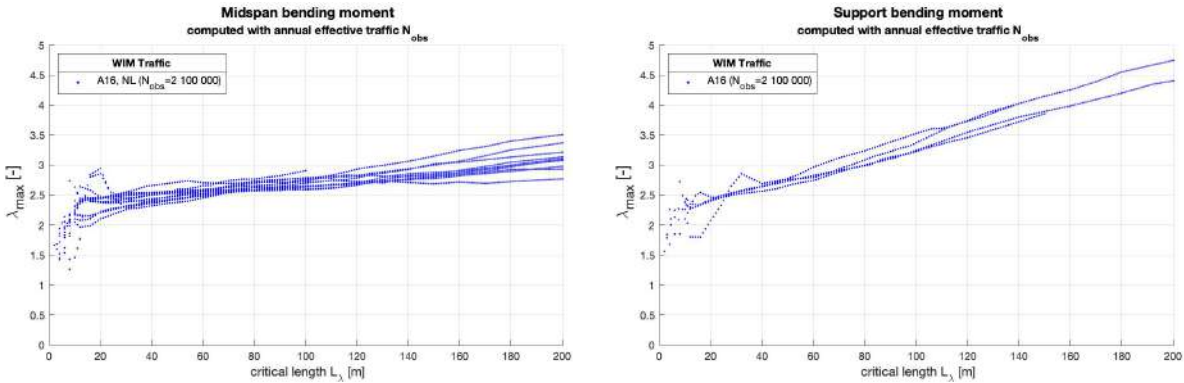


Figure 5.4. λ_{max} for mid-span (L) and support bending moments(R) - A16, Netherlands

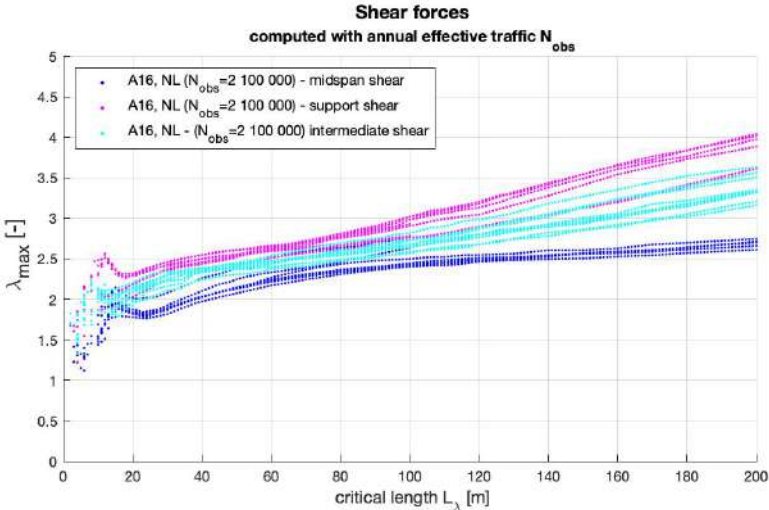


Figure 5.5. λ_{max} for shear forces - A16, Netherlands

When the various influence lines for shear force are grouped on the same graph, 3 distinct behaviours are observed depending on the location of the section. Mid-span locations being the lowest λ_{max} curves and support shear influence lines being the highest. Concerning the intermediate sections, their behaviour lies between these two extremes defined for support and mid-span locations.

5.2.2 Switzerland

λ_{max} Results of Weight in Motion from Ceneri, Gotthard and Denges stations are determined here. The interpolated results are directly presented in figures 5.6, 5.7, 5.8 and 5.9 the method is the same as described in the previous section. Once again, the simulations use a sample of 100'000 lorries from each WIM measurement. But this time the estimated number of lorries per year on slow lane is quite different from the A16. The number of passages is obviously much lower for Swiss traffic and the simulations therefore use the estimated annual number of heavy vehicles:

- Ceneri: $N_{obs} = 675'000$
- Gotthard: $N_{obs} = 400'000$
- Denges: $N_{obs} = 500'000$

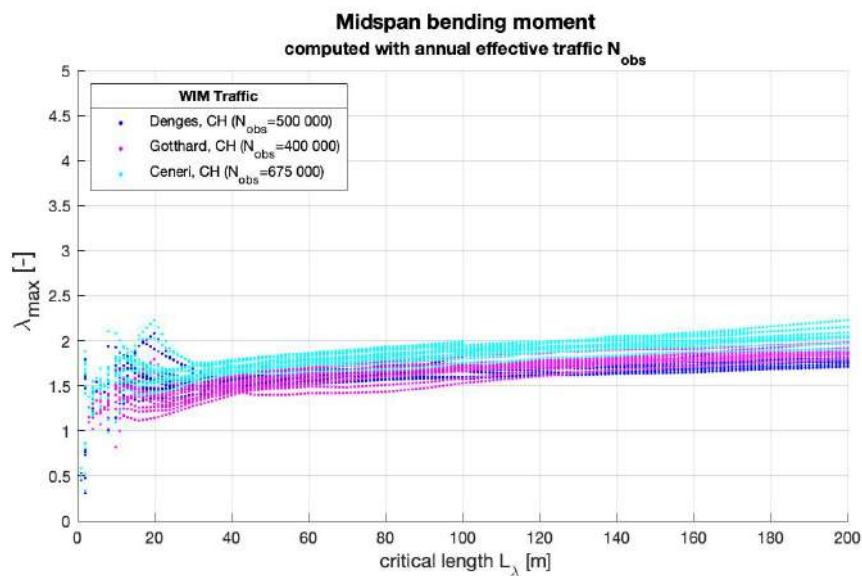


Figure 5.6. λ_{max} for mid-span bending moments - Switzerland

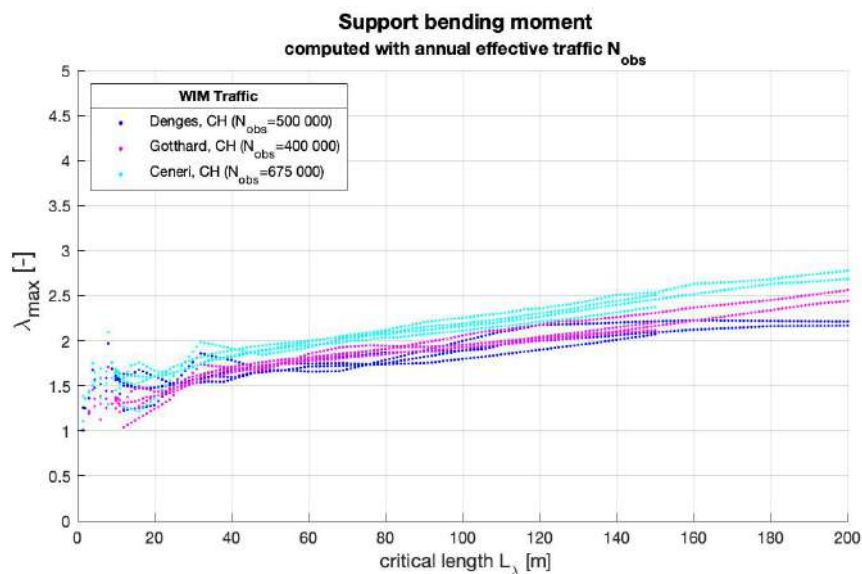


Figure 5.7. λ_{max} for support bending moments - Switzerland

The results are quite similar between the 3 WIM stations, the same behaviour of the curve is observed, with some slight shifts between the traffics. However, the difference with the results from A16 is quite large. It should be highlighted that the fatigue action is quite different because of the number of heavy vehicles (four times larger for A16, NL). The volume of traffic seems to have a great influence on the λ_{max} results.

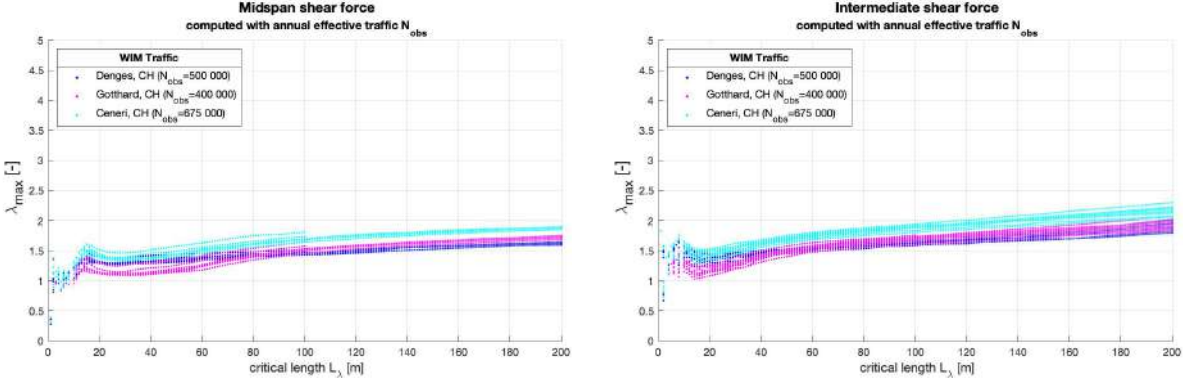


Figure 5.8. λ_{max} results for mid-span(L) and intermediate shear forces(R) - Switzerland

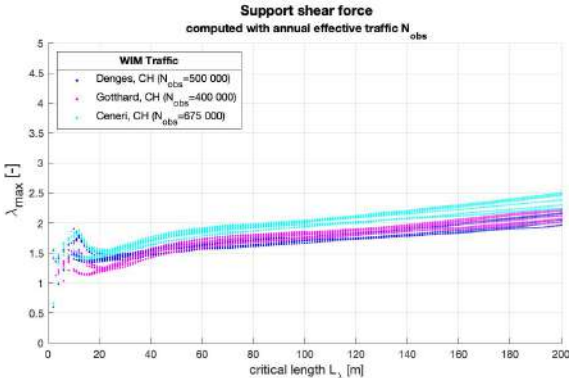


Figure 5.9. λ_{max} results for support shear force - Switzerland

The same tendency is found with fairly similar results for all the influence lines studied. Concerning shear forces, we distinguish 3 slightly different behaviours when grouped by mid-spans, supports and intermediates sections. It is noticeable that the results of the Ceneri are always higher than the other two traffic which could support the idea that the traffic volume has a real influence on λ_{max} .

5.2.3 Sweden

For the Swedish traffic, 2 available Weight in Motion measurements are used for the numerical simulations. The first WIM measurement is located at Löddeköping and the second one is a combination of measurements from various stations across Sweden. The Löddeköping measurement is however quite small, the sample size is only from 10'000 vehicles, so one has to be careful with the results of this traffic data as it is not as representative as the other available samples. The estimation of the traffic volume is difficult for the WIM measurements from Sweden, since it takes into account several different stations, nevertheless an average estimation has been made, so the traffic volumes used are the following: $N_{obs}=400'000$ for sweden and $N_{obs}=500'000$ for Löddeköping. The interpolated λ_{max} results are presented in figures 5.10, 5.11, 5.12 and 5.13

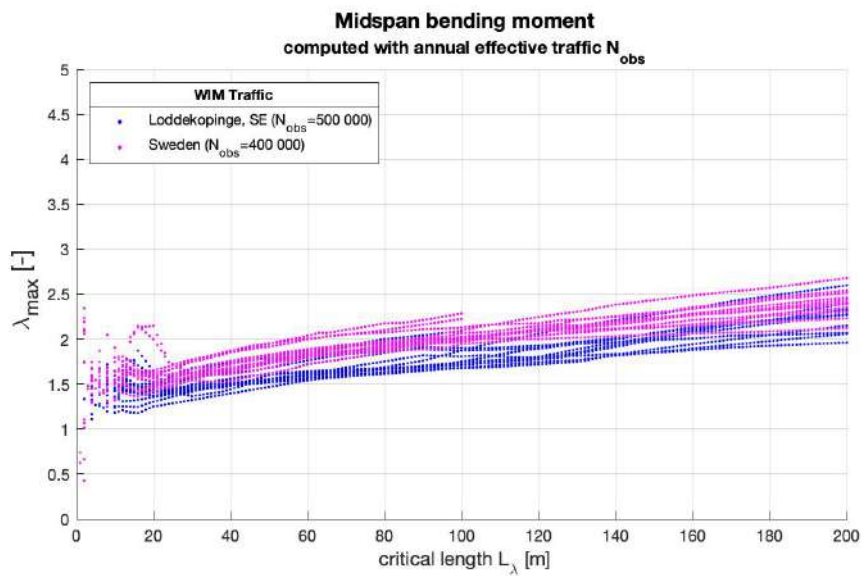


Figure 5.10. λ_{max} for mid-span bending moments - Sweden

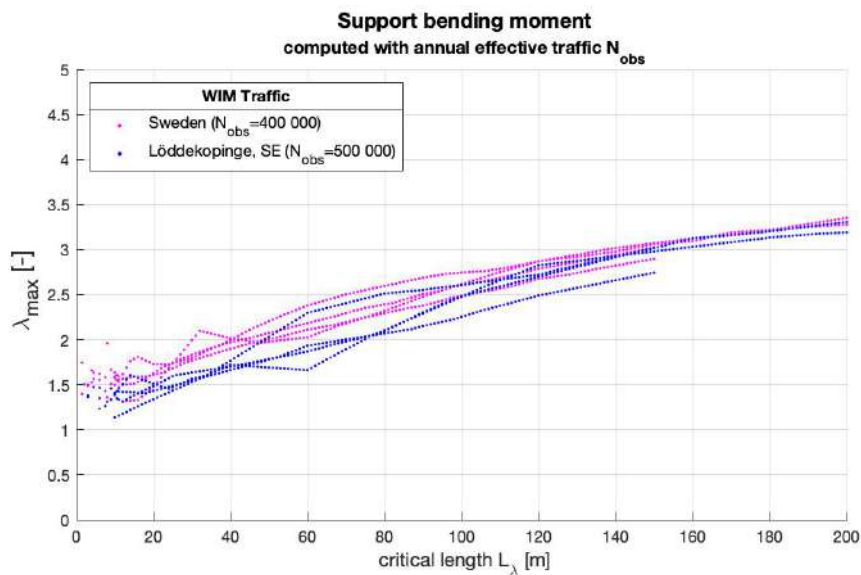


Figure 5.11. λ_{max} for support bending moments - Sweden

The results are quite similar, but there is a slightly steeper slope for Swedish traffic than for Swiss and A16 traffic. All results are compared together in the next section, but it is important to note that the Swedish traffic is significantly different as the traffic is heavier. This is due in particular to the large part of lorries that are much longer with more than 5 axles. These heavy loaded vehicles seem to have a direct impact on the λ_{max} results. This is especially true since in the Swiss and A16 traffic there are very few lorries with more than 5 axles and therefore the traffic appear to be less aggressive.

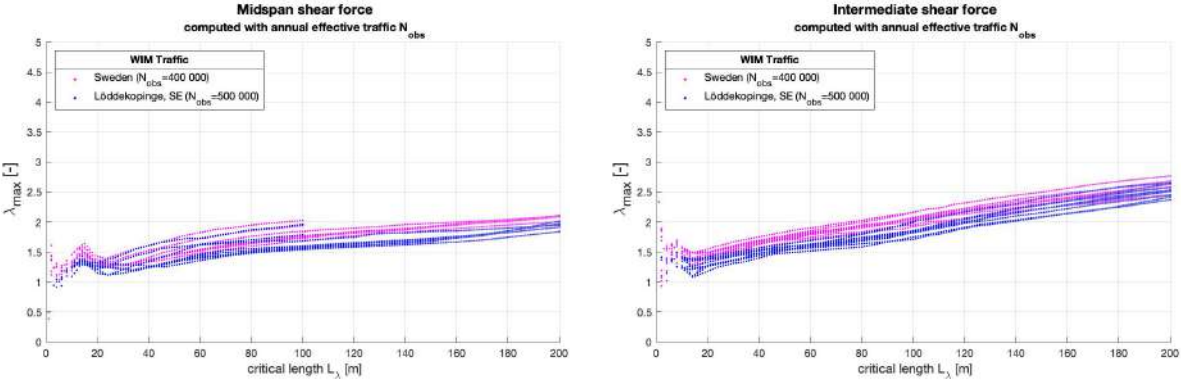


Figure 5.12. λ_{max} results for mid-span(L) and intermediate shear forces(R) - Sweden

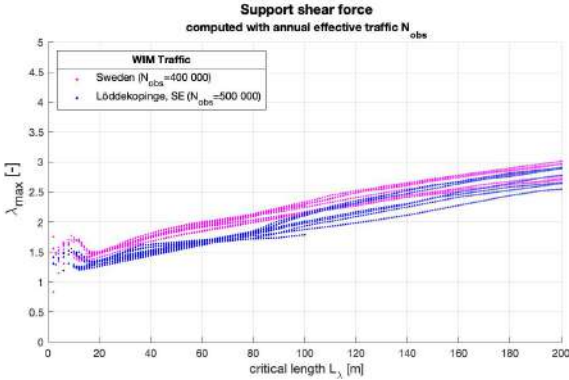


Figure 5.13. λ_{max} results for support shear force - Sweden

Same behaviour is determined as for the other Weight in Motion measurement results for shear forces. Namely, λ_{max} for mid-span shear forces is always the lowest in contrast to the support section which is always the highest. Every WIM measurements shows the same kind of behaviour, sometimes to different scale, but the results seems homogeneous.

In the next section, the WIM results are compared and put together on order to subsequently opt for the definition of new λ_{max} curves. This definition must take into account the variety of European traffic which can be described with the different WIM measurements that are used for numerical simulations. Following the results of the shear influence lines, it was decided to keep only the influence lines for mid-span and support sections. Even though the intermediate sections have a distinct behaviour, it always stays between the curves for mid-span and support shear and could be assimilated to the worst case (i.e. support shear forces). The λ_{max} curves defined in the following sections are for 4 cases; mid-span bending moment, support bending moment, mid-span shear force and support shear force

5.3 λ_{max} results comparison

In this section, the results of the different WIM traffic are compared. The results are put together to determine whether the λ_{max} correction factor behaves the same for the different traffic types. This part is necessary to subsequently produce new λ_{max} curves that are as representative as possible of European traffic. In figure 5.14, the comparison of λ_{max} results for each WIM is presented.

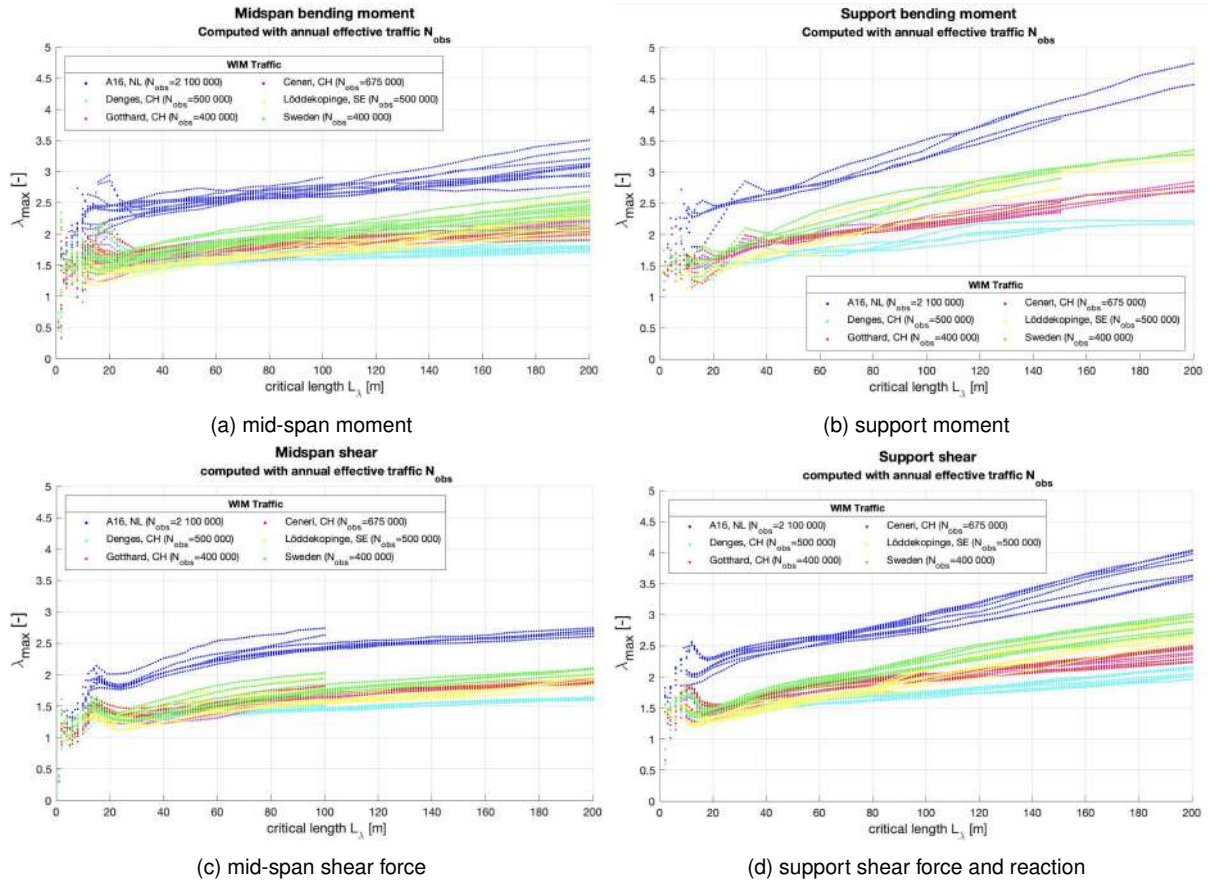


Figure 5.14. λ_{max} comparison for WIM measurements

The same trend can be observed in the various comparisons, namely that λ_{max} is much higher for traffic from the A16 in the Netherlands. However, the curves have a rather similar behaviour, especially a vertical shift between these curves. It should be noted that the simulations used the real estimated number of trucks per year, i.e. the traffic volume is relatively different, especially for the A16 which is about 4 times higher than the other available WIM measurements. It seems therefore that the traffic volume has a real influence on the λ_{max} factor. The volume of traffic has an impact on the damage caused because the structure is subjected to a greater number of cycles if the number of passages increases, but it must also have an impact on the distance between vehicles. Effectively, if the traffic increases, the road is more and more saturated, which leads to much smaller distances between vehicles. In this case, more configurations with interactions between vehicles are expected. This will lead to higher solicitations and therefore higher stress ranges. The λ_{max} factor should therefore be corrected with a factor close to the λ_2 factor which takes into account the traffic volume.

However, the λ_2 factor as described in EN 1993-2 [20] considers both the annual traffic and average weight of heavy vehicles. The problem here is that the average vehicle weight is not determinant in the calculation of λ_{max} because it is mainly function of the maximum loads acting on road-bridges and not

average loads. It therefore seems rather incorrect to apply a correction factor that takes into account the average vehicle weight. In order to correct the λ_{max} values, it is proposed to use an adjusted λ_2^* factor which only takes into account the annual number of heavy vehicles.

$$\lambda_2^* = \left[\frac{N_{obs}}{N_0} \right]^{1/5} \quad (21)$$

The value of the lambda correction factor should this time be bounded not by λ_{max} but by $\lambda_{max} \cdot \lambda_2^*$

$$\lambda = \lambda_1 \cdot \lambda_2 \cdot \lambda_3 \cdot \lambda_4 \leq \lambda_{max} \cdot \lambda_2^* \quad (22)$$

The table 5.1 presents the λ_2^* factor for each WIM measurements for $N_0 = 500'000$ and $N_0 = 2'000'000$.

	A16, NL	Gotthard, CH	Ceneri, CH	Denges, CH	Löddekopinge, SE	Sweden
N_{obs}	2'100'000	400'000	675'000	500'000	500'000	400'000
$\lambda_2^*(500'000)$	1.332	0.956	1.062	1.000	1.000	0.956
$\lambda_2^*(2'000'000)$	1.010	0.725	0.805	0.758	0.758	0.725

Table 5.1. λ_2^* factor for $N_0 = 500'000$ and $N_0 = 2'000'000$ heavy vehicles

5.3.1 λ_{max} corrected results - mid-span moment

Now, for all the results presented, the correction factor λ_2^* is applied. The figure 5.15 shows the comparison of λ_{max} for mid-span bending moment corrected for $N_0 = 500'000$ and $N_0 = 2'000'000$.

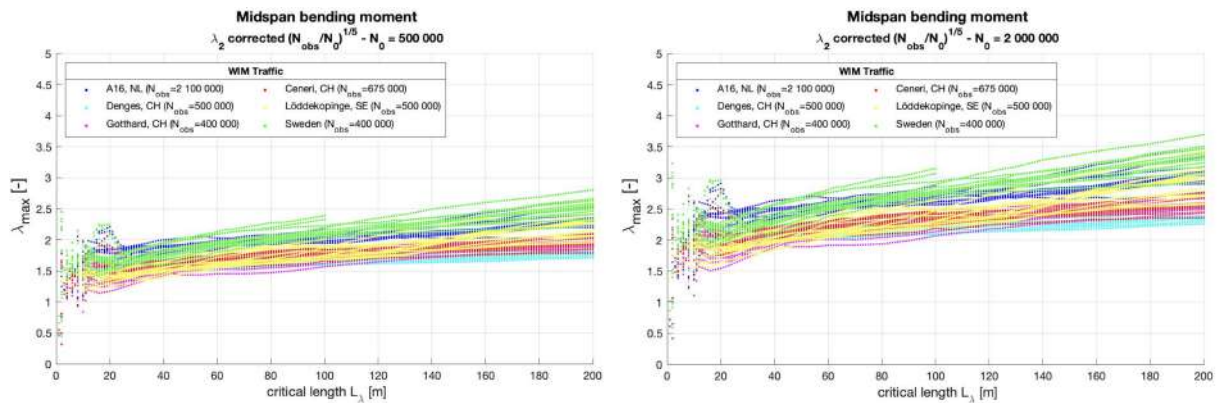


Figure 5.15. λ_{max} results for mid-span moment corrected with $N_0 = 500'000$ (L) and $N_0 = 2'000'000$ (R)

The correction seems to work well, as the results are quite well grouped regardless of the type of traffic. There are of course some small differences, especially between Swiss traffic which is quite light compared to Swedish and Dutch traffic. The A16 traffic is very dense and the Swedish traffic is very heavy with a large proportion of long vehicles with a large number of axles which could explain an increase in the λ_{max} factors for longer critical length.

5.3.2 λ_{max} corrected results - support moment

For the support moments, the correction reduces the gap between the curves as well, but we can notice 2 distinct groups between the very heavy traffic measurements (Sweden and A16) and the Swiss traffic measurements. Indeed, the slope of the curve is much lower for Swiss traffic. The influence lines for

the support moments seem to be more sensitive to heavy traffic, which is probably due to the axle arrangement and the heavier loads.

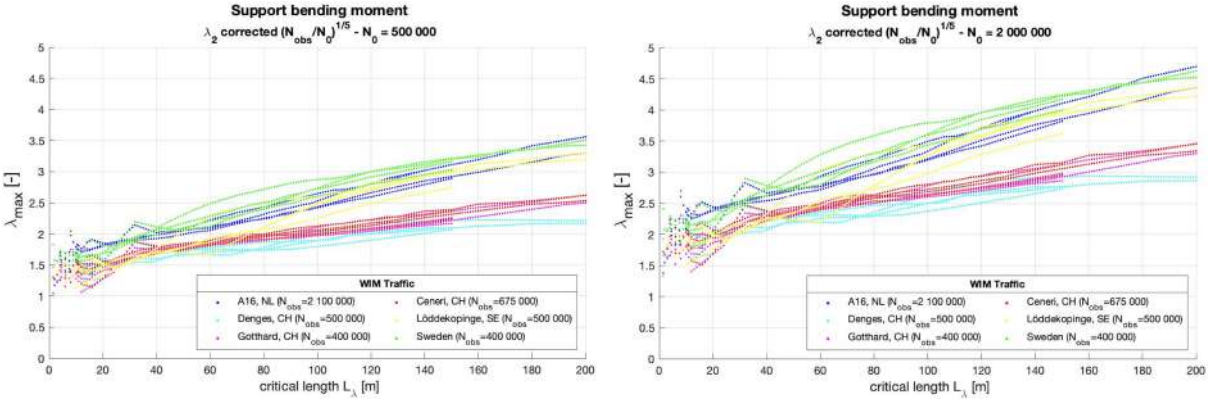


Figure 5.16. λ_{max} results for support moment corrected with $N_0 = 500'000$ (L) and $N_0 = 2'000'000$ (R)

The clear difference between the results is probably due to the distribution of traffic. In fact, in the Swiss traffic there are hardly any trucks with more than 5 axles, whereas the Swedish traffic is very heavy with a large part of lorries with 6, 7 or 8 axles (which represent about 30% of the traffic). As an example, the λ_{max} calculation was carried out for the 3S-SM influence line with a 5-axle truck and a 7-axle truck with the average weight distribution according to WIM measurements. This is not an exact picture of reality, as only one vehicle passes over the influence line, but it shows an idea of the effect of the two types of vehicle on fatigue loading.

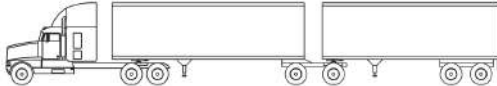


Figure 5.17. Typical 7-axles lorry from swedish WIM measurement

The example considers the "European" lorry described in the previous sections and assigns the average weights observed in the Swiss measurements. As for the 7-axle lorry, the layout most frequently found in the measurements is the one shown in figure 5.17. The ratio between the 2 curves presented below is close to 1.35 which corresponds roughly to the difference between the WIM results in figure 5.16.

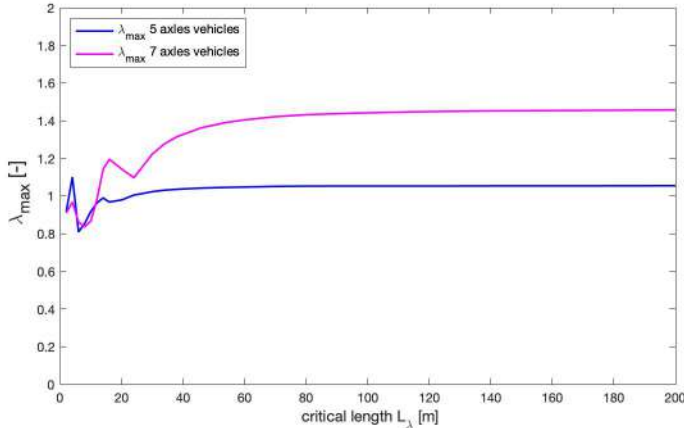


Figure 5.18. comparison 5-axle and 7-axle lorry

5.3.3 λ_{max} corrected results - mid-span shear

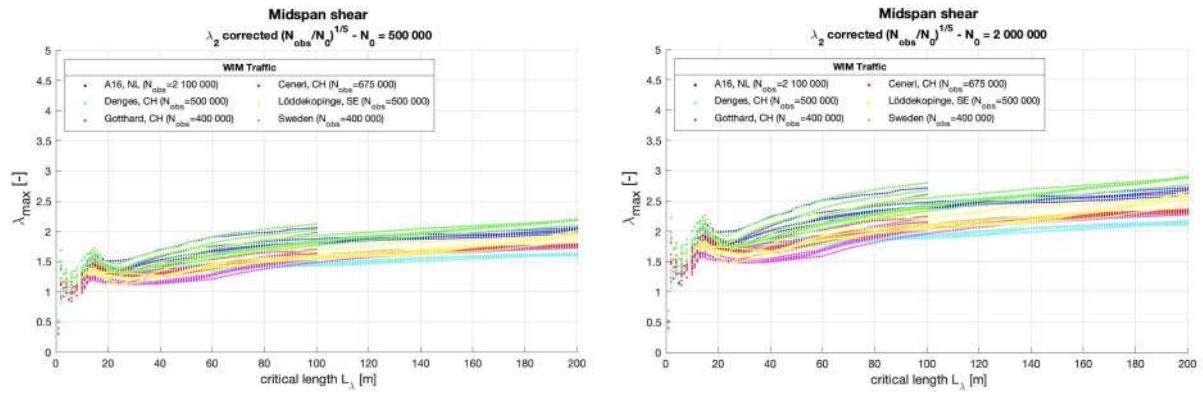


Figure 5.19. λ_{max} results for mid-span shear corrected with $N_0 = 500'000$ (L) and $N_0 = 2'000'000$ (R)

5.3.4 λ_{max} corrected results - intermediate shear

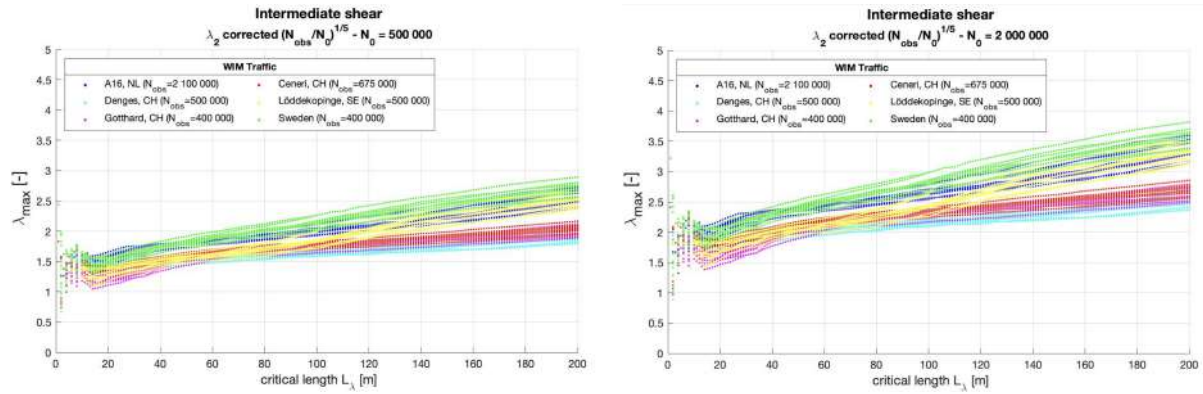


Figure 5.20. λ_{max} results for intermediate shear corrected with $N_0 = 500'000$ (L) and $N_0 = 2'000'000$ (R)

5.3.5 λ_{max} corrected results - support shear

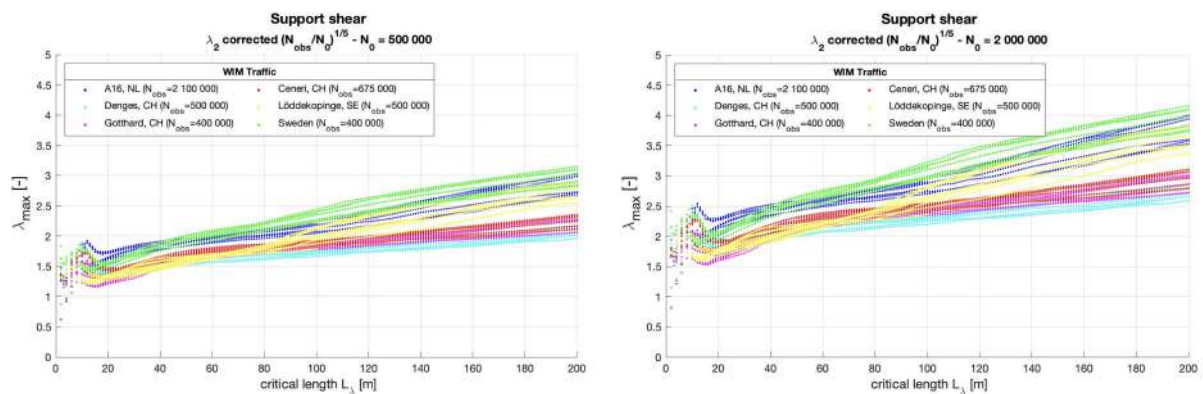


Figure 5.21. λ_{max} results for support shear corrected with $N_0 = 500'000$ (L) and $N_0 = 2'000'000$ (R)

For the three shear force groups, the correction makes it possible to bring the various λ_{max} curves and results closer together, and once again we observe a detachment between very heavy traffic and Swiss traffic for longer critical length. Indeed, a steeper slope can be observed for the Swedish and A16 traffic for intermediate and support shear forces. For mid-span shear force, the slope remains the same but there is a slight vertical shift between Swiss traffic and very heavy European traffic. Nevertheless the grouping of these results is a good basis for the proposal of new λ_{max} curves.

5.4 λ_{max} curves proposition

To propose new λ_{max} curves, the WIM results are corrected with the previously determined λ_2^* factor. The curves are interpolated meter by meter, which makes it possible to determine the mean and the standard deviation for each critical length value. For each group of results, the proposed λ_{max} curve is based on the 95% fractiles using approximating curve segments. The 4 groups of results from which the proposed curves are derived are:

- Mid-span bending moment
- Support bending moment
- Mid-span shear force
- Support shear force and reaction

5.4.1 λ_{max} proposition - mid-span moment

The figures 5.22 presents the interpolated results regrouping all the WIM measurements and the 95% confidence interval for each length L_λ . The proposed curve is divided into 3 segments, a plateau up to 20m, a convex curve between 20m and 30m, and a straight line from 30m. The interpolation occurs from 10 to 200 meters, for shorter spans, the calculated results are directly plotted without interpolation. The confidence interval is also determined for short spans, but the number of values is not always the same depending on the critical length due to the correction applied on the critical length for certain influence lines.

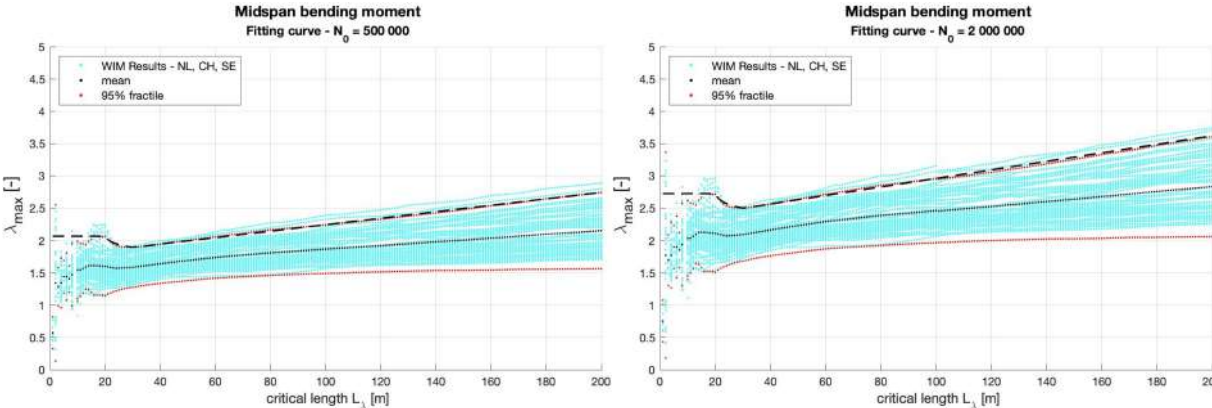


Figure 5.22. λ_{max} fitting curve for mid-span moment corrected with $N_0 = 500'000$ (L) and $N_0 = 2'000'000$ (R)

The same approach is applied for 2 references values, $N_0 = 500'000$ and $N_0 = 2'000'000$. The curve is the same for both figures, it is simply fitted with the same λ_2^* factor used for the results correction. The proposed reference curve is that for 500'000 heavy vehicles per year, as N_0 is actually described in Eurocode EN 1993-2 [20]. However, the curve should be corrected upwards for heavier traffics using the λ_2^* correction.

5.4.2 λ_{max} proposition - support moment

As for the previous proposition, the support bending moments curves are also determined in figure 5.23. However, the difference between the various WIM is greater for support moments due to the sensitivity of these influence lines, as seen in figure 5.16. Then, to compute the confidence interval, only the Swedish and A16 traffic data were used. The behaviour of Swiss traffic is too different from the ones from Sweden and the Netherlands and the correction factor is not able to cope for this effect. Therefore, it was preferable to use only the most unfavorable traffics in order to find an upper bound curve for λ_{max} .

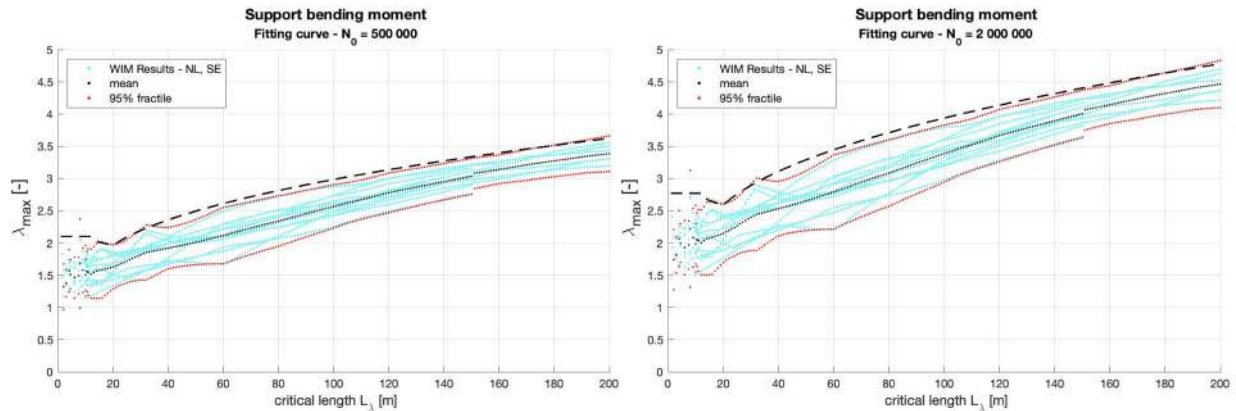


Figure 5.23. λ_{max} fitting curve for support moment corrected with $N_0 = 500'000$ (L) and $N_0 = 2'000'000$ (R)

Here again, the curve is composed of 3 segments in order to best follow the confidence interval. A plateau up to 12m, a convex curve from 12m to 18m, and this time the third part of the curve is a concave curve instead of a straight curve. It is clear that the values obtained are much higher than for mid-span moments, especially for longer spans.

5.4.3 λ_{max} proposition - mid-span shear force

For mid-span shear forces, the proposition curve presented in figure 5.24 is also composed of 3 curve segments to follow the confidence interval. For short spans, between 5 and 15 meters, we clearly see that the results are smaller than the proposed curve, however it has been decided to keep the same definition of the curve with a plateau for short spans to stay on the safe side. In addition to that, it allows to have a homogeneous definition between the λ_{max} curves for the different influence lines.

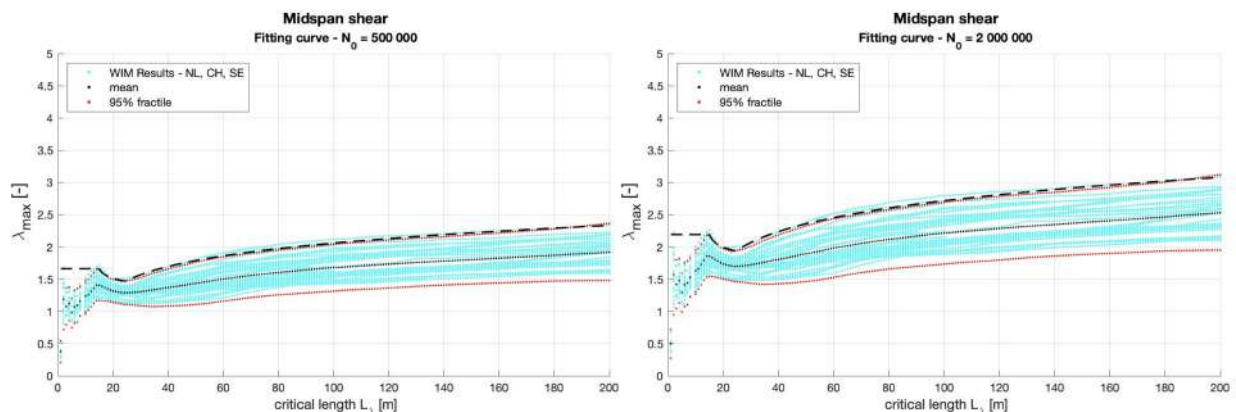


Figure 5.24. λ_{max} fitting curve for mid-span shear corrected with $N_0 = 500'000$ (L) and $N_0 = 2'000'000$ (R)

5.4.4 λ_{max} proposition - support shear force and reaction

In comparison to the mid-span shear, there is a clear upward shift in the results for support shear forces. The proposed curve in figure 5.25, is again composed of 3 segments. As for the proposed curve for mid-span bending moments, the third segment is a straight line. The curve follows the confidence interval for longer spans extremely well. For the short spans, as for the mid-span shear the curve has been plotted with some safety margin.

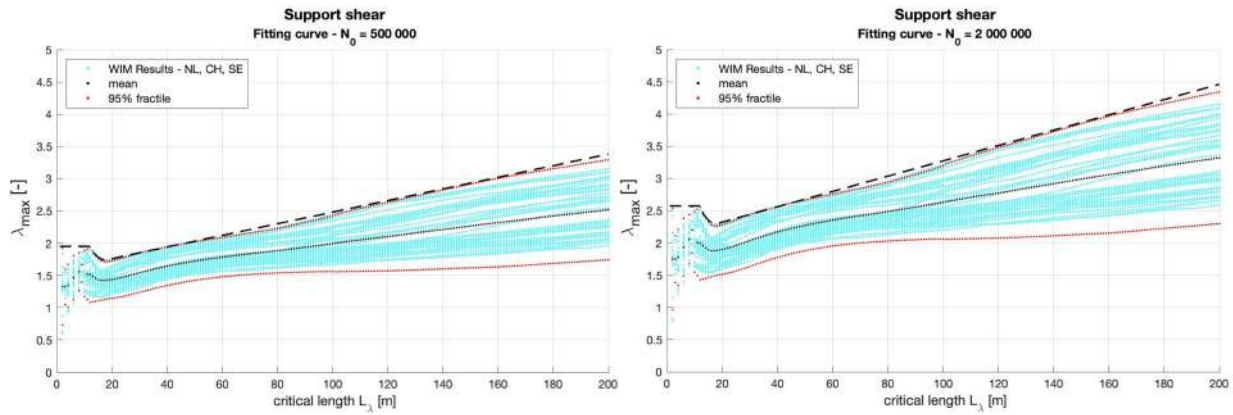


Figure 5.25. λ_{max} fitting curve for support shear force and reaction corrected with $N_0 = 500'000$ (L) and $N_0 = 2'000'000$ (R)

5.5 Comparison with current eurocode curves

In this section, the curves length proposition presented in the previous section are compare to the current λ_{max} curves in EN 1993-2 [20]. We recall, however, that we are comparing the current EN curves which use the FLM3 2-vehicles, whereas the curves simulated here only use the FLM3 single vehicle model this time.

5.5.1 Mid-span bending moment

The figure 5.26 shows this comparison for mid-span bending moments. The right side determine the relative difference from the proposed and the actual EN curves to the confidence interval of 95% for each critical length. (if the relative difference is negative, it means that the λ_{max} curve is higher than the confidence interval).

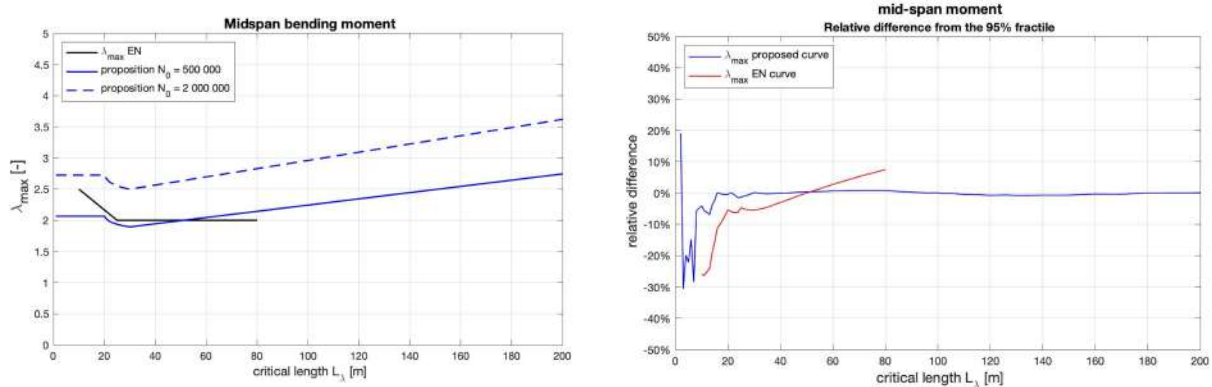


Figure 5.26. Mid-span moment - λ_{max} fitting curve comparison(L) and gap to confidence interval comparison(R)

The comparison between the current EN curve and the proposed λ_{max} curve for $N_0 = 500'000$ shows that the curves are relatively close. However the plateau described for the EN curve does not seem quite accurate with today's results. It should be remembered that the Sedlacek and Merzenich simulations used a fixed distance of 50 meters between vehicles and only 4 vehicle types derived from the Auxerre traffic. The fixed distance greatly reduces the possibilities and adverse combinations of vehicle interactions. This could explain to a large extent why the results differs a little with the ones for real traffic data. With these WIM measurements we have a fairly good confidence in these results since they are not subjected to a traffic model but derived directly from the actual measurements, on top of that several different traffics have been used and they all show the same trend in λ_{max} results. The new proposed curve follows much better the results than the current EN curve. Moreover, from about 50m, the λ_{max} curve of the Eurocode seems to underestimate the value of λ_{max} , which is not safe. For short spans, the gap is a little wider, but is still on the safety side.

5.5.2 Support bending moment

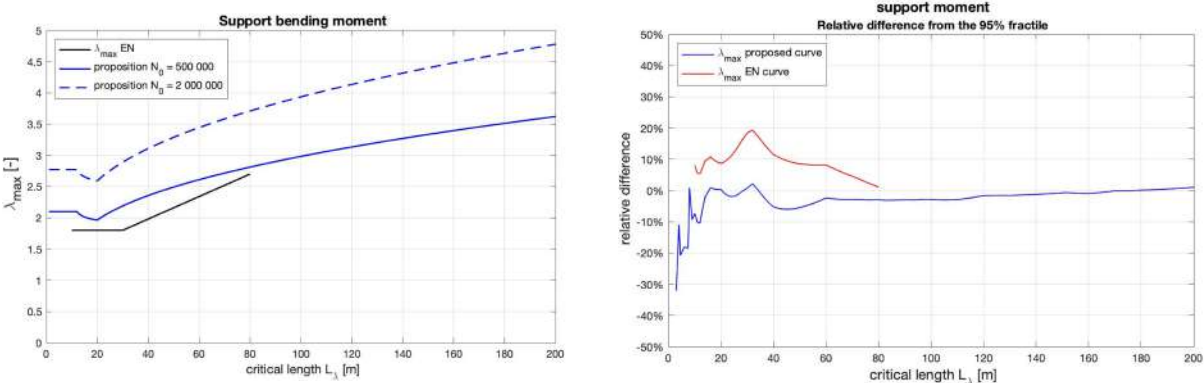


Figure 5.27. Support moment - λ_{max} fitting curve comparison(L) and gap to confidence interval comparison(R)

The figure 5.27 presents the same comparison for support bending moments. Similarly, when examining the λ_{max} values for traffic at $N_0 = 500'000$, the results are quite close to the current EN curve. The use of a curve for the third part of the proposed λ_{max} curve seems necessary as it allows to best fit the confidence interval than a straight line. Indeed, using a straight line would have overestimate λ_{max} values for spans longer than 100m. The EN curve, for its part, is not on the safe side. The curve slightly underestimates the λ_{max} values, which is no longer the case with the new curve. The use of real traffic data seems to improve the accuracy of the values obtained while confirming the trend that was obtained with the traffic models used at the time.

5.5.3 Mid-span shear force

To compare the shear forces at mid-span, an adaptation must be made to compare the values on the same level. The definition of the critical length used for the new proposals is not the same as the current definition in EN 1993-2 [20]. Indeed, the critical length for mid-span shear in the Eurocode is defined as 0.4 times the length of the considered span. In the new numerical simulations, it has been decided to use directly the length of the considered span as the critical length L_λ . In the comparison figure 5.28, the λ_{max} EN curve is therefore corrected with this factor of 40%. The curve described from 10 to 80 meters becomes a curve from 25 to 200 meters using the new definition of the critical length.

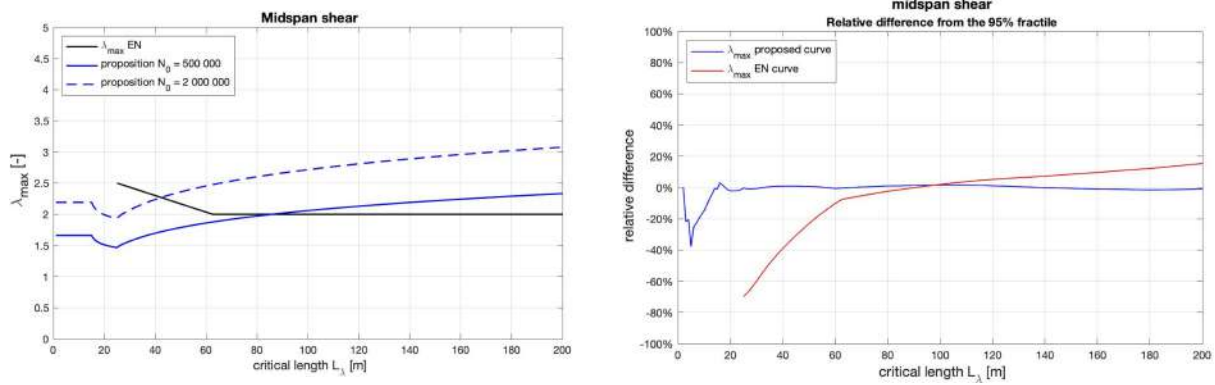


Figure 5.28. Mid-span shear - λ_{max} fitting curve comparison(L) and gap to confidence interval comparison(R)

The difference is quite large compared to the current curve. The curve described in the Eurocode does not follow at all the same trend as the results that are performed. In the comparison with the confidence interval, the difference is very high (up to 65%). Moreover, for longer spans, the curve is not on the safe side when relying on the results obtained with the WIM measurements.

5.5.4 Support shear force and reaction

When comparing with the current curve defined in the European standards, it can be seen that the behaviour is quite similar, however the slope is a little more attenuated than for the current λ_{max} curve which is based mainly on the support moments influence lines. Here the curve is more representative because it is only described for shear forces in contrast to the actual curves which is used for support moments and shear forces.

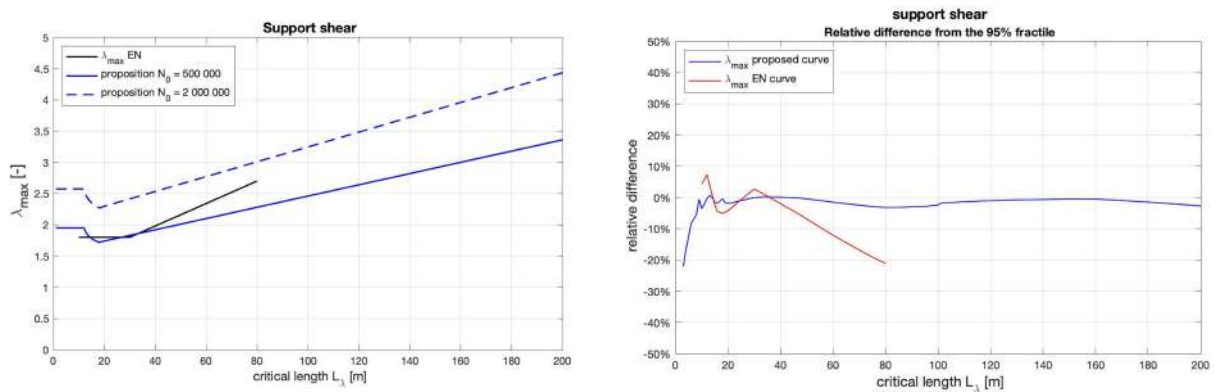


Figure 5.29. Support shear - λ_{max} fitting curve comparison(L) and gap to confidence interval comparison(R)

The current curve is not optimal and appears to overestimate the λ_{max} values for shear forces. This is probably due to the fact that currently the same curve is used for moments and shear force. Because the values are higher for the support bending moments, the curve when applied to the shear forces is a little overestimated.

5.6 New λ_{max} curves

The final λ_{max} curves presented below are calibrated for a number of 500'000 lorries per year, as currently defined in the European standard with $N_0 = 500'000$. The curves are all defined for critical lengths L_λ ranging from 5 to 200m. They are defined according to the same principle, the curve is composed of 3 curve segments (a plateau, a convex curve, and then a linear or a concave curve).

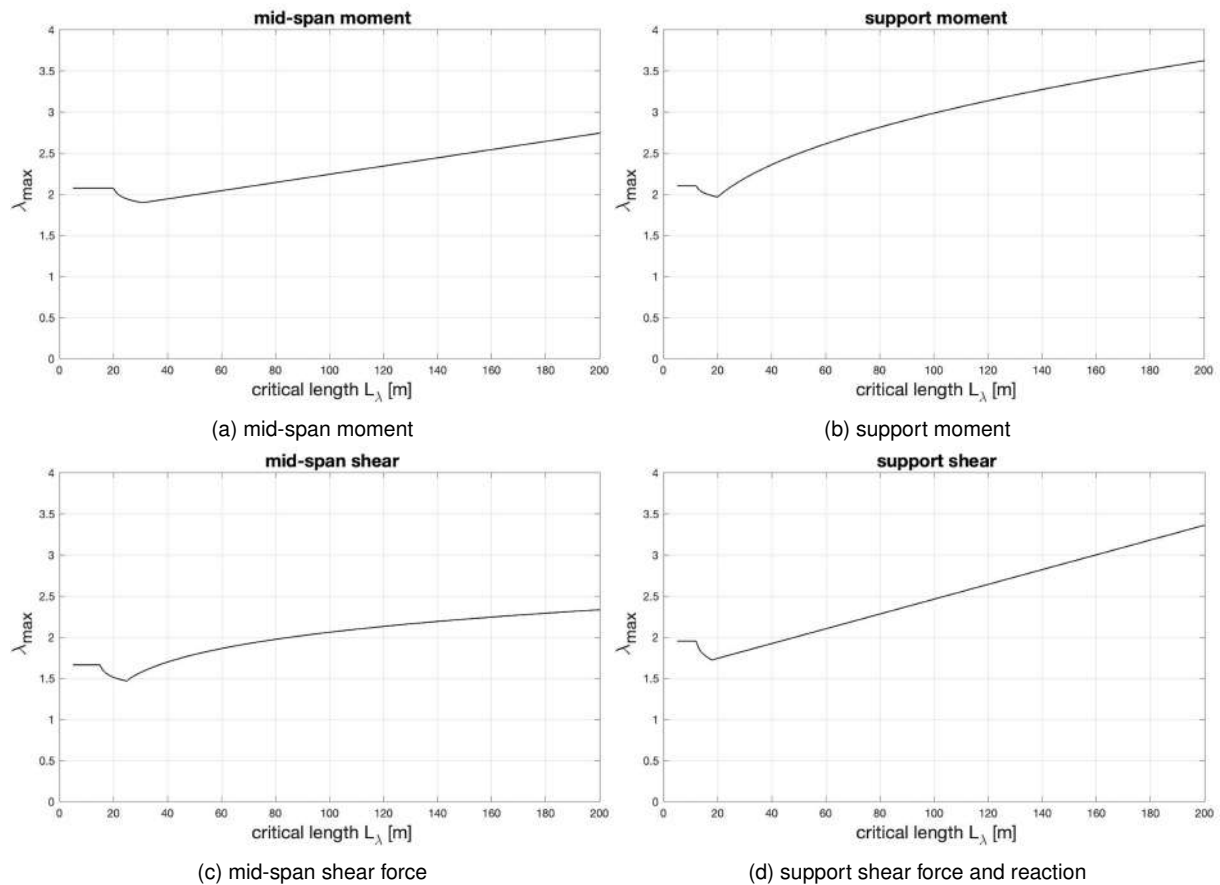


Figure 5.30. λ_{max} final curves

The curves presented in figure 5.30 are derived from the proposals presented in the previous section. The table 5.2 also presents the equations of the different curves, as well as the boundaries between each part of the curves defined by L_1 and L_2 .

	midspan moment	support moment	mid-span shear	support shear
L_1, L_2	20m, 30m	12m, 20m	15m, 25m	12m, 18m
$5 \leq L_\lambda \leq L_1$	2.07	2.10	1.66	1.95
$L_1 \leq L_\lambda \leq L_2$	$0.55 + \frac{1.52}{(L_\lambda - 19)^{0.05}}$	$0.65 + \frac{1.45}{(L_\lambda - 11)^{0.045}}$	$0.55 + \frac{1.11}{(L_\lambda - 14)^{0.081}}$	$0.65 + \frac{1.30}{(L_\lambda - 11)^{0.1}}$
$L_2 \leq L_\lambda \leq 200$	$1.74 + 0.005 \cdot L_\lambda$	$1.40 + 0.21(L_\lambda - 11)^{0.45}$	$(L_\lambda - 14)^{0.162}$	$1.56 + 0.009L_\lambda$

Table 5.2. λ_{max} curves equations

All the equations follow the same types of functions, so it is also possible to represent the curves in a general way by indicating the parameters to be used for each line of influence. The tables 5.3 and 5.4 therefore shows the equation in general form with the parameters to be applied for each curve.

λ_{max}	
$5 \leq L_\lambda \leq L_1$	A
$L_1 \leq L_\lambda \leq L_2$	$B + \frac{(A-B)}{(L_\lambda - (L_1 - 1)^a)}$
$L_2 \leq L_\lambda \leq 200$	$C + c \cdot L_\lambda + d \cdot (L_\lambda - (L_1 - 1))^b$

Table 5.3. λ_{max} curves parametric equations

	L_1	L_2	A	B	C	a	b	c	d
MM	20	30	2.07	0.55	1.74	0.050	-	0.005	0
SM	12	20	2.10	0.65	1.40	0.045	0.45	0	0.21
MV	15	25	1.66	0.55	0	0.081	0.162	0	1.00
SV	12	18	1.95	0.65	1.56	0.100	-	0.009	0

Table 5.4. λ_{max} curves parameters

As explained in the previous sections, it is necessary to correct this value for the actual traffic volume. The number of trucks on the slow lane is the parameter to be taken into account. As the reference is set for 500'000 lorries per year, the correction is made by keeping the same value $N_0 = 500'000$ described in the Eurocode EN 1993-2 [20].

$$\lambda_2^* = \left[\frac{N_{obs}}{N_0} \right]^{1/5} \quad (23)$$

$$\lambda = \lambda_1 \cdot \lambda_2 \cdot \lambda_3 \cdot \lambda_4 \leq \lambda_{max} \cdot \lambda_2^* \quad (24)$$

5.7 Effects of the slopes of the Wöhler curve

All previous results were based on the standard resistance curve with double slope $m|k=3|5$. In order to determine the difference that is obtained when using other resistance curves with different slopes, the simulations were also carried out with the other slopes described in Chapter 4. The figure below shows the comparison of the different slopes used for the λ_{max} calculation.

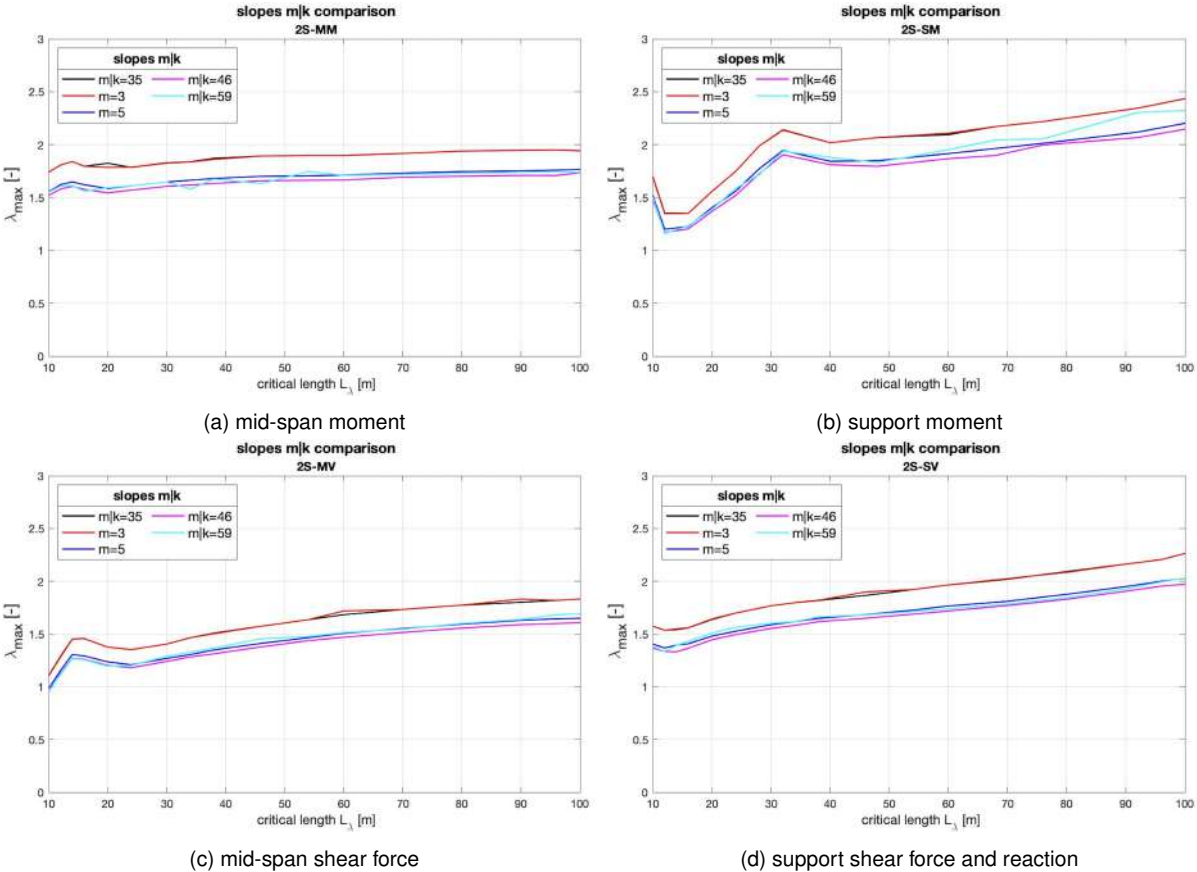


Figure 5.31. λ_{max} comparison for different slopes of the fatigue strength curve

It is clear that the behaviour of the curves is identical, the curves have exactly the same shape whatever the resistance curve used. However, it is necessary to determine the factor to be applied to find each curve. Moreover, we notice that the difference between the curves is the same whatever the influence line that we calculate. The correction to be applied is nevertheless not so trivial, because the slope is not the only determining parameter. Indeed, it can be observed for example that λ_{max} is lowest when the $m|k=4|6$ strength curve is used and does not lie between the values for $m=3$ or $m=5$ slopes. This may seem surprising at first, but it should be remembered that not all slopes have exactly the same construction. In particular for curves $4|6$ and $5|9$, these observe a slope change for $N = 2 \cdot 10^6$ cycles whereas the other slopes have a change in slope at the CAFL which is located at $N = 5 \cdot 10^6$. The position of the slope change is of great importance as the most important factor is the relationship between the strength category at 2 millions cycles and the stress threshold at the CAFL. The relationship between these two values is important because the criterion for determining λ_{max} is directly related to the constant amplitude fatigue limit, but the relationship for determining λ_{max} takes into account the fatigue strength category.

To illustrate this, the following figure shows the difference between the various resistance curves by setting the CAFL threshold at the same point for all curves. This allows the λ_{max} value to be determined graphically for any resistance curve if the constant amplitude fatigue limit is set at the same level for each curve.

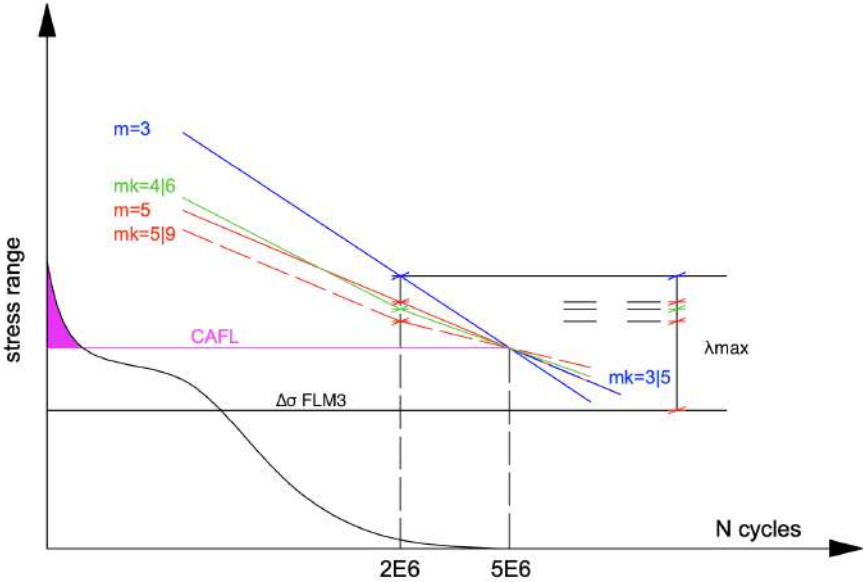


Figure 5.32. Comparison of $\Delta\sigma_C$ for various slopes $m|k$

Assuming that CAFL is the same for all curves, it is normal that λ_{max} values are higher for curves 3 and 3|5. These curves are also identical because the change in slope occurs below the CAFL and should not affect the λ_{max} values. It is simply larger because it is the case where the ratio between $\Delta\sigma_C$ and $\Delta\sigma_D$ is the largest. The table 5.5 shows the ratios between these two values according to the resistance curve used (assuming that the CAFL is set at the same level for each slopes), the last column represents the ratio between the value for the slope used compared to the reference slope which is $m|k=3|5$.

	$\Delta\sigma_C$	$\Delta\sigma_D$	$\Delta\sigma_C/1.357$
$m = 3$	1.357	1	1
$m = 3 5$	1.357	1	1
$m = 5$	1.201	1	0.885
$m = 5 9$	1.107	1	0.815
$m = 4 6$	1.164	1	0.857

Table 5.5. Comparison of fatigue strength curves

Here the assumption was made that the CAFL was at the same level regardless of the resistance curve used, but in reality the threshold will not be at the same level for each curve because the damage of 0.01 will not be reached at the same time. If we take as reference the slope $m|k=3|5$, it is above all others for the diagram region where $N < 5$ millions cycles. This indicates that the damage generated for the part of the stress histogram above the CAFL will be lower than for all other resistance curves. This means that the threshold will be a little shifted upwards when using the other resistance curves. The ratios calculated in the previous table are minimum limits. The λ_{max} can still be higher due to the shift of the threshold. Applying these factors described in the table 5.5, we find values quite close to the results of the simulations for slopes with $m=5$ and $m|k=4|6$. For slope $m|k=5|9$, on the other hand, it does not

correspond to the correction defined in table 5.5. Indeed, the factor to be used is equal to 0.815 whereas the results presented in the figure 5.32 show that slope 5|9 corresponds to the values of slope $m=5$.

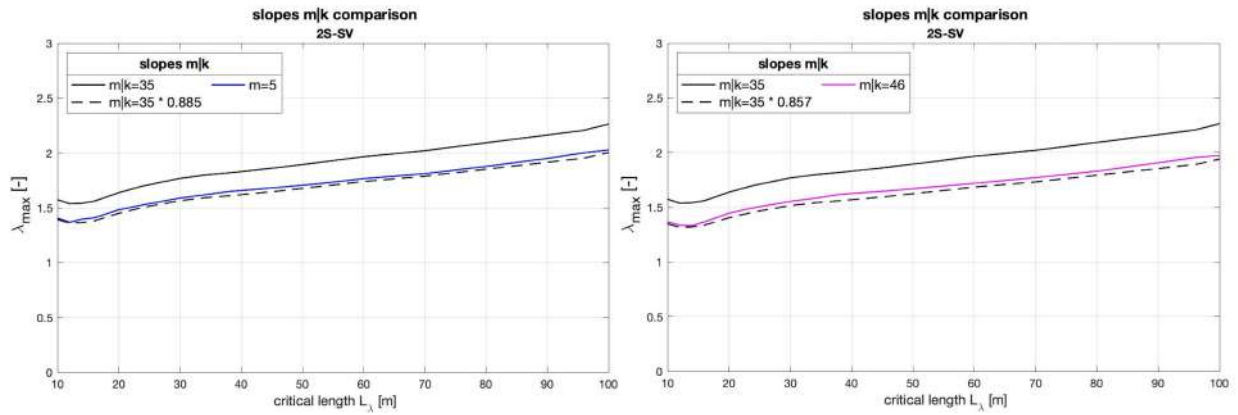


Figure 5.33. λ_{max} corrected for $m=5$ (L) $m|k=4|6$ (R)

What may explain this is that since curve 5|9 is the lowest of all, the damage caused is much lower for the same CAFL location, so it is likely that the CAFL threshold is shifted downwards and the gap is less than this proportion between the reference curve 3|5 and this curve with $m|k=5|9$.

Analytically it is possible to define the correction to be applied for curves $m=5$ and $m|k=4|6$ with respect to the λ_{max} results described for a the curve with $m|k=3|5$.

$m=5$:

$$\Delta\sigma_{C(5)} = \left(\frac{2}{5}\right)^{-1/m} \cdot \Delta\sigma_D \quad (25)$$

$$\lambda_{max(5)} = \lambda_{max(3|5)} \cdot \frac{\Delta\sigma_{C(5)}}{\Delta\sigma_{C(3|5)}} = \lambda_{max(3|5)} \cdot \left(\frac{2}{5}\right)^{-1/m+1/3} = \lambda_{max(3|5)} \cdot \left(\frac{2}{5}\right)^{(m-3)/(m \cdot 3)} \quad (26)$$

$m|k=4|6$:

$$\Delta\sigma_{C(4|6)} = \left(\frac{2}{5}\right)^{-1/k} \cdot \Delta\sigma_D \quad (27)$$

$$\lambda_{max(4|6)} = \lambda_{max(3|5)} \cdot \frac{\Delta\sigma_{C(4|6)}}{\Delta\sigma_{C(3|5)}} = \lambda_{max(3|5)} \cdot \left(\frac{2}{5}\right)^{-1/k+1/3} = \lambda_{max(3|5)} \cdot \left(\frac{2}{5}\right)^{(k-3)/(k \cdot 3)} \quad (28)$$

The λ_{max} curve must therefore be corrected with respect to the slope of the fatigue strength curve in the region between N_C and N_D . In the case where the change in slope of the fatigue strength curve occurs at $N_C=2$ millions cycles, m must be replaced by k as in equation 28.

$$\lambda_{max(m|k)} = \lambda_{max(3|5)} \cdot \left(\frac{2}{5}\right)^{(m-3)/(m \cdot 3)} \quad (29)$$

5.7.1 Comparison for concrete bridge decks - reinforcing steel

For concrete bridge decks, the verification is similar to that for steel highway bridges. The lambda verification method use similar partial factor as expressed below.

$$\Delta\sigma_{s,equ} = \Delta\sigma_{s,Ec} \cdot \lambda_s \quad (30)$$

$$\lambda_s = \varphi_{fat} \cdot \lambda_{s,1} \cdot \lambda_{s,2} \cdot \lambda_{s,3} \cdot \lambda_{s,4} \quad (31)$$

However, the verification method presented for bridge decks does not use a λ_{max} limit in contrast to the verification for steel road bridges. The calculation also applies to Fatigue Load Model 3, but this time the values from the FLM3 model must be multiplied by the following coefficients:

- 1.75: for verification at intermediate supports in continuous bridges
- 1.40: for verification in other areas

The comparison done here, is for reinforcing steel. In this case, the fatigue strength curve defined in EN 1992-2 [19] is with double slope $m|k=3|5$. The $\lambda_{s,1}$ values are presented graphically in the same way as for steel bridges. In order to get an idea of the λ_{max} values that would be valid for the strength curve 5|9, the values have been plotted on the current Eurocode EN 1992-2 [19] graph for the $\lambda_{s,1}$ values.

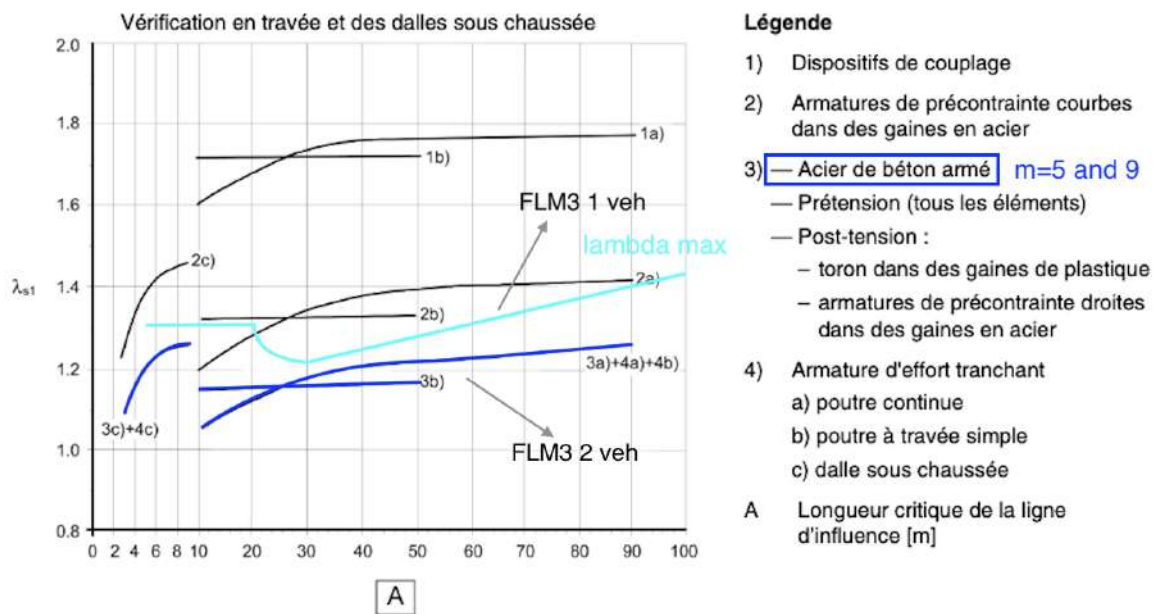


Figure 5.34. Comparison with EN 1992-2 [19] for reinforcing steel - in span verification

This figure 5.34 determines $\lambda_{s,1}$ for a verification of elements located at mid-span. In order to represent the λ_{max} values in relation to the $\lambda_{s,1}$ values, the proposed curve for the mid-span moment with the standard curve 3|5 has been corrected. To correct it, first the results have been modified with the equation 29. Then, the factor presented in EN 1992-2 [19] to correct the equivalent stress value from FLM3 (1.40 for span sections) has to be considered. The λ_{max} value therefore have been divided by the correction factor of 1.40 since the numerical simulations have been developed using the FLM3 single vehicle model without any additional amplifications.

In figure 5.35, the same approach is used. The curve proposed for support bending moment in the previous section is corrected following the fatigue strength curve 5j9 and with the factor applied in EN 1992-2 [19], which equals 1.75.

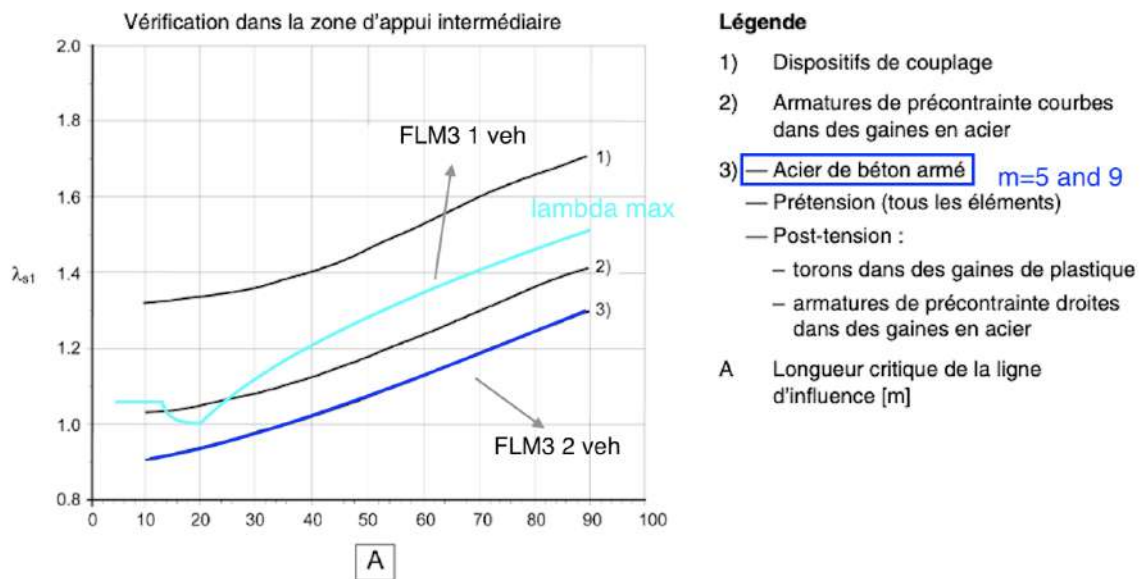


Figure 5.35. Comparison with EN 1992-2 [19] for reinforcing steel - support area

The λ_{max} curves are relatively close to the $\lambda_{s,1}$ curves, and it can be seen that they are always located above the $\lambda_{s,1}$ curves, which is consistent, so it would be possible to add a λ_{max} limit in the verification method for concrete bridge decks. Further investigations would be useful to propose plausible curves for bridge decks components.

5.8 λ_1 and λ_{max} - possible update to EN 1993-2

The curves shown below represent the λ_1 and λ_{max} curves together. The λ_1 results are obtained from the work of Gianluca Bianchi[3]. In order to harmonise the results, the curves for both λ_1 and λ_{max} all have the same curve characterisation.

- 5 to 20 m: they use a polynomial equation with power 2
- 20 to 200m they use a polynomial equation with power 3

In this case, the curves are defined from 5 to 200m. In order to define them, the same approach has been used based on the 95% confidence interval. The harmonisation of the curves has therefore slightly modified the λ_{max} curves presented in the previous sections, but they remain close to the calculated 95% confidence interval.

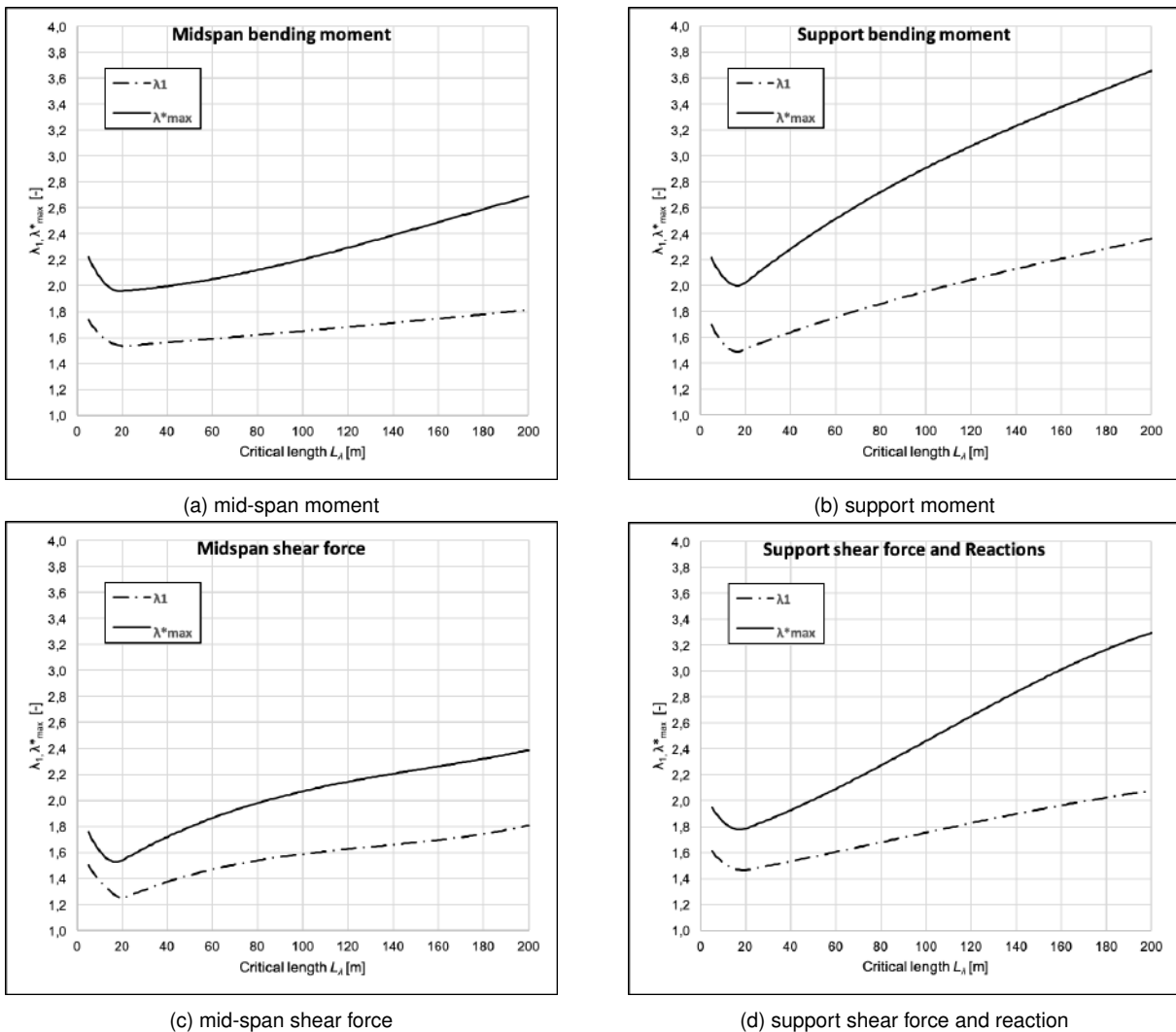


Figure 5.36. λ_1 and λ_{max} curves

The curves presented in figure 5.30 are derived from the proposals presented in the previous section. The curves present similar behaviour between λ_1 and λ_{max} . The λ_1 curve always remaining below λ_{max} . This grouping of curves makes it possible to see that the results found are consistent. As the definition of the curves is of the same type for each influence line, the results are clear and allow a certain readability. The representation on the same graph of the λ_1 and λ_{max} curves allows to easily apprehend the difference and the cases where λ_{max} will be likely to become determining.

6 Conclusions

This work allowed to study in depth the behaviour of the λ_{max} factor used in the simplified fatigue verification method for road bridges. This verification method has to be updated and recalibrated according to the traffic that can be observed on European roads nowadays. Indeed, the lambda factors of this simplified method reflect the difference between the damage caused by the fatigue load model and the damage that would be caused by a real traffic. It is therefore important to carry out this update to ensure that the verification method is consistent and guarantees the safety of structures.

A review of the previous simulations has been carried out to assess the assumptions that were applied, in particular on the traffic conditions for the calculation of the cumulative damage. It was also shown that some assumptions were not necessarily appropriate, particularly with regard to inter-vehicles distances and that only free-flowing traffic was considered. These assumptions greatly underestimate the influence in terms of damage as they do not take into account the possible interaction between heavy vehicles. In addition, the number of influence lines evaluated was relatively small and the results were determined only for span lengths ranging from 10m to 80m.

The calibration of the new λ_{max} curves is based on WIM measurements from 6 different stations (located in Switzerland, Sweden and in the Netherlands). This allowed to evaluate several types of traffic with parameters that could be very different. To determine the new curves, a new criterion was used. This criterion allows an exceed of 1% of absolute damage for stress ranges above the constant amplitude fatigue limit. It has been shown that this criterion is more adequate and remains safe. The choice to use WIM measurements is explained by the fact that it accounts for real traffic and in particular the extreme values of traffic loads that can occur. In contrast to traffic models, which report characteristic values of heavy vehicles and do not represent the plurality of maximum loads. In the case of λ_{max} calibration, it seems preferable to use WIM measurements, which allow an evaluation of the traffic in its entirety. WIM data also allows the dynamic effects contained in the measurements to be considered, and it has been shown that WIM measurements do not necessarily require additional dynamic amplification. In the simulations done during this project, 44 influence lines were therefore calculated in order to cover a larger number of cases than in previous simulations. The influence lines were also evaluated for span lengths up to 200m. These new numerical simulations allowed the influence lines to be classified into 4 groups; mid-span bending moment, support bending moment, mid-span shear forces and support shear forces. It was therefore possible to determine 4 λ_{max} curves.

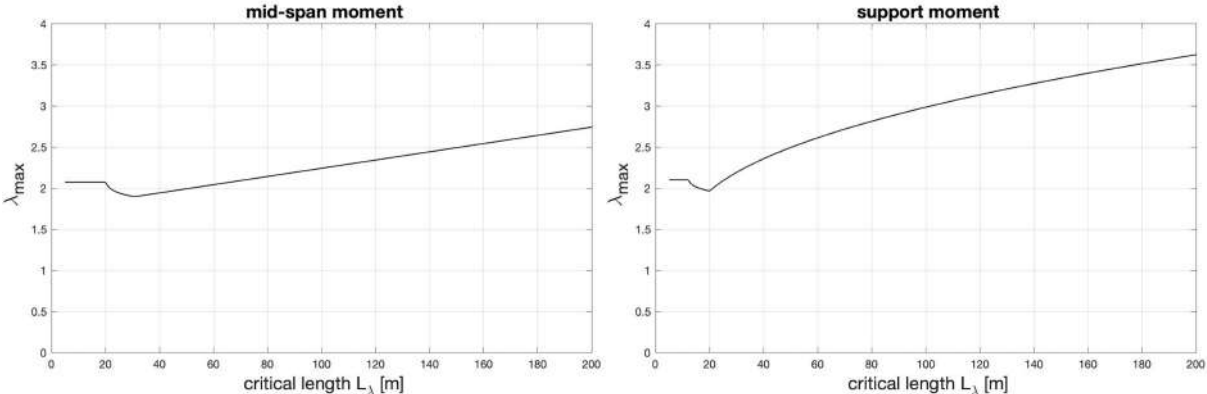


Figure 6.1. λ_{max} final curves - bending moments

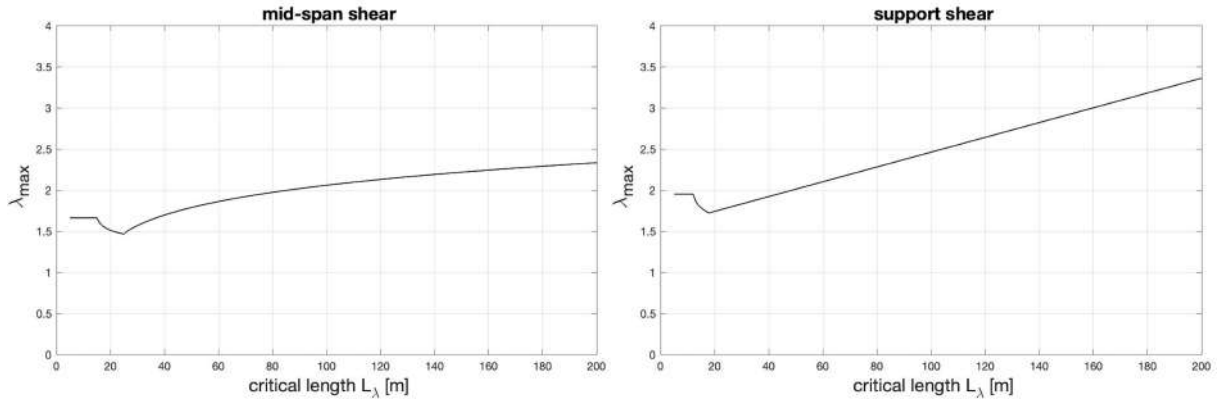


Figure 6.2. λ_{max} final curves - shear forces

The curves have been calibrated according to a traffic volume for a number of heavy vehicles per year equal to 500'000. This is in line with the value N_0 described in the current version of the Eurocode EN 1993-2 [20]. However, it has been shown that the traffic volume has a real influence on the λ_{max} values to be adopted. The traffic volume influences the number of stress cycles but also the traffic configuration. The higher the traffic volume, the smaller the distance between the vehicles, which have a real influence on λ_{max} . By using an adapted correction of the λ_2 factor, it was possible to combine the curves from the 6 different WIMs. A correction must therefore be applied to the λ_{max} factor during the verification according to the type of road evaluated. The correction factor λ should therefore be determined using this equation:

$$\lambda = \lambda_1 \cdot \lambda_2 \cdot \lambda_3 \cdot \lambda_4 \leq \lambda_{max} \cdot \lambda_2^* \quad (32)$$

$$\lambda_2^* = \left[\frac{N_{obs}}{N_0} \right]^{1/5} \quad (33)$$

The curve was determined according to a fatigue resistance curve with a double slope $m|k=3|5$. A correction was also determined in order to apply the λ_{max} values to other resistance curves with different slopes. The correction to apply is the following:

$$\lambda_{max(m|k)} = \lambda_{max(3|5)} \cdot \left(\frac{2}{5} \right)^{(m-3)/(m \cdot 3)} \quad (34)$$

In the case where the change in slope of the fatigue strength curve occurs at $N_C = 2$ millions cycles, m must be replaced by k in the equation.

The work has therefore made it possible to propose new λ_{max} curves that are in line with current European traffic. In addition, the new curves consider a larger number of influence lines covering spans from 5m to 200m. Taking into account a larger set of influence lines including various static configurations allows to define λ_{max} . Finally, an adapted proposal together with λ_1 curves has been presented and allows to have both curves on the same graphs. This makes it possible to have a clear approach to the results and to directly see the difference between the λ_1 and λ_{max} curves.

6.1 Future works

The numerical simulations are now well developed with a large number of parameters that allow the evaluation of a large number of influence lines with different traffic models, be it FLM4, Auxerre, A16 models, or traffic measurements with the help of WIM stations. Further investigations could be carried out regarding dynamic amplification factors. This would provide confirmation of the assumptions done in this work.

Now that the behaviour of the λ_1 and λ_{max} factors have been studied, it would be interesting to perform simulations with multi-lanes traffics. Indeed, all the simulations that were carried out in this work only considered a model for a single traffic lane, an adaptation of the algorithm in order to study the effect of 2 traffic lanes for example would be interesting and would allow the study of the λ_4 factor. This would allow the study of the behaviour of the lambda factor according to different traffic configurations (2 lanes in the same direction, 2 lanes with opposite directions).

In addition, it would be interesting to pursue the work started in order to be able to apply the λ_1 and λ_{max} results for other fatigue resistance curves. In particular, it would be possible to find results for bridge deck elements using the various strength curves for standard reinforcement, pre- and post-tensioning reinforcement, coupling devices and shear reinforcement. This would allow to complete the current algorithm and to compare these results with the actual curves defined in Eurocode EN-1992-2.

References

- [1] Nariman Maddah, *Fatigue Life Assessment of Roadway Bridges based on Actual Traffic Loads*, EPFL Thèse N°5575, 2013.
- [2] Cláudio Alexandre Pereira Baptista, *Multiaxial and variable amplitude fatigue in steel bridges*, EPFL Thèse N°7044, 2016.
- [3] Gianluca Bianchi, *European traffic on road bridges and recalibration of damage equivalence factor for fatigue verification*, EPFL Master Thesis, 2019
- [4] A. Nussbaumer and S. Wallbridge, *Background for determination of the fatigue load correction factor in SIA codes*, EPFL, 2009
- [5] Manfred A. Hirt, Rolf Bez and Alain Nussbaumer, *Construction Métallique (TGC volume 10)*, PPUR, 2009
- [6] Jean-Paul Lebet and Manfred A. Hirt, *Ponts en acier (TGC volume 12)*, PPUR, 2009
- [7] A. Nussbaumer, J. Oliveira Pedro, C.A. Pereira Baptista and M. Duval, *Fatigue damage factor calibration for long-span cable-stayed bridge decks*, in *Structural Integrity*, 2019, chapter 7, pp. 369–376
- [8] G. Sedlacek, G. Merzenich, M. Paschen, A. Brules, L.Sanpaolesi, P.Croce, J.A. Calgaro, M. Pratt, Jacob, M. Leendertz, v. de Boer, A. Vrouwenfelder and G. Hanswille, *Background document to EN 1991 - Part 2 - Traffic loads for road bridges - and consequences for the design*, JRC Scientific and Technical Reports, 2008
- [9] P. Croce, *Background to fatigue load models for Eurocode 1: Part 2 Traffic Loads. Progress in Structural Engineering and Materials*, 2001
- [10] G. Merzenich and G. Sedlacek, *Hintergrundbericht zum Eurocode 1 - Teil 3.2: "Verkehrslasten auf Straßenbrücken"*, *Forschung Heft Straßenbau und Straßenverkehrstechnik*, 1995
- [11] P. Kunz, Manfred A. Hirt, *Grundlagen und Annahmen für den Nachweis der Ermüdungssicherheit in den Tragswerksnormen des SIA*, 1991
- [12] M. Sjaarda, T. Meystre, A. Nussbaumer, Manfred A. Hirt, *system-atic approach to estimating traffic load effects on bridges using weigh- in-motion data*, *Stahlbau* 89, H. 7, S. 585–598, 2020

- [13] G. Sedlacek, H. Eisel, W. Hensen, B. Kuhn, *Leitfaden Zum DIN-Fachbericht 103 Stahlbrücken*, John Wiley Sons, 2004
- [14] J. Maljaars, *Evaluation of traffic load models for fatigue verification of European road bridges*, Engineering Structures, Volume 225, 2020, 111326, ISSN 0141-0296
- [15] J. Leander, *Reliability evaluation of the Eurocode model for fatigue assessment of steel bridges*, Journal of Constructional Steel Research, Volume 141, 2018, Pages 1-8, ISSN 0143-974X
- [16] J.-A. Calgaro, M. Tschumi, H. Gulvanessian, *Designers' Guide to Eurocode I: Action on bridges*, 2010
- [17] *SETRA: Eurocodes 3 and 4 - Application to steel-concrete composite road bridges*, Paris, 2007
- [18] *Eurocode 1 - Actions on structures - Part 2: Traffic loads on bridges*, European committee for standardization, 2003
- [19] *Eurocode 2 - Design of concrete structures - Part 2: Concrete bridges*, European committee for standardization, 2005
- [20] *Eurocode 3 - Design of steel structures - Part 2: Steel Bridges*, European committee for standardization, 2006
- [21] *Eurocode 3 - Design of steel structures - Part 1-9: Fatigue*, European committee for standardization, 2005
- [22] *Swiss standard SIA 261 - Actions sur les structures porteuses*, 2014
- [23] *Swiss standard SIA 263 - Construction en acier*, 2013
- [24] António J. Reis, José J. Oliveira Pedro, *Bridge Design: Concepts and Analysis*, Ed. John Wiley Sons Ltd, Abril de 2019 (524 pags). ISBN: 9780470843635.

Annex A

Influence lines

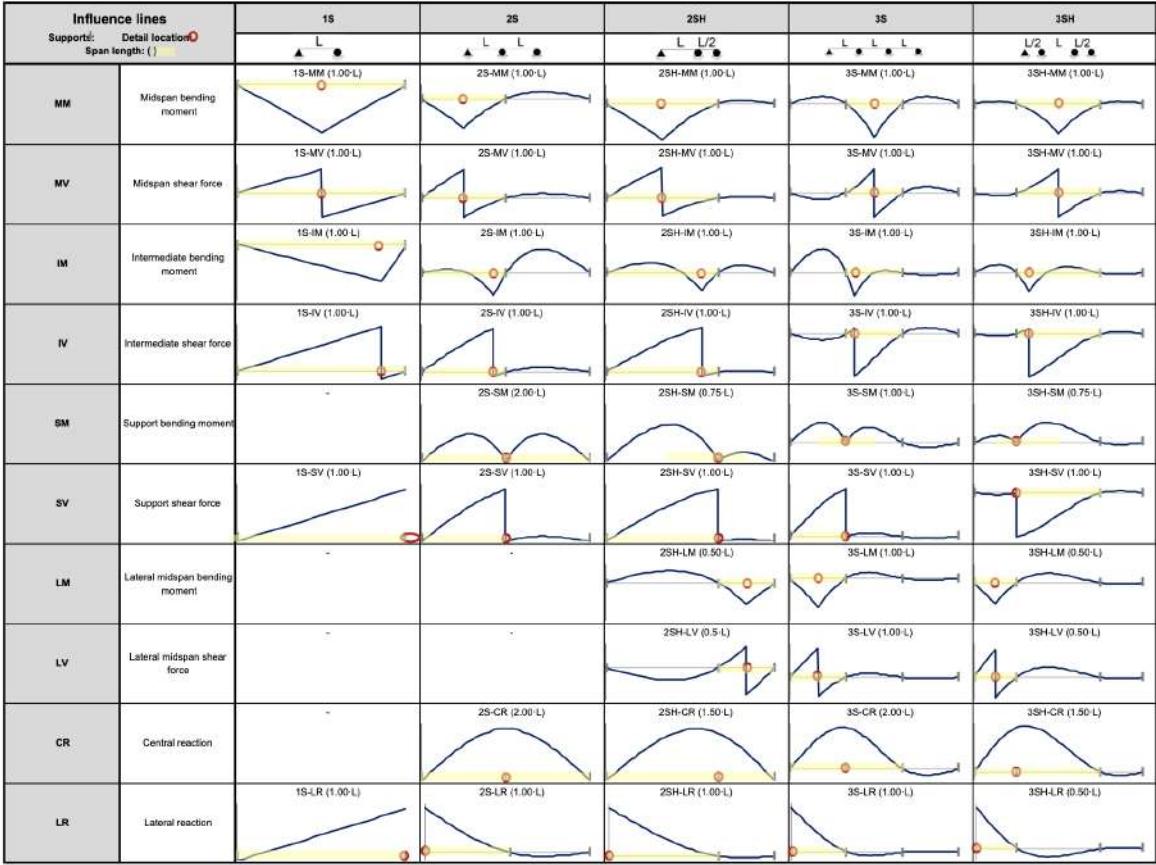


Figure A.1 Influence lines and critical length L_{λ}

Annex B

λ_{max} equations

mid-span moment

$$1.35 \cdot 10^{-3}x^2 - 5.10 \cdot 10^{-2}x + 2.44 \quad \text{for } 5m \leq L_\lambda \leq 20m \quad (35)$$

$$- 6.16 \cdot 10^{-8}x^3 + 2.98 \cdot 10^{-5}x^2 + 2.11 \cdot 10^{-4}x + 1.94 \quad \text{for } 20m \leq L_\lambda \leq 200m \quad (36)$$

support moment

$$1.80 \cdot 10^{-3}x^2 - 5.73 \cdot 10^{-2}x + 2.46 \quad \text{for } 5m \leq L_\lambda \leq 20m \quad (37)$$

$$- 8.55 \cdot 10^{-8}x^3 - 4.73 \cdot 10^{-5}x^2 + 1.57 \cdot 10^{-2}x + 1.72 \quad \text{for } 20m \leq L_\lambda \leq 200m \quad (38)$$

mid-span shear force

$$6.52 \cdot 10^{-4}x^2 - 3.10 \cdot 10^{-2}x + 1.9 \quad \text{for } 5m \leq L_\lambda \leq 20m \quad (39)$$

$$1.31 \cdot 10^{-7}x^3 - 6.15 \cdot 10^{-5}x^2 + 1.24 \cdot 10^{-2}x + 1.31 \quad \text{for } 20m \leq L_\lambda \leq 200m \quad (40)$$

support shear force and reaction

$$1.85 \cdot 10^{-3}x^2 - 5.69 \cdot 10^{-2}x + 2.19 \quad \text{for } 5m \leq L_\lambda \leq 20m \quad (41)$$

$$- 1.44 \cdot 10^{-7}x^3 + 4.55 \cdot 10^{-5}x^2 + 4.76 \cdot 10^{-3}x + 1.67 \quad \text{for } 20m \leq L_\lambda \leq 200m \quad (42)$$